# Battery Pack Design of Cylindrical Lithium-Ion Cells and Modelling of Prismatic Lithium-Ion Battery Based on Characterization Tests

By

Ruiwen Chen, B.Eng. & Co-op.

A Thesis
Submitted to the Department of Mechanical
Engineering and the School of Graduate Studies
of McMaster University
in Partial Fulfilment of the
Requirements for the Degree of
Master of Applied Science

Master of Applied Science (2022) McMaster University

Department of Mechanical Engineering Hamilton, Ontario, Canada

| | |
|---|---|
| TITLE: | Battery Pack Design of Cylindrical Lithium-Ion Cells and Modelling of Prismatic Lithium-Ion Battery Based on Characterization Tests |
| AUTHOR: | Ruiwen Chen<br>B.Eng. &Co-op.<br>McMaster University, Hamilton, Canada |
| SUPERVISOR: | Dr. Saeid R. Habibi, Ph.D., P.Eng, FCSME, FASME<br>Professor and Senior NSERC Industrial Research chair<br>Director, Centre for Mechatronics and Hybrid Technologies<br>McMaster University, Hamilton, Canada |
| NUMBER OF PAGES: | 120 |

# Abstract

With increasing research on lithium batteries, the technology of electric vehicles equipped with lithium battery packs as the main energy storage system has become more and more mature, and the design and testing of lithium ion battery packs are becoming extremely important. As the battery system becomes more complex, it is necessary to optimize its structural design and to monitor its dynamic performance accurately. This research considers two related topics. The first is the design of a battery submodule made up of cylindrical lithium cells. The objective of this design is to improve its energy density and optimize the heat dissipation performance according to the installation position and space constraints in Ford Focus EV 2013, and, produce a submodule prototype based on this design; The second objective is to derive and verify an equivalent circuit model for a prismatic lithium battery cell of high energy capacity based on experimental results.

In terms of mechanical structure, the basic structure of a battery pack is determined by the desired performance as well as cell characteristics. In this research, the Samsung 35E 18650 cylindrical cells are chosen. 20 battery cells are connected in parallel to form a battery submodule, and 13 battery submodules are connected in series to form a battery pack. The battery pack design process mainly includes positioning and connection of battery cells, heat dissipation mechanism, cabling and inside the pack. The above considerations were applied to prototype battery submodule with an energy density of 216.87 Wh/kg. Some key considerations in the design of the battery pack include checking the conductivity and the welding connection.

Chemistry of lithium-ion batteries are constantly evolving with industrial demands which call for higher energy storage capacity. Therefore, this research selected a new high-capacity prismatic

cell to establish an equivalent circuit model using characterisation and experiments, followed by verification. A 280 Ah Lithium Iron Phosphate (LFP) prismatic battery cell was selected and characterized by testing under various operating conditions for validation, the Urban Dynamometer Driving Schedule (UDDS) was used.

# Acknowledgements

With the completion of my thesis, my student career at McMaster University has come to an end. Looking back on my studies in the past few years, I have been helped and encouraged by many people in my studies and life.

First of all, I would like to thank my supervisor, Dr. Saeid Habibi. Since I joined the Centre for Mechatronics and Hybrid Technologies (CMHT), Dr. Saeid Habibi has been committed to building a perfect scientific research platform for us. In the research, regardless of the required hardware and software resources, Dr. Saeid Habibi has spared no effort to strongly support. With the endless help and guidance of Dr. Saeid Habibi, I completed my researches and this thesis. He not only helped me in my studies, but also gave me great supports in my professional career and life. Here, I deeply express my respect and gratitude to Dr. Saeid Habibi. I also want to thank Dr. Ryan Ahmed who also provided me with countless technical support during my research continuously.

I would like to thank Dana Incorporated for providing me with the co-op experience, which gives me the opportunity to gain valuable working knowledge and understand the cutting-edge development of the automotive industry.

I would have not been able to complete my thesis without my partner Han Xuesong for unconditionally supporting me and understanding me when I was at a loss. You didn’t give me up when everything was messed up back then. You are and will always be my biggest driving force to continue and move forward. I would also like to thank my brother Chen Ruiwu, who always

gives me economic and spiritual support since childhood. You are always my strongest backing. I'll forever be grateful to my mother, you are the strongest woman I ever know, thank you for tolerating my bad temper and paving the forwarding way for me. Finally I want to thank my grandpa in heaven who gave me and my twin brother everything you cherished, your teaching us kindness and tolerance will always encourage us to make continuous progress, I hope us to always make you proud.

# Abbreviations

| | |
|---|---|
| **BEV** | Battery electric vehicle |
| **BMS** | Battery management system |
| **CC** | Constant current |
| **CTC** | Cell to Chassis |
| **CV** | Constant voltage |
| **DOD** | Depth of Discharge |
| **EPA** | Environmental Protection Agency |
| **EV** | Electric vehicle |
| **HEV** | Hybrid electric vehicle |
| **HPPC** | Hybrid pulse power characteristic |
| **HV** | High voltage |
| **ICE** | Internal combustion engine |
| **KF** | Kalman Filtering |
| **LCO** | Lithium cobalt oxide |

| | |
|---|---|
| **LFP** | Lithium iron phosphate |
| **LMO** | Lithium manganese oxide |
| **LTO** | Lithium Titanate oxide |
| **LV** | Low voltage |
| **NMC** | Lithium Nickel Manganese Cobalt Oxide |
| **NCA** | Lithium Nickel Cobalt Aluminium Oxide |
| **PHEV** | Plug-in hybrid electric vehicle |
| **PTC** | Product Temperature Control |
| **RMSE** | Root mean square error |
| **SOC** | State of charge |
| **SOH** | State of health |
| **OCV** | Open circuit voltage |
| **UDDS** | Urban dynamometer driving schedule |

# Contents

Abstract ..... iii

Acknowledgements ..... v

Abbreviations ..... vii

Chapter 1 Introduction ..... 1

1.1 Background and Motivation ..... 1

1.1.1 Research status of power lithium battery pack structure ..... 2

1.1.2 Research status of SOC Estimation ..... 4

1.2 Objectives and Contributions ..... 5

1.3 Thesis Organization ..... 6

Chapter 2 Lithium-ion Battery Cell ..... 8

2.1 Classification of Lithium-ion Battery Cells ..... 8

2.1.1 Classification by Chemistry Factor ..... 9

2.1.2 Classification by Form Factor ..... 11

2.2 Terminology and Definitions of Lithium-ion Batteries ..... 13

2.2.1 State of Charge (SOC) ..... 13

2.2.2 State of Health (SOH) ..... 15

2.2.3 Charge/ Discharge Rate (C-rate) ..... 17

2.2.4 Fully Charged/ Discharged ..... 17

2.2.5 Energy Density ..... 18
2.2.6 Life Cycle ..... 19
2.2.7 Self-Discharge ..... 20
2.2.8 Nominal Capacity and Useable Capacity ..... 21
2.2.9 Battery Voltage ..... 22
2.2.10 Depth of Discharge ..... 23
2.2.11 Internal Resistance ..... 24
2.3 Characteristics of Lithium-ion Battery ..... 25
2.3.1 Battery open-circuit voltage (OCV) ..... 25
2.3.2 Correspondence characteristics of Charge-discharge rate and terminal voltage ..... 26
2.3.3 Temperature characteristics ..... 27
2.3.4 Group efficiency of batteries ..... 28
2.4 Common Methods of SOC estimation ..... 28
2.4.1 Coulomb Counting method ..... 28
2.4.2 Open circuit voltage (OCV) method ..... 29
2.4.3 Fuzzy reasoning and neural network method ..... 29
2.4.4 The equivalent circuit model method ..... 29
2.4.5 Kalman filtering method ..... 30
2.4.6 Summary ..... 30
Chapter 3 Design of a Power Battery Pack ..... 31
3.1 Mechanical structural requirements of designing battery packs ..... 32
3.2 Parameter Determination of Battery Pack ..... 33

3.2.1 Power Design ..... 33
3.2.2 Battery pack frame design ..... 39
3.3 Battery submodule design and fabrication ..... 41
3.3.1 Battery submodule layout ..... 42
3.3.2 Design of current collectors and conductive copper columns ..... 42
3.3.4 Battery submodule energy density ..... 47
3.3.5 Fabrication of battery submodule ..... 48
Chapter 4 Battery Testing Setup ..... 52
4.1 Test Setup Components ..... 53
4.1.1 Battery Selection ..... 53
4.1.2 LFP Battery Advantages ..... 53
4.1.2 Digatron cell cycler ..... 56
4.1.3 Experimental Chamber ..... 57
4.1.4 Connection Set ..... 58
4.1.5 Rack and Fixture ..... 60
4.1.6 Thermocouples ..... 62
4.1.7 Thermocouple Placement ..... 63
4.2 Test Software ..... 65
4.2.1 Battery Manager Workstation Software ..... 65
4.2.2 Program ..... 66
4.2.3 Temperature Reading ..... 68
Chapter 5 Characterization Tests and Improved Pulse Tests ..... 70

5.1 Level-out Test ..... 71
5.2 SOC-OCV Test ..... 75
5.3 Different C-rates Test ..... 81
5.4 Improved Pulse Test and Parameter Identification ..... 85
Chapter 6 Battery Model and Parameter Identification ..... 91
6.1 Battery management system ..... 91
6.2 Lithium-ion battery studying model ..... 92
6.3 Equivalent Circuit Model for Lithium-ion Batteries ..... 94
6.3.1 Rint Model ..... 94
6.3.2 Thevenin Equivalent Circuit Model ..... 95
6.3.3 General Non-Linear (GNL) Comprehensive Model ..... 96
6.4 Parameter Identification ..... 98
6.4.1 Improved First-Order RC Model ..... 99
6.4.2 Modified Pulse Width and Pulse Numbers ..... 100
6.4.3 Parameter Estimation ..... 102
6.4.4 Initial Values of Model Parameters ..... 103
6.5 The Optimization Process using Genetic Algorithms ..... 105
6.6 Validation using Driving Schedule ..... 107
Chapter 7 Conclusion and Future Work ..... 112
7.1 Conclusion ..... 112
7.2 Future Work ..... 113
References ..... 114

# Chapter 1

# Introduction

## 1.1 Background and Motivation

Currently, the world is faced with environmental pollution and energy shortages with limited availability of oil resources, not easy to extract. Conventional cars are dependent on petroleum fuel, which require oil consumption, and entail intensifying air pollution. In contrast, electric vehicles have the advantages of clean energy and no pollutant emissions [1]. Therefore, various countries attach great importance to the research and development of electric vehicles.

The three main types of electric vehicles, are Hybrid Electric Vehicles (HEV), Battery Electric Vehicles (BEV), and Fuel Cell Electric Vehicles (FCEV). Electric vehicles are driven by electric motors, which have the advantages of low noise, fast acceleration, high energy conversion efficiency, and reduced emissions (when considering well-to-wheel energy supply) compared with traditional vehicles [2]. With the continuous developments in their technology, the use of wind, solar, and nuclear energy sources are becoming more and more mature, and the environmental advantages of electric vehicles will be increasingly significant.

Battery-powered vehicles have been developing rapidly. As a key component and the main source of energy in electric vehicles, batteries and their performance directly determine the performance of vehicles and their utility. Global automotive companies are committed to finding high-efficiency batteries with currently the lithium-ion battery being the preferred choice for electric vehicles. Lithium-ion batteries have comparatively outstanding features such as light weight, high energy density, high power density, low self-discharge rate, and a long life cycle [3]. In order to meet the capability of having a long range, the battery pack needs to have a high capacity with a large number of cells. Therefore, it is particularly important to design a battery pack that is compact, efficient, reliable, and can adapt to different ambient temperatures and working conditions.

To better manage and control batteries, experts and researchers have conducted in-depth studies on their characteristics, and a variety of different lithium-ion battery models have been proposed. The operating characteristics of a lithium-ion battery are affected by many factors such as battery internal resistance, charge and discharge currents, working temperature, the number of charge/discharge cycles, and State of Charge (SOC), all needing to be considered comprehensively. Building a battery model is important for effective battery management, including SOC estimation and State of Health (SOH) estimation [4].

### 1.1.1 Research status of power lithium battery pack structure

Since 1990, when a zero-emission vehicle program was introduced in California, USA, forcing automakers to develop electric vehicles, significant progress has been made in the development of electric vehicles and their energy storage systems. The global demand in electric vehicles is also driving battery technology.

Milestone achievements in electric vehicle commercialization within the last two decades include the development of vehicles such as the Chevrolet Volt and Tesla. The Chevrolet (Volt)

battery pack consists of 4 battery modules connected by a high-voltage wiring harness. It has a T-shaped structure as shown in Figure 1.1, which effectively improves its overall space utilization [5]. Japanese automakers also achieved breakthroughs in the power pack design. The Nissan Leaf battery pack consists of 48 battery modules, each containing 4 single cells. The battery pack uses natural cooling to dissipate heat, and the structure of the Nissan Leaf battery pack is shown in Figure 1.2 [6]. In recent years, Tesla has led the field of electrification. Tesla uses cylindrical cells and also introduced innovative architectures like Cell to Chassis (CTC), which means the electric cell is directly integrated into the whole vehicle chassis, omitting the module and battery pack. The classic Model 3 has 2,976 cylindrical cells in the whole battery pack, with each set of 31 cells forming a battery brick. These 96 battery bricks are further divided into 4 modules, 2 small modules containing 23 battery bricks and 2 big modules containing 25 battery bricks. The Model 3 battery pack structure is shown in Figure 1.3.

Figure 1.1: Structure of Volt battery pack

Figure 1.2: Structure of Leaf battery pack

Figure 1.3: Structure of Tesla Model 3 battery pack

Shashank.A [7] comprehensively expounded the design theory and some patents demonstration of some key points on the robustness of the structural design of the battery pack. US Patent No. 8663824 discloses a design in which the cells are fixed by flange brackets in battery modules, and an air gap is created between the nearby cells to ensure that heat conduction does not occur. Another design proposed in US Patent No. 7507499, there is a small air gap between the areas on both the left and right sides of the battery modules, forming a thermal barrier to prevent the spread of thermal runaway. US Patent No. 8481191 provides a spacer assembly for cylindrical battery cells, each spacer only having 5% height of one battery cell.

### 1.1.2 Research status of SOC Estimation

Lithium-ion battery models are typically categorized as empirical, electrochemical, or equivalent circuit models. The equivalent circuit model has features that include: a simple structure, low computational complexity, and ease of implementation. It is widely used in Battery Management Systems (BMS). Therefore, an equivalent circuit model is a common way to study lithium-ion batteries. To build an equivalent circuit model it is necessary to determine the model parameters which represent the internal characteristics of the battery and reflect the battery state.

SOC estimation is an important function of electric vehicle battery management systems. Researchers have done considerable research to improve the accuracy of EV battery SOC

estimation. The widely used methods are coulomb counting, the open circuit voltage, the internal resistance, neural network, and using the Kalman filter [8]. This research discusses the definition of battery SOC; introduces the principles and advantages/disadvantages of various SOC estimation methods; analyzes the influence of factors on battery SOC; and focuses on building an equivalent circuit model to estimate SOC. Figure 1.4 is the general diagram of model-based SOC estimation methods [8].

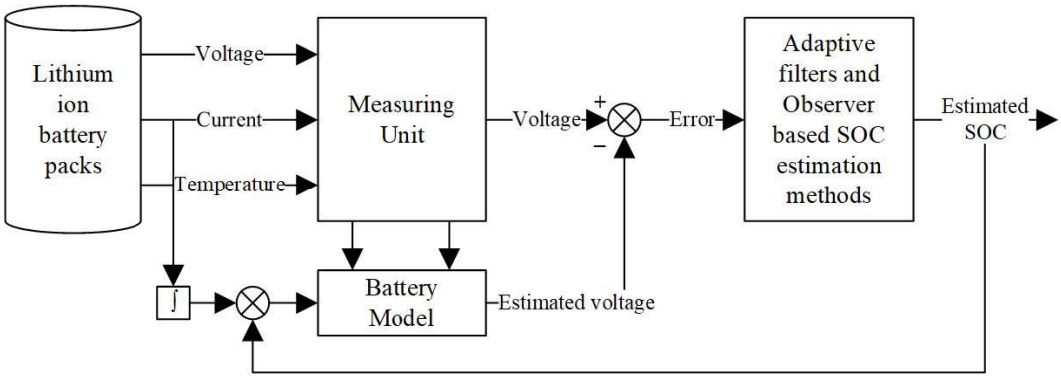


Figure 1.4: General diagram of model-based SOC estimation methods

## 1.2 Objectives and Contributions

The objective of this research is to design new battery packs for their implementation in a 2013 Ford Focus. The intention is to:

- Improve the electric vehicle driving range to 400 km with one charge.
- Use multiple modules with different types of battery cells and chemistries.
- Simplify the battery pack structure using passive air cooling.
- Minimize the weight of battery packs.
- Control the operating temperature of battery packs.

One type of cell considered was a high energy-density prismatic cell with a large capacity of 280 Ah. As part of this research, the prismatic cell was characterized, modeled, and validated by simulation. The contributions from this research include conducting a comprehensive characterization test on the 280 Ah battery cell to study its performance under different working conditions, establishing an equivalent circuit model using Matlab and Simulink to estimate the State of Charge, and validating the feasibility of the battery model by testing using drive cycles.

## 1.3 Thesis Organization

This thesis is organized as follows:

**Chapter 1** outlines the context as well as the main objectives and contributions of the research.

**Chapter 2** provides a literature review on energy storage systems in electric vehicles and on characterization of lithium-ion batteries.

**Chapter 3** presents a battery module design. An architectural comparison is made with existing battery pack design strategies to show the benefits of the new design that minimize the pack weight, volume and cost. The possible advantages of a battery pack with multiple different types of cells is also examined.

**Chapter 4** describes the experimental set up used for battery characterization. The testing equipment and procedures are described.

**Chapter 5** provides an overview of the characterization tests. In this chapter, Level-out test, State of Charge (SOC) test and the Pause Charge test are described and performed on a 280Ah LFP battery cell

**Chapter 6** outlines an equivalent circuit model with optimized parameters using Genetic Algorithms. A coulomb counting method combined with an equivalent circuit model was chosen

to model one high-capacity prismatic cell. The performance and the accuracy of the model was examined using a real driving schedule test.

**Chapter 7** provides the concluding remarks, as well as recommendations and improvements for future work.

# Chapter 2

# Lithium-ion Battery Cell

The battery cell is the smallest unit of the energy storage system in an electric vehicle. It mainly consists of four key components: cathode, anode, electrolyte, separator and terminals [9]. The battery is classified according to its shape and chemistry. The characteristics of the battery pack have a large influence on the overall performance of the electric vehicle. A battery module consists of multiple battery cells connected together in series and/or in parallel, housed in a mechanical enclosure. The compact arrangement or stacking of the battery cells inside a module is an important consideration for integration of the pack. , Also required are the battery management system, the thermal management system, and sensors.

## 2.1 Classification of Lithium-ion Battery Cells

A high-voltage battery pack as the power source of electric vehicles has been regarded as a key enabling technology, but is also a bottleneck limiting the development of electric vehicles. At

present, Lithium Nickel Manganese Cobalt Oxide (NMC) batteries are more commonly used in North America [10].

### 2.1.1 Classification by Chemistry Factor

Early in the 1990s, Nickel-Metal Hydride batteries (NiMH) began to dominate the EV sector with their use in the Toyota Prius. The NiMH battery has a moderate energy density (70–100 Wh/kg), which is better than Nickel–Cadmium batteries (NiCd). However, the voltage of NiMH battery is only 1.2 V which is 1/3 of a lithium-ion battery, so in the case of a certain required voltage, its associated battery pack volume is comparatively much larger than a lithium-ion battery pack, which is the main disadvantage of NiMH batteries [11].

In the early stages of development of new energy vehicles, lithium iron phosphate (LFP) batteries were commonly used. Using $LiFePO_4$ as the cathode material provides a long service life of more than 2,000 cycles. The LFP batteries also showed thermal stability. Furthermore, the LFP battery cell chemistry does not contain cobalt and other precious elements, and its raw materials of phosphorus and iron are readily available, making it relatively cheap compared to other lithium-ion batteries. With the rapid development of new energy vehicles, the technical requirements for their battery also has become increasingly higher. Given the latest developments, the energy density of a single LFP battery is relatively lower compared to the latest lithium ion batteries causing vehicle weight with LFP batteries to be higher, which is obviously unfavorable. In the past two years some car companies have abandoned the use of LFP batteries and switched to other lithium-ion battery chemistries for better energy density. However, LFP batteries have a lower cost while offering a moderate operating voltage (3.2 V), acceptable energy density (170 Wh/kg), and high discharge power, fast charging performance, long cycle life, and high stability in high temperature environments [12]. The spider chart in Figure 2.1 summarizes the overall performance of an LFP battery.

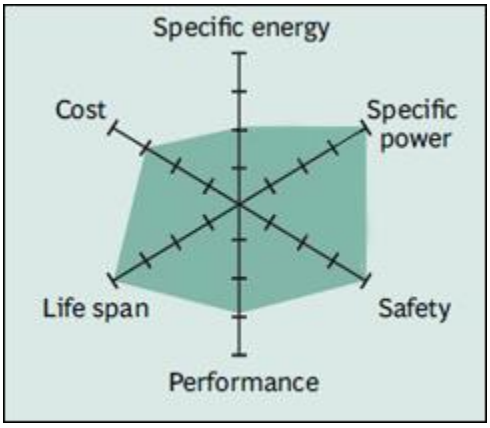


Figure 2.1: Hexagonal spider graphic of a typical Li-phosphate battery [10].

Compared with LiFePO4 and NiMH batteries, the most dominant battery chemistries in the EV industry are currently the Lithium Nickel Manganese Cobalt Oxide (NMC) and Lithium Nickel Cobalt Aluminum Oxide (NCA). In Figure 2.2, these batteries have a more balanced performance, higher energy densities, and higher volumetric specific energies compared to LFP batteries. These batteries are being mass produced, making them cost competitive in recent years. In addition, these battery chemistries lead to the overall energy storage density for the battery pack to reach above 200 Wh/kg that is more suitable for long range travel [13]. Beside better overall performance, batteries with Nickel and Cobalt can also be mixed with Manganese or Aluminum to adapt to the wide range of applications in energy storage systems that require reliable cycles. NMC/NCA batteries are becoming the main choice for new energy vehicles.

However, NMC/NCA batteries have high demands on the battery management system as well as the mechanical design of the pack, requiring good over-charge/over-discharge protection and over-temperature protection in both the design and production process.

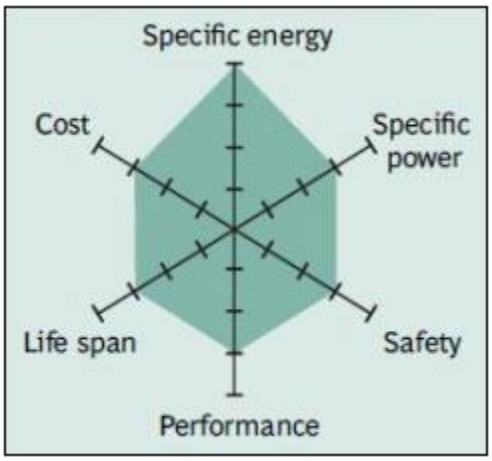


Figure 2.2: Hexagonal spider graphic of a NMC/NCA battery [10].

With the development of energy storage technology, a variety of different battery chemistries are constantly emerging to improve the EV performance.

### 2.1.2 Classification by Form Factor

The cells are categorized according to their form factor as follows.

a) **Cylindrical Cell**- A battery with a cylindrical casing and connecting elements.

Lithium-ion cylindrical cells have a long history dating back to the 18650 cylindrical cell invented by SONY in 1992 [14]. The performance consistency of cylindrical cells stays high, which makes battery packs with cylindrical cells provide better thermal performance. Lower cost and better heat dissipation are the main reasons why cylindrical cells have become the dominant power battery today. However, due to their low energy density, thousands of 18650 cells have to be connected in parallel and series to reach common energy and power targets. This increases the complexity of the internal battery pack structure, as well as the battery management system. Therefore, 21700 cylindrical cells of higher energy density emerged to meet market requirements, increasing the

energy density by 30%. The resulting energy density of automotive battery pack were increased (typically from about 250 Wh/kg up to 300 Wh/kg or nearly by 20% overall) [7].

The introduction of the 21700 cylindrical cell illustrates a trend of increasing the volume of the cylinder in order to obtain a larger battery pack capacity. The new 46800 cylindrical cell by Tesla will increase the cell's capacity 5 times compared to 18650 cells and the power by 6 times.

b) **Pouch cell -** A battery with a flexible composite film shell and connecting elements.

Pouch cells use an aluminum plastic film as the outer shell and have a laminated structure inside that can be customized into any size and shape according to customer requirements [15]. The weight of a pouch cell is on average nearly 20% lower compared to prismatic cells with the same capacity, while the capacity is nearly 50% higher compared to prismatic cells with the same volume. At the same time, the aluminum plastic film will only expand or rupture when a safety hazard happens, which means that it is less likely to explode, thus enhancing the safety of a battery pack. However, the application of aluminum plastic film also results in a lower mechanical strength. This makes the production process more complicated compared to cylindrical and prismatic cells. Furthermore, the encapsulation requirements are higher, and the problem of liquid leakage is more likely to arise, subsequently requiring a better battery management system.

c) **Prismatic Cell -** A battery with a rectangular casing and connecting elements.

Prismatic battery cells usually have an aluminum alloy shell and use square winding or a stacked sheet inside. Due to the higher hardness of the shell, the cell is better protected than that of pouch cells using aluminum-plastic film. Prismatic cells do not have a unified standard, and can be customized to different sizes and larger capacities according to customers' needs, thus reducing the complexity of the battery pack's structure and the overall volume. However, because there is no unified standard, there are thousands of different battery sizes in the market, and the production process for each size is different. Therefore, the characterization consistency of prismatic cells is quite poor, and the degree of production automation is relatively low.

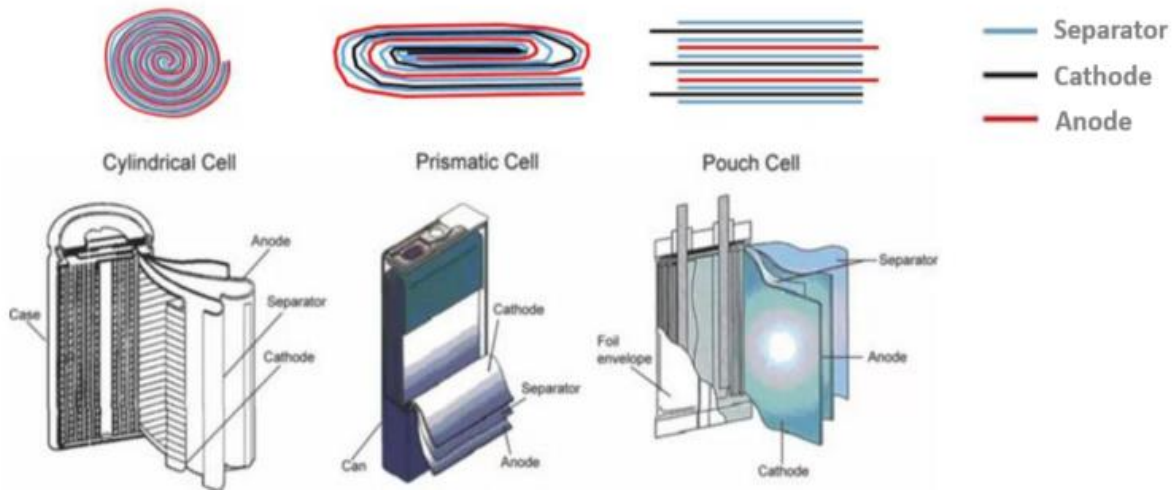


Figure 2.3: Schematic of cylindrical-type, prismatic-type, and pouch-type battery cells [16].

The three forms of lithium cells are not only different in appearance but also in their internal winding, which results in different working performance levels, as shown in Figure 2.3. In this thesis 3.5 Ah 18650 cylindrical cells and 280 Ah prismatic cells are used for testing and characterization.

## 2.2 Terminology and Definitions of Lithium-ion Batteries

The research on lithium-ion batteries mainly focuses on their technical indicators to describe the "pros and cons" of the performance.

### 2.2.1 State of Charge (SOC)

The State of Charge (SOC) is defined as the state of available electrical energy in a battery, usually expressed as a percentage as shown in Figure 2.4. It represents the ratio of the remaining capacity of a battery after discharging to its fully charged capacity.

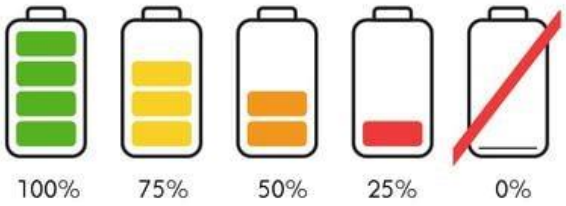


Figure 2.4: Battery state of Charge in a percentage reading.

Its value range is 0~100%. When SOC = 0%, it means the battery is completely discharged, and when SOC = 100%, it means the battery is fully charged. The Battery Management System (BMS) controls the battery, mainly monitoring SOC and making estimates to ensure efficient battery operation. Because the available electrical energy varies with the charging/discharging current, temperature, and aging, the definition of charge state is also categorized into two kinds: absolute charge state and relative charge state. The absolute State of Charge is a reference value calculated according to the designed fixed capacity value when the battery is manufactured. The absolute State of Charge of a new fully charged battery is 100%. Even if an aged battery is fully charged, it will not reach 100% under different charge and discharge conditions.

Figures 2.5 and 2.6 show the relationship between the measured voltage and capacity of a battery under different discharging rates and temperatures. When the discharging rates are high, the battery capacity decreases. When the temperature decreases, the battery capacity also decreases accordingly.

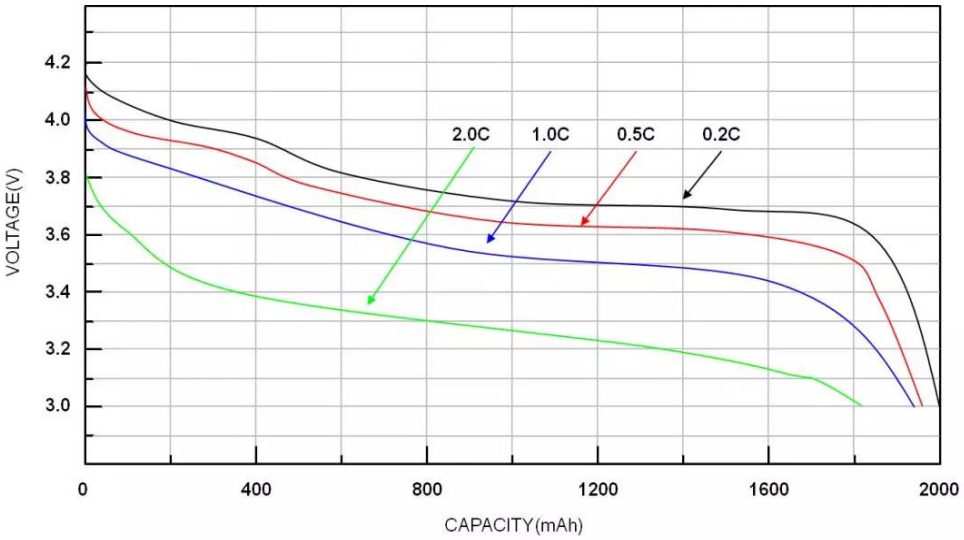


Figure 2.5: Curves of measured voltage and capacity under different discharging rates. [17]

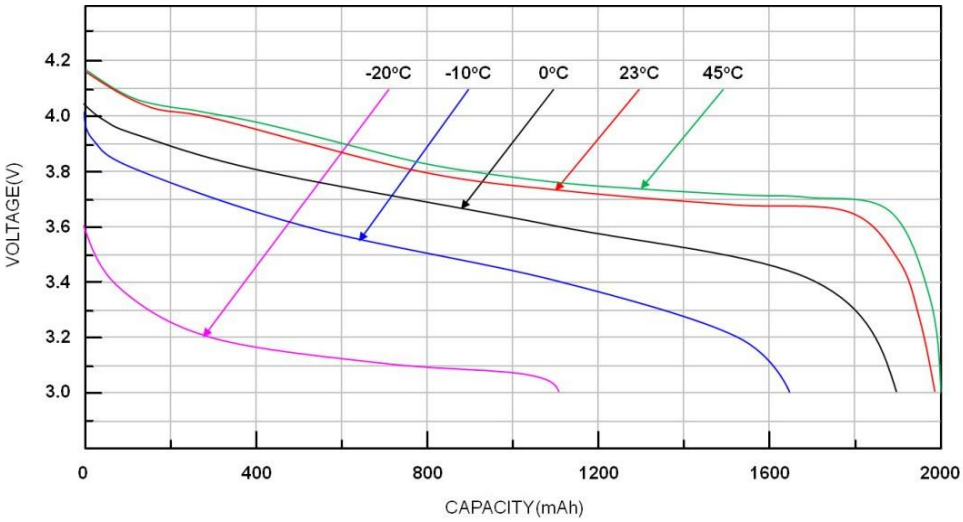


Figure 2.6: Curves of measured voltage and capacity under different temperatures. [17]

### 2.2.2 State of Health (SOH)

The State of Health (SOH) characterizes the battery's ability to store electrical energy relative to a new battery. It represents the state of a battery from the beginning to the end of its life as a percentage and is used to quantify the battery's performance state. There are many performance

indicators of batteries. SOH has many definitions referring to the battery's capacity, discharge rate, internal resistance, cycle times, and peak power.

**Capacity defines SOH**

The most common definition for SOH uses the decay of battery capacity for defining the SOH, as follows:

$$SOH = \frac{Capacity_{aged}}{Capacity_{rated}} \times 100\% \qquad (2.1)$$

Where $\mathrm{Capacity}_{\mathrm{aged}}$ is the current capacity of the battery and $\mathrm{Capacity}_{\mathrm{rated}}$is the rated capacity of the battery.

**Charge quantity defines SOH**

The maximum discharge rate has also been used to quantify SOH, as follows:

$$SOH = \frac{Q_{aged\_\max}}{Q_{new\_\max}} \times 100\% \qquad (2.2)$$

Where: $\mathrm{Q}_{\mathrm{aged\_max}}$ is the maximum discharge quantity of the current battery and $\mathrm{Q}_{\mathrm{new\_max}}$ is the maximum discharge quantity of a new battery.

**Internal resistance defines SOH**

The increase in the internal resistance of a battery is an important indicator of battery aging. Many users use the internal resistance to define SOH.

$$SOH = \frac{R_{EOL} - R_C}{R_{EOL} - R_{new}} \times 100\% \qquad (2.3)$$

Where: $\mathrm{R}_{EOL}$ is the internal resistance at the end of the battery life, $\mathrm{R}_C$ is the internal resistance of the current battery, and $\mathrm{R}_{new}$ is the internal resistance of a new battery.

**Remaining cycles defines SOH**

Cycle life has also been used for defining the SOH as follows:

$$SOH = \frac{Cnt_{ramain}}{Cnt_{total}} \times 100\% \qquad (2.4)$$

Where: $Cnt_{remain}$is the number of remaining is cycles and $Cnt_{total}$is the total number of cycles.

The above mentioned definitions of SOH are all very common. The most common is the SOH definition based on capacity. The internal resistance is related to SOC and temperature, and it is not easy to measure. The remaining cycles and total cycles are also difficult to measure and predict accurately. In addition, the battery's operating temperature, charge-discharge rate, depth of discharge, cycle interval, and charge-discharge cut-off voltage will also affect the health and life of the battery.

### 2.2.3 Charge/ Discharge Rate (C-rate)

The charge/discharge rate refers to the current value required to charge/discharge the battery with respect to its rated capacity. For example, one C-rate is the current that would fully charge or discharge the battery within one hour, and is numerically equal to the battery's rated capacity.

For example, for a battery cell with a capacity of 24 Ah: with 48 A discharge, the discharge rate is 2C, and the discharge is completed in 0.5 hours; and, when charging occurs at 12 A, the charge rate is 0.5C, and the charging is completed in 2 hours.

### 2.2.4 Fully Charged/ Discharged

When the difference between the output voltage and the maximum voltage of the battery terminal is less than 100 mV, and the charging current drops to a certain value, the battery can be regarded

as fully charged. When the battery voltage is less than or equal to the minimum discharge voltage it can be called a complete discharge. The battery characteristics are different and the fully charged/discharged conditions are also different. Figure 2.7 shows a typical lithium-ion battery charging characteristic curve [17].

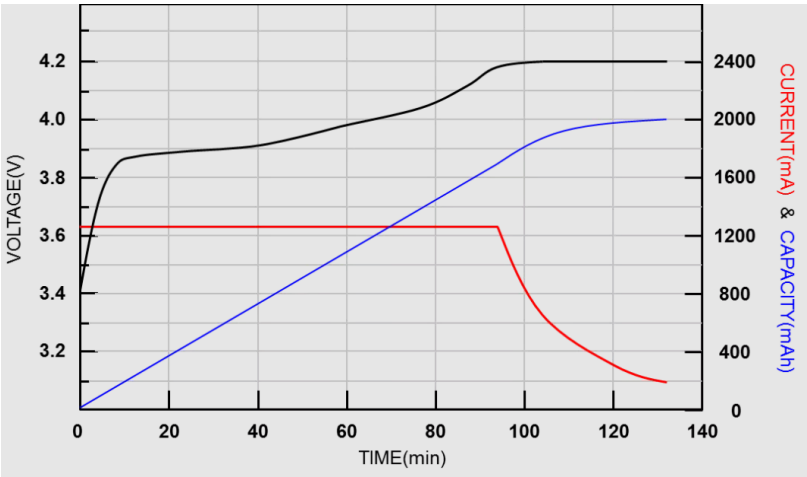


Figure 2.7: A typical lithium-ion battery charging characteristic curve [17].

## 2.2.5 Energy Density

Energy density refers to the energy released per unit volume or per unit mass, expressed as volume energy density (Wh/L) or mass energy density (Wh/kg), which is a key factor affecting the range of electric vehicles.

Energy density is mainly divided into unit energy density and system energy density. The energy density of a single cell is the minimum unit energy density. For example, if a battery weighs 325 g with a rated voltage of 3.7 V, and a capacity of 10 Ah, its energy density is 113 Wh/kg. The system energy density refers to the energy density of the battery pack or of the entire vehicle.

The battery pack consists of a number of single-cell batteries, the battery pack frame, protective plates, sensors, and electronic components for battery management. Therefore, the system energy

density is affected by the unit energy density and the weight of the packaging components, making it less than a single cell energy density. According to the "Energy-saving and New Energy Vehicle Technology Roadmap", a rough idea of the development trend of power batteries can be predicted. As shown in Figure 2.8, by 2030 the specific energy density of pure electric vehicle battery cells will reach 500 Wh/kg [18].

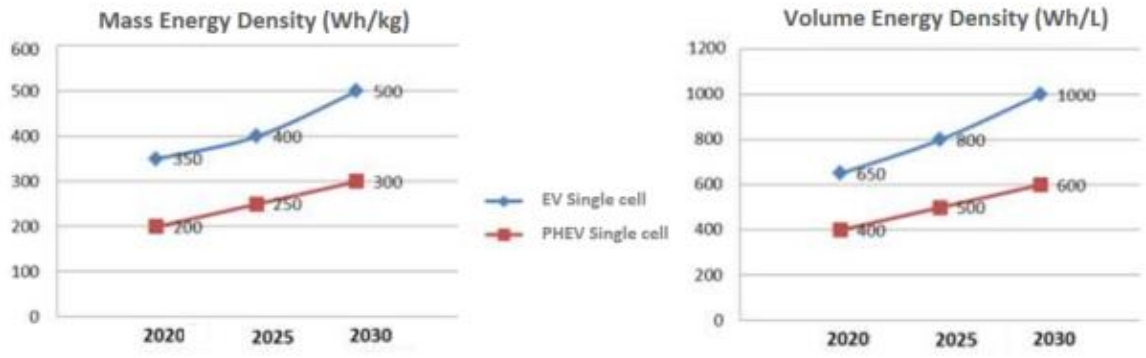


Figure 2.8: Energy-saving and New Energy Vehicle Technology Roadmap [18].

## 2.2.6 Life Cycle

The life cycle is the number of times a battery has undergone complete charging and discharging until it reaches its end of life. The battery life is defined by two parameters: cycle life and calendar life. Cycle life refers to the number of times the battery can be charged and discharged in cycles before it reaches end of life defined as the time when the battery capacity decays to 80%.

The calendar life refers to the time span for the battery to reach the end of life condition (capacity decays to 80%) under specific operating conditions or the environmental conditions of use. The calendar life usually depends on working conditions and storage environmental conditions.

Cycle life is a theoretical parameter and calendar life is more practical. However, the calculation of calendar life is complicated and takes a long time, so generally battery manufacturers only provide data on cycle life. Usually after 500 charge and discharge cycles the capacity of a fully charged battery drops by 10% to 20%, as shown in Figure 2.9. [19]

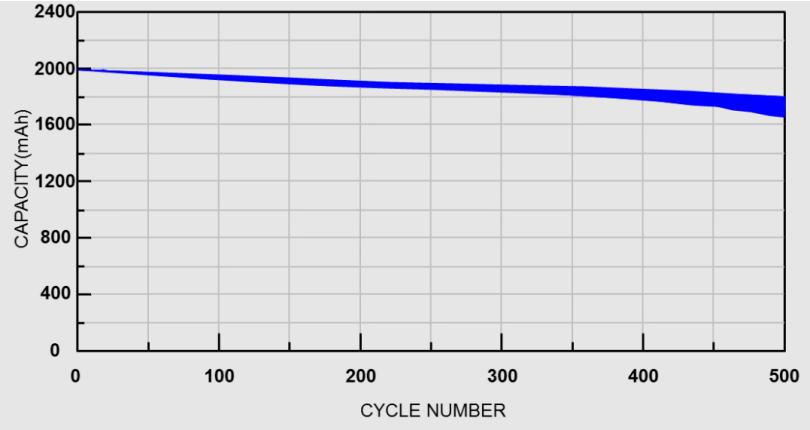


Figure 2.9: Capacity changing curve of a lithium-ion battery over cycles. [19]

## 2.2.7 Self-Discharge

The self-discharge of all batteries will increase as the temperature rises. Self-discharge is basically not a manufacturing defect, but a characteristic of the battery itself. Generally the self-discharge of the battery is mainly affected by the manufacturing process, materials, and storage conditions. Figure 2.10 indicates typical self discharge rates of a lithium-ion battery under different temperatures. Generally, the self-discharge rate doubles for every 10°C increase in battery temperature. The monthly self-discharge of lithium-ion batteries is about 1% to 2%, while the monthly self-discharge of various nickel-based batteries is 10% to 15%.

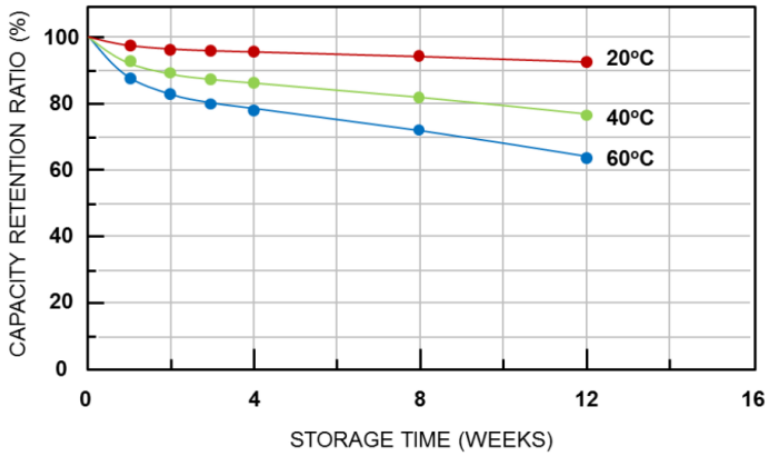


Figure 2.10: Typical self discharge rates of a lithium-ion battery under different temperatures. [20]

## 2.2.8 Nominal Capacity and Useable Capacity

The battery capacity $Q_{max}$ refers to the amount of Charge quantity that can be released from a fully charged battery before the battery reaches the End-of-Discharge Voltage (EDV). In practice, a current of 0.1C or less is used to measure the battery capacity.

In the actual use of a battery its capacity cannot be fully released because there must be a certain discharge current and the battery itself has internal resistance. Therefore, the actual usable capacity $Q_{use}$ must be less than $Q_{max}$ as shown in Figure 2.11.

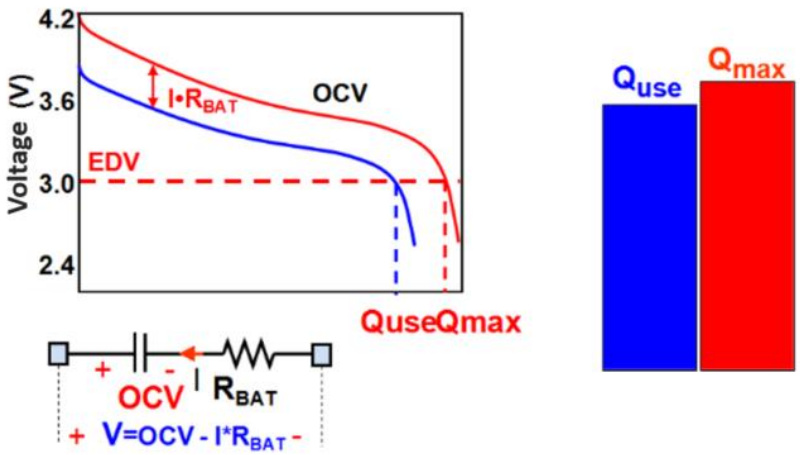


Figure 2.11: Discharge curve of a lithium-ion battery under different load conditions. [20]

### 2.2.9 Battery Voltage

According to Figure 2.11, the battery terminal voltage (V) is equal to the Open Circuit Voltage (OCV) minus the voltage drop across the internal resistance inside a battery. The actual use curve is lower than the open circuit curve of the battery, and also a smaller capacity can be released. It is also easy to note that the larger the current and the larger the load, the smaller the available capacity. Therefore, the available battery capacity will change as the load changes. In reality, it can sometimes be seen that the battery capacity is increasing because of the load current decreasing.

The voltage measures of interest in batteries include the terminal voltage, nominal voltage, open circuit voltage, operating voltage, end of charge voltage, and end of discharge voltage as follows:

**Terminal voltage:** the potential difference between the terminals.

**Nominal voltage**: the voltage that a battery can reach when working under standard and specific conditions. The nominal voltage is determined by the electrode material and the internal electrolyte

concentration. The lithium iron phosphate battery is 3.2 V while a NMC/NCA material battery is 3.6 V.

**Open circuit voltage:** the terminal voltage of the battery when there is no load.

**Working voltage:** also called load voltage, which refers to the terminal voltage of the battery after a load is connected to a battery.

**End of charge voltage:** when the battery is fully charged, the active material on the electrode plate has reached a saturated state, and if you continue to charge, the battery voltage will not rise anymore. The voltage at this time is called end of charge voltage. The end of charge voltage of a lead-acid battery is about 2.7 V, the metal hydride nickel battery is 1.5 V, and the lithium ion battery is 4.25 V.

**End-of-Discharge Voltage (EDV):** when the battery is discharged under certain conditions the battery voltage gradually drops. When the battery is no longer suitable for discharging, the lowest working voltage at this time becomes end of discharge voltage. The EDV is related to the discharge rate and is directly affected by the discharge current.

If the battery continues to discharge after being lower than the EDV, the voltage at both terminals of the battery will drop rapidly, forming a deep discharge, so that the products formed on the electrode plate will not be easily restored during further normal charging, which will affect the life of the battery.

### 2.2.10 Depth of Discharge

Depth of Discharge (DOD) is the fraction or percentage of the capacity which has been removed from the fully charged battery. It is an alternative method to indicate a battery's State of Charge (SOC).

All battery manufacturers recommend keeping the DOD below the maximum limit of 100%. Ideally 80% DOD or less is recommended. The rule is that the smaller the DOD the larger the number of cycles. With 50% DOD the LiFePO4 cells may have well above 5,000 cycles. However it is important to keep the DOD at the central part of the capacity range. If the DOD is not in the center of the capacity range, the cell performance may degrade faster. Figure 2.12 illustrates the depth of discharge of a battery.

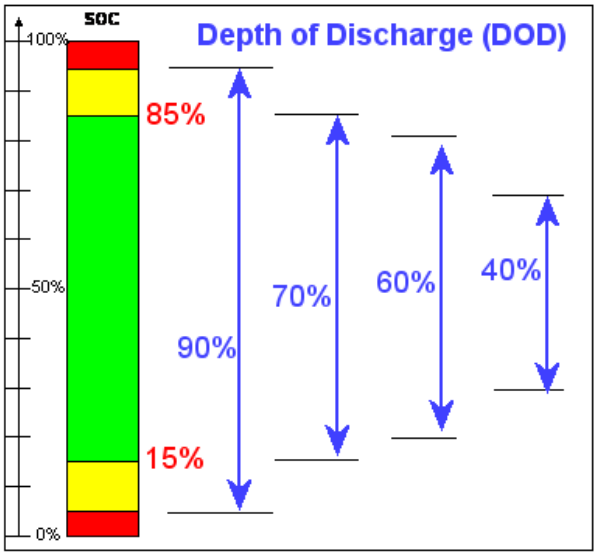


Figure 2.12: Diagram of Depth of Discharge (DOD) of a battery. [23].

## 2.2.11 Internal Resistance

Internal resistance refers to the resistance experienced by the current flowing through the battery including ohmic internal resistance and polarization internal resistance. Ohmic internal resistance relates to resistances in the electrode material, electrolyte, separator resistance, and various parts in between terminals; polarization internal resistance includes electrochemical polarization resistance and concentration polarization resistance.

Figure 2.11 shows a battery discharge curve. The horizontal axis represents the discharge capacity and the vertical axis represents the battery open circuit voltage. The ideal battery

discharge state is a red curve, and the blue curve is the true state when the internal resistance of the battery is taken into account.

It can be seen from the figure that the actual battery capacity $Q_{use}$ is less than the theoretical maximum capacity $Q_{max}$. Due to the existence of resistance, the actual capacity of the battery will be reduced. It can also be learned that the actual battery capacity $Q_{use}$ depends on two factors: the product of the discharge current I and the internal resistance of the battery $R_{BAT}$, and the end-of-discharge voltage (EDV). It should be pointed out that the internal resistance of the battery is mainly affected by the ambient temperature (T), State of Charge (SOC), and battery aging (Aging). The internal resistance of the battery generally increases with the temperature decreasing and SOC decreasing. As shown in Figure 2.6, the lower the temperature is, the larger the internal resistance, causing a lower available capacity.

The unit of internal resistance is generally milliohms (mΩ). A battery with a large internal resistance will cause high internal energy consumption and serious heat generation during charging and discharging, which will cause accelerated aging and life decay to a battery, and will also limit the discharging process at a large rate. Thus the smaller the internal resistance is, the better the battery life and rate performance will be gained. Generally there are AC and DC test methods for measuring the internal resistance of the battery.

## 2.3 Characteristics of Lithium-ion Battery

### 2.3.1 Battery open-circuit voltage (OCV)

The open circuit voltage of the battery refers to the potential difference between the positive and negative terminals when the battery is in a static state. Shown in the Figure 2.13 below are the OCV-SOC curves of two types of lithium-ion batteries. The NMC/NCA battery is strictly monotonous, due to the good correspondence between SOC and OCV, and the difference in OCV

is clearly depending on SOC changes. However, in the case of $LiFePO_4$ battery, the middle section is flat, the difference in OCV is small, and it is not strictly monotonous, and so some OCV values corresponds to several SOC points. There are difficulties such as lack of maintenance time and lack of accuracy. Therefore, the open circuit voltage is often combined with other methods to use.

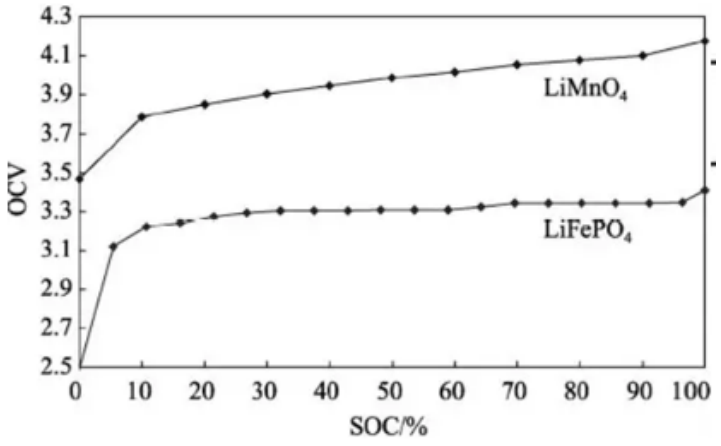


Figure 2.13: OCV-SOC curves of two types of lithium batteries [24]

## 2.3.2 Correspondence characteristics of Charge-discharge rate and terminal voltage

The battery voltage measured in a dynamic operating mode is actually the terminal voltage of the battery rather than OCV. Therefore, when the battery is charging or discharging, the terminal voltage is significantly different from the OCV.

When a constant current goes through a battery a correspondence between a set of voltages and SOC can be easily obtained. Figure 2.14 shows the voltage curves at different C-rates of a $LiFePO_4$ battery at a certain temperature. In fact, except for the constant current charging phase of the battery, the actual working current of the battery rarely has a long time constant current phase. Different current switches will cause the predicted voltage deviating from the actual terminal voltage curve, this phenomenon is called polarization.

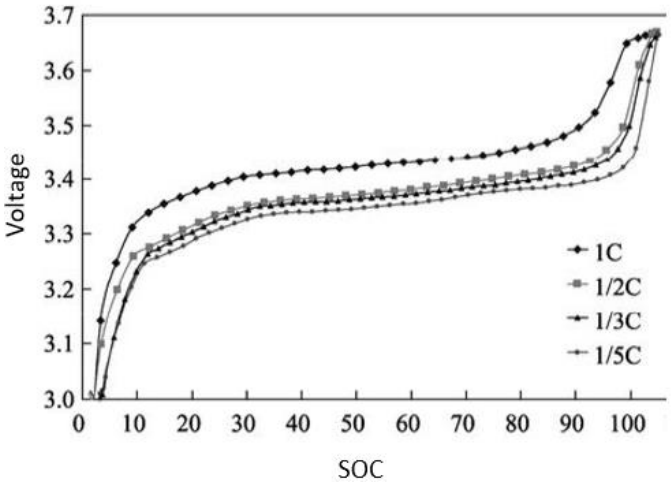


Figure 2.14: Voltage curves of a $LiFePO_4$ battery under different C-rates [24]

### 2.3.3 Temperature characteristics

It is known that batteries of different materials exhibit different temperature characteristics. Taking a $LiFePO_4$ battery as an example, Figure 2.15 shows the relationship between SOC and internal resistance at different temperatures. In general, the internal resistance of the battery changes with temperature and SOC, and is very sensitive to low temperatures. In the same way OCV, polarization, and other parameters will also change with temperature, undoubtedly making predictions more difficult.

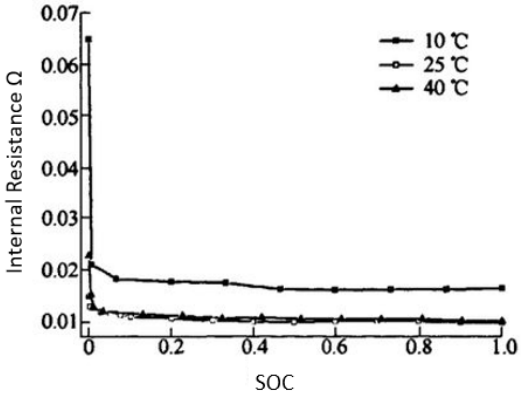


Figure 2.15: Curves of SOC and internal resistance under different temperatures. [24]

### 2.3.4 Group efficiency of batteries

The above-mentioned characteristics are the characteristics of a single cell. In the actual pack, the considerations become more complex due to the series-parallel connections of the cells. It is inevitable that there are differences in internal resistance, polarization resistance, self-discharge rate, and initial capacity amongst different batteries. The different performances during battery charging and discharging make it more difficult to estimate the SOC for the pack.

## 2.4 Common Methods of SOC estimation

State of Charge (SOC) represents the amount of energy stored in a battery. The SOC can be estimated using various methods as follows.

### 2.4.1 Coulomb Counting method

Coulomb Counting is current integration method used to estimate the SOC of the battery when the initial $SOC_0$ is known. By evaluating the integral of the charging/discharging current within the corresponding time and given the initial $SOC_0$, the SOC is calculated in time as:

$$SOC(t) = SOC_0 + \frac{\eta}{C}\int_0^t I(t)\mathrm{d}t \qquad (2.5)$$

Where SOC (t) is the SOC value of the battery at time-t; **η** is the Coulomb efficiency; C is the battery capacity; I (t) is the current flowing in the battery at time-t. For lithium-ion batteries **η**≈1.

It should be noted that the initial $SOC_0$ is not easy to determine and there is a certain error in the accuracy, and the error will increase cumulatively with time. It is therefore important to have a very high level of accuracy in current measurement. In addition, the error will increase under

severe current fluctuations. In practical applications, the ampere-hour integration method is usually used in combination with other methods to improve the prediction accuracy.

### 2.4.2 Open circuit voltage (OCV) method

Through the OCV characteristics, the steady state voltage is used as the basis for SOC estimation. The open circuit voltage method is simple and easy to implement. The accuracy is high when the battery has been in a steady state mode for a long time, but it is not applicable under actual working conditions. Therefore, the open circuit voltage method is generally combined with other methods to jointly predict the SOC. The most widely used method in industry is the open circuit voltage (OCV) combined with the ampere-hour integration method.

### 2.4.3 Fuzzy reasoning and neural network method

The battery has a highly non-linear characteristic. Fuzzy reasoning and neural networks can be used to model the battery's performance as they can capture nonlinear dynamics as it relates to SOC estimation. A three-layer neural network model is often used to estimate SOC, where the number of neurons in the input and output layers is determined by the needs of the actual problem. The terminal voltage and temperature are measured and used as input variables.

### 2.4.4 The equivalent circuit model method

The equivalent circuit model has a good applicability to various working states of the power battery, and it is easy to derive. Figure 2.16 shows a simple 1$^{st}$ order equivalent circuit model of the battery. The voltage source on the left represents OCV, R represents internal resistance, $R_1$ represents the polarization resistance, $C_1$ represents the polarization capacitance, and the right output represents terminal voltage which can be measured.

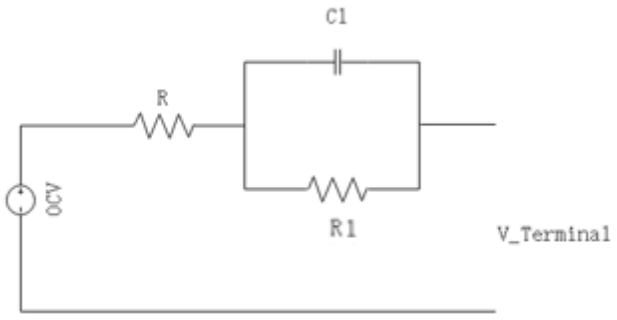


Figure 2.16: The 1st order equivalent circuit model of a lithium battery.

### 2.4.5 Kalman filtering method

The core of the Kalman Filtering (KF) algorithm is to make the best estimate of the state of the dynamic system. When applied to batteries, the state and observation equations must first be established. The KF algorithm can be used to estimate SOC with relatively high accuracy [21]. The dynamic estimation of the system can be realized theoretically by using this method. However, the premise is that the established state and observation equations must be accurate.

### 2.4.6 Summary

Comparing the above methods, the current flow will change greatly during the operation of electric vehicles, and the open circuit voltage method for estimating SOC requires a stable voltage environment, which is only suitable for the estimation of the initial state. Although the neural network algorithm has high accuracy, it must have huge experimental data ahead of time to train the network which is time-consuming and complex. Therefore, combining the above advantages and disadvantages, the Coulomb Counting method combined with the 1st order equivalent circuit model is chosen to estimate SOC in this thesis.

# Chapter 3

# Design of a Power Battery Pack

The battery pack involves mechanical and electrical integration of battery cells for creating the energy storage system for electric vehicles. This chapter analyzes and studies the design of a battery pack further to the requirements pertaining to its capacity, layout, configuration and mechanical components. The performance indicators of the electric vehicle such as the maximum speed, acceleration, climbing ability and driving range need to be considered and met, as well as the battery specific requirements pertaining to the voltage, the current, and the temperature.

The energy density of a lithium-ion battery module can reach 150-200Wh/kg, which is higher compared to the batteries of other chemistries. Therefore, the lithium-ion battery has become the mainstream in the field of electric vehicles. The objective in this research is to develop a 48 V battery pack with a high energy density using passive air-cooling techniques to both extend the range and minimize the curb weight of a selected electric vehicle model. The target energy density aims to reach 200Wh/kg on the level of battery submodule.

## 3.1 Mechanical structural requirements of designing battery packs

The mechanical structure of a battery pack for electric vehicles should have [25]:

(1) Good electrical insulation: the output voltage of the battery pack in electric vehicles is much higher than the safety voltage of the human body, so in the design process the insulation between the battery modules and the battery enclosure, as well as between the enclosure and the car, should be fully considered.

(2) Shock absorption and anti-collision ability: the car is running on the open road, and so the battery module should be firmly fixed in the car to meet the basic requirements pertaining to the car's vibration, rollover, and potential for collision.

(3) Good heat dissipation: the battery will generate a lot of heat during its operation. The design of the battery pack needs to not only meet the requirements of suppressing the temperature rise inside the enclosure, but also to make sure the temperature difference inside the battery pack is well controlled.

(4) Good waterproofing and dustproofing: the battery enclosure needs waterproofing and anti-settling ability for dust.

(5) Meet the installation conditions of the vehicle: the maximum dimensions of the battery pack should meet the requirements of the vehicle installation space.

The energy density of commercial battery cells can be as high 200Wh/kg, but the energy density of the battery pack composed of cells in series and parallel will be reduced due to other components and subsystems., Therefore in the design process, the desired energy density should be taken as a target for optimizing the parameters of the battery pack. Referring to the Tesla Model-S, the weight of the whole battery system is 450 kg, and the energy density is up to 120Wh/kg on a pack level. In summary, the energy density target of the pack is set to be 150Wh/kg.

In this research, the Samsung's INR18650-35E lithium-ion battery cell were selected for designing and fabricating a 48V battery pack.

## 3.2 Parameter Determination of Battery Pack

Upon meeting the power requirements of a power battery pack, appropriately selecting the battery capacity and quantity and rationally distributing the battery layout can improve the dynamic and thermal performance, possibly reducing the cost to a large extent. At the same time, a reasonable and efficient battery management system is also of vital importance for accurately monitoring the battery working state, so as to maximize the performance of its power output and prolong its cycle life.

### 3.2.1 Power Design

This thesis consider the design of a modular battery pack for the 2013 Ford Focus Electric vehicle, to extend its range to 400km. According to this desired driving range while considering curb weight, air damping coefficient, maximum speed, average driving speed, and wheel parameters, the maximum power required by the motor of the whole vehicle is calculated. The power requirements enable sizing of the battery pack, its capacity, number and configuration of the cells.

#### 3.2.1.1 Basic parameters of 2013 Ford Focus EV

It is assumed that a driver with a maximum weight of 100kg will drive for 400km at one charge under the average speed of 80km/h during the entire trip and the maximum speed of up to 120km/h. Designated technical parameters of 2013 Ford Focus Electric Vehicle are listed in Table 3.1.

Table 3.1: The parameters of the 2013 Ford Focus EV [26]

| Parameter | Value | Parameter | Value |
|---|---|---|---|
| Curb Weight /kg | 1900 | Coefficient of air damping $(N \cdot S^2 / m^4)$ | 0.3 |
| Curb weight with Full Load /kg | 2000 | Coefficient of rolling damping $(N \cdot S^2 / m^4)$ | 0.0076+ 0.000056Vu |
| Windward area/$m^2$ | 1.7 | Maximum speed km/h | 120 |
| Range /km | 400 | Average speed km/h | 80 |

### 3.2.1.2 Motor Parameter confirmation

According to the technical parameters of the vehicle speed, curb weight, air damping coefficient, rolling damping coefficient and windward area, the power demand of the motor can be calculated to satisfy the two conditions of the maximum vehicle speed and the maximum climbing degree, taking the greater value as the maximum power. The power demand follows the relationship [27]:

$$P_V = \frac{1}{\eta_T} \cdot \left( \frac{m \cdot g \cdot f \cdot u_a}{3600} + \frac{m \cdot g \cdot i \cdot u_a}{3600} + \frac{C_D \cdot A \cdot u_a^3}{76140} + \frac{\delta \cdot m \cdot u_a}{3600} \frac{du}{dt} \right) \qquad (3.1)$$

The variable $P_V$ represents the power demanded by the vehicle in kW; $\eta_T$ represents the efficiency of the transmission system, and the wheel valley motor is selected for this criteria whose transmission efficiency is 1; $u_a$ represents the vehicle speed in km/h; $C_D$ represents the air damping coefficient; $f$ is the automobile rolling damping coefficient; $i$ represents climbing degree; and A represents the windward area of the car in $m^2$.

The maximum power demand of a car should meet the power both during climbing and at the highest vehicle speed as follows.

(1) Maximum vehicle speed $u_{max}$ needs vehicle power:

$$P_{max1} = \frac{1}{\eta_T} \cdot \left( \frac{m \cdot g \cdot f \cdot u_{max}}{3600} + \frac{C_D \cdot A \cdot u_{max}^3}{76140} \right) \qquad (3.2)$$

The variable $P_{max1}$ represents the power demanded under highest vehicle speed in kW; $u_{max}$ represents the highest vehicle speed in km/h; $C_D$ represents the air damping coefficient; $f$ is the automobile rolling damping coefficient; and A represents the windward area of the car in $m^2$. Assuming the car is driving on a flat road at a constant speed, so the climbing degree term and the acceleration term are both 0.

(2) Maximum climbing degree $i = 0.2$, and the climbing speed $u_a$ = 15 km/h, the power required by the electric vehicle is:

$$P_{max2} = \frac{1}{\eta_T} \cdot \left( \frac{m \cdot g \cdot f \cdot u_a}{3600} + \frac{m \cdot g \cdot i \cdot u_a}{3600} + \frac{C_D \cdot A \cdot u_a^3}{76140} \right) \qquad (3.3)$$

The variable $P_{max2}$ represents the power demanded under maximum climbing degree in kW; $u_a$ represents the vehicle speed under maximum climbing degree in km/h; $i$ represents maximum climbing degree. Assuming the car is driving at a constant speed below the maximum value, so the acceleration term should be 0.

(3) Average driving speed needs the power:

$$P_{ave} = \frac{u_{ave}}{3600\eta_T} \cdot \left( m \cdot g \cdot f + \frac{C_D \cdot A \cdot u_{ave}^2}{21.15} \right) \qquad (3.4)$$

The variable $P_{ave}$ represents the power demanded under average driving speed in kW; $u_{ave}$ represents the average driving speed of 80km/h. Assuming the car is driving on a flat road at a constant speed, so the climbing degree term and the acceleration term are both 0.

The target maximum vehicle speed is 120km/h and average driving speed of 80km/h. The power demands for maximum vehicle speed power, maximum climbing power and average speed calculated are 21.125 kW, 12.022 kW and 8.789 kW respectively.

The motor has the highest efficiency near the rated power [27]. The calculation above shows that the maximum power of the car is usually determined to be 21.125 kW according to the maximum speed result, and a certain amount of backup power should be reserved. Therefore, upon choosing the wheel valley motor the climbing power should be greater than 12.022 kW, and the average power of the motor should be higher than 8.789 kW. The rated power of the existing motor in 2013 Ford Focus EV is 107 kW, which can cover the theoretical needs of the target value of 21.125 kW.

#### 3.2.1.3 Basic parameters and structure of the battery submodule and pack

(1) Nominal voltage and electric range of the battery pack

Further to the project requirements, the rated voltage of the extended-range battery pack for the electric vehicle was specified as 48V. The battery cell usually operates in the range of 3.2 V to 4.2 V, and the rated voltage is 3.6 V. Thirteen battery submodules are needed to be connected in series to make the battery pack voltage reach 46.8 V, close to target 48V.

(2) Capacity of the battery pack

As the driving range of the original existing pack at one charge is about 123 km, the designed mileage of one cylindrical battery pack in this chapter is responsible for another 20 km range extension. And the selected electric vehicle needs to travel for a distance of no less than 400 km under the average speed of 80 km/h. From (3.4) it can be calculated that the average output power of the car is 8.789 kW at 80 km/h, and as the energy consumed by the car accessories does not exceed 15% of the energy storage system [27], so the energy consumption of the accessories is 1.318 kW. As the nominal voltage is close to 48 V, the capacity of the battery pack can be calculated using (3.5) as following:

$$\frac{Power(W)\times Mileage(km)}{Velocity(km/h)\times Voltage(V)} \quad (3.5)$$

$$\frac{(8789W+1318W)\times 20km}{80km/h\times 48V}=52.64Ah$$

Considering that the actual effective capacity of a battery cell is lower than its theoretical value, researchers usually take the effective capacity factor as 0.8, so the actual battery pack capacity should not be less than 65.8 Ah.

(3) Selection of battery cells

The assembly of a battery pack is complicated, as energy storage systems need to consist of cells connected in parallel or in series. This thesis uses Samsung INR18650-35E cylindrical battery cell. The reasons for this choice are as follows:

1) The INR18650-35E battery cell can withstand 5C rate discharge at the maximum, which can meet the demand of peak power. The battery capacity reaches 3500mAh, the weight is as small as 50 g, and therefore it has a high energy density.

2) The INR18650-35E battery is a cylindrical cell with a large specific surface area, and heat can be quickly dissipated reducing the operating temperature of the battery submodule and pack.

3) The INR18650-35E model has a large production run and has various applications in the field of the EV industry. Its reliability has been verified, which can reduce the cost of manufacturing and risk of safety, and they also have little maintenance issues during use.

Table 3.2: INR18650-35E battery cell parameters are shown

| Samsung INR18650-35E 3500mAh | | | |
|---|---|---|---|
| Item | Specification | Item | Specification |
| Cell Model Name | INR18650-35E | Chemistry | LiNiCoAlO2 |
| Charging Voltage | 4.2 V | Max. Discharge Current | 8 A |
| Nominal voltage | 3,6 V | Height | Max. 65.25 mm |

| | | | |
|---|---|---|---|
| Nominal capacity | 3500mAh | Diameter | Max. Φ 18.55 mm |
| Discharge end voltage | 2,65 V | Operating Temperature | 0 to 45°C |
| Weight | 50g Max | Operating Temperature | -10 to 60°C |

The parameters of the battery pack must match the requirements of maximum power, voltage, maximum current, and mileage. The nominal voltage of the battery cell is 3.6 V. Assuming that the battery pack requires m cells in series, n cells in parallel, there are:

$$m \times 3.6\ V \approx 48\ V \quad (3.6)$$

$$n \times 3.5\ Ah \geq 65.8\ Ah \quad (3.7)$$

Where $m \approx 13.33$ and $n \geq 18.8$, making $m = 13$ and $n = 20$, therefore the entire battery pack is composed of 260 battery cells with 13 in series and 20 in parallel.

Table 3.3 Battery pack parameter matching

| Parameter | Value |
|---|---|
| Single cell voltage | 3.6 V |
| Quantity of cells | 260 |
| Battery pack voltage | 46.8 V |
| Battery pack capacity | 70 Ah |

The whole battery pack is connected in series and in parallel with 260 battery cells. Considering the large size and weight of the battery pack, which is not conducive to the overall assembly, it is better to adopt a design scheme of multiple battery submodules. This thesis uses 13 submodules in series for fabrication and easier maintenance. All 13 submodules have the same size and structure. Each battery submodule has 20 cells connected in parallel, with a nominal voltage of 3.5 V and a nominal capacity of 70 Ah.

### 3.2.2 Battery pack frame design

The connection method of the battery cells affects the consistency, reliability, and service life of the pack.

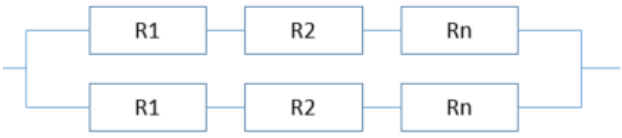


Figure 3.1: Series Model

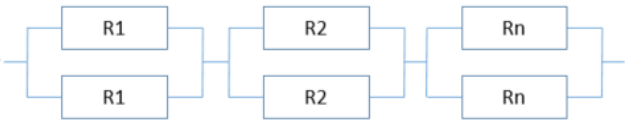


Figure 3.2: Parallel Model

Figure 3.1 and Figure 3.2 are two commonly used series-parallel models. Assuming that the failure rates of the single cell in the model are the same, and the cells are independent from each other, the following mathematical model can be established [22],

Series-Parallel:

$$R(t) = 1 - [1 - \prod_{t=1}^{n} R_i(t)]^m \qquad (3.8)$$

Parallel-Series:

$$R(t) = \prod_{t=1}^{n} \{1 - [1 - R_i(t)^m\} \qquad (3.9)$$

Where $R(t)$ represents the reliability （durability and service life） of the system, $R_i$= (1, 2, ,...,n) represents the reliability of the i-th unit, m represents the number of batteries connected in parallel, and n represents the number of batteries connected in series.

It was calculated that 260 battery cells are required to build a battery pack. Assuming that the reliability of each battery cell is 0.9 (in fact, it should be greater than 0.9), the reliability calculation results using different methods are as follows:

Adopting parallel connection before series connection, the reliability of the system:

$$R(t) = [1-(1-0.9)^{20}]^{13} = 0.9999 \qquad (3.10)$$

Adopting series connection before parallel connection, the reliability of the system:

$$R(t) = 1-(1-0.9^{13})^{20} = 0.9971 \qquad (3.11)$$

Through the above calculations, it can be concluded that the connection in parallel and then in series has a better reliability. If a single battery of one parallel battery module is damaged, it will not affect the operation of other battery modules, only the capacity of the battery module will decrease. As long as the design is reasonable, the parallel connection of battery modules will also improve the reliability of the battery pack.

Wang Zhenpo, Sun Fengchun and others compared the two series-parallel battery packs in the BYD 6100 model after running for 500 km and standing for 10 hours [28]. They tested the battery pack voltage consistency and found that the battery voltage distribution is more concentrated by adopting the parallel connection before the series connection. The voltage differences between cells are acceptable. The method of connecting in series before in parallel has a balancing voltage distribution range. If it is used continuously, it will affect the uniformity of the battery voltage and accelerate the aging of the battery. The battery cells connected in parallel can be charged and discharged with each other, which has a certain balancing effect on the voltage of the battery.

The lithium-ion battery charging method is usually constant current first and then constant voltage, and each voltage value during the charging corresponds to a SOC value. If the lithium-ion battery is over charged or over discharged, it will age more rapidly or be damaged, so the BMS must monitor the voltage of each battery cell [29].

**Layout of Battery Pack**

Connecting in parallel before in series has great advantages in reliability and the consistency of the battery voltage. The basic layout of the battery pack is shown in Figure 3.3.

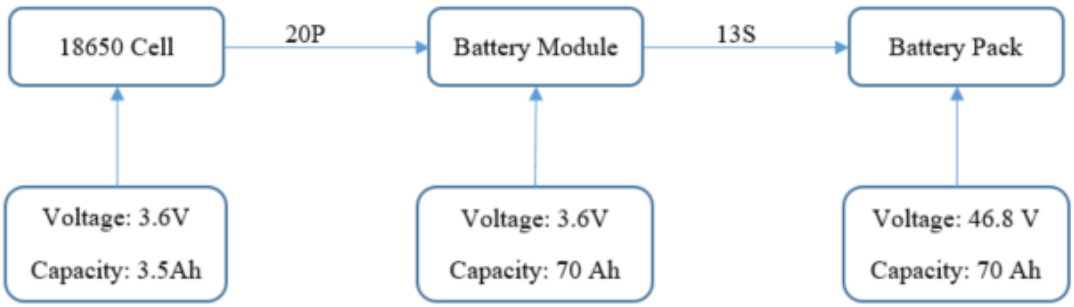


Figure 3.3 Composition of power battery pack

The battery pack adopts a layered model. Every 20 battery cells are connected in parallel to form a battery submodule. According to the voltage requirements of the battery pack, 13 battery submodules are connected in series. The basic parameters of the battery submodule are as follows:

$$U_1 = U_0 \bullet n = 3.6\ V \times 1 = 3.6\ V \qquad (3.12)$$

$$C_1 = C_0 \bullet m = 3.5\ \ Ah \times 20 = 70\ \ Ah \qquad (3.13)$$

In the formula, $C_0$ and $C_1$ respectively represent the rated capacity of the battery cell and the battery submodule, $U_0$ and $U_1$ respectively represent the rated voltage of the battery cell and the battery submodule, n and m respectively represent the number of battery cells in series and parallel.

## 3.3 Battery submodule design and fabrication

The battery submodules are the components of the battery pack. One battery submodule includes 20 INR18650-35E batteries, current collectors, battery holders, conductive copper columns, temperature sensors, and other components. In the process of designing a battery submodule the insulation and the fixing of the battery submodule should be fully considered.

### 3.3.1 Battery submodule layout

The size of the battery submodule has a strong relationship to the arrangement of the battery cells. For the cylindrical cells, the battery arrangement includes parallel and staggered arrangement. Figure 3.4 shows the battery submodule areas in the two arrangements. The staggered arrangement battery submodule occupies a smaller volume. Lu Yanhui [30] studied the influence of different configurations on the battery temperature uniformity and found that the temperature uniformity of the staggered battery submodule battery is poor. Based on the consideration of heat dissipation, the battery cells will be arranged in parallel.

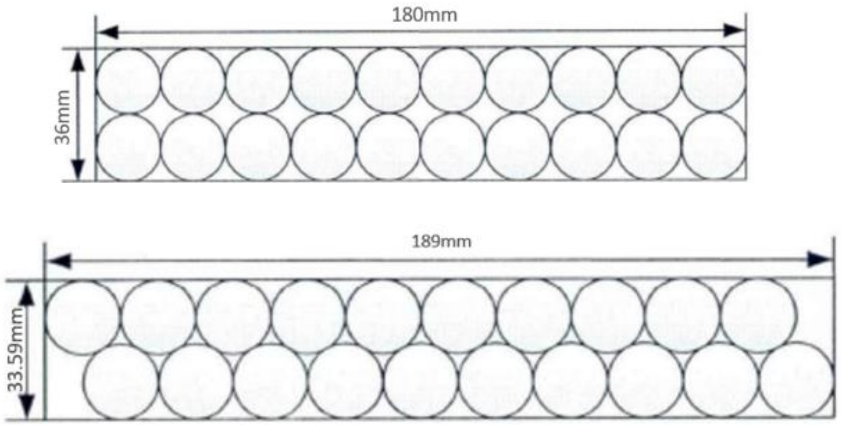


Figure 3.4 Comparison of the two arrangements of cylindrical cells [30]

### 3.3.2 Design of current collectors and conductive copper columns

**Current collectors**

The current collectors are mainly used for carrying the current of the battery submodule, and in this case, should be designed to carry 70 A continuous current [31]. At present the more commonly used metals are copper and nickel. Copper has good electrical conductivity and low resistivity and

so a copper sheet was selected as the current collector. Figures 3.5 and 3.6 show the size and the conceptual diagram of current collectors.

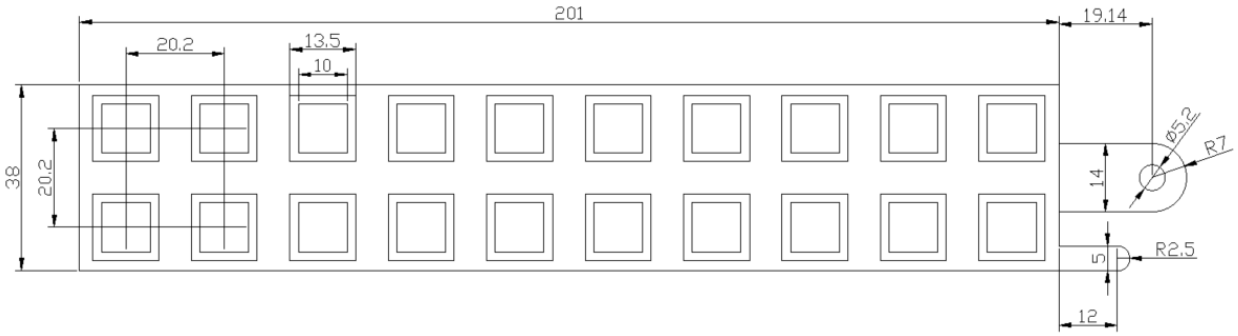


Figure 3.5 Size diagram of current collector

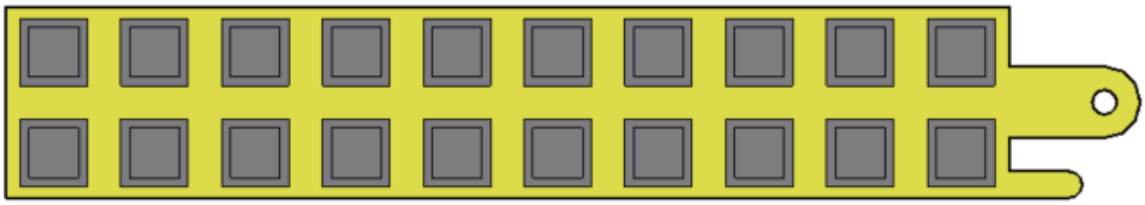

Figure 3.6 Conceptual diagram of current collector

Nickel is preferred to do spot welding with the cell terminals compared to copper, because copper is more easily oxidized in the air and less resistant to corrosion than nickel. Therefore, 0.2 mm thick nickel is set at the spot weld between the current collector and the battery, which not only ensures that the current carrying capacity is met, but also improves the weld quality. The end tab of the copper sheet has a 5.2 mm mounting hole, which is mainly installed with the copper column. The copper sheet is also designed with voltage detection points. To account for the welding stress caused by heat expansion and contraction during the welding process, the thickness of the copper sheet of the current collector is 0.3 mm and the width is 38 mm. Cross sectional area of current collector shown in Figure 3.7

$$A = 38\ mm * 0.3\ mm = 11.4\ mm^2 \quad (3.14)$$

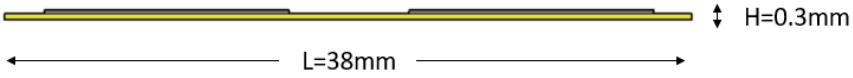


Figure 3.7 Cross sectional of current collector

If the safe current capacity of the copper sheet is 7 A/ $mm^2$, the maximum current that can be passed in the proposed current collector is 79.8 A. When the battery submodule is discharged at a rate of 1C, the current is 70 A, and the copper sheet meets the above requirement.

**Conductive copper columns**

The conductive copper column of the battery submodule shown in Figure 3.8 is used as the output terminal of the battery submodule, and the current carrying capacity of the copper column is the main consideration in the design process. The battery submodule capacity is 70 Ah, considering that the battery system will be discharged at maximum 1C rate during its operation, the rated current of the battery pack is also 70 A. The designed conductive electrode column has a diameter of 9 mm with a 5.2 mm diameter through-hole in the center.

Figure 3.8 Conductive copper columns

Minimum cross-sectional area of copper:

$$S = \pi(R^2 - r^2) = 42.38\ mm^2 \quad (3.15)$$

The conductivity of copper is usually based on the temperature rise, and the calculation formula for the current carrying capacity of copper is:

$$I_{cu} = 101.7St^{-1/2}$$

Where:

$I_{cu}$ $-A\ current\ carrying\ capacity\ of\ copper\ at\ room\ temperature$

S −The cross-sectional area of copper

t −When a current is continuously discharged, t = 3600 s, when intermittent discharge is t = 30 s, and when starting discharge, t = 10 s.

Then the withstand current of the conductive copper columns is shown in Table 3.5:

Table 3.5 Current capacity of the conductive copper columns

| Conductive state | Continuous | Intermittent | Starting |
|---|---|---|---|
| Withstand current | 71.7825 A | 786.9 A | 1362.96 A |

The design requires that the battery pack is continuously discharged at a rate of 1C, and the battery system discharge current is 70 A. During the starting and accelerating process of the battery pack the conductive copper columns can be continuously discharged at 71.78A, and the starting current reaches 1362.96A, and so the design meets the requirements.

**Peripheral design of battery submodule**

When designing battery submodules, each part of the battery submodule is required to have a certain strength and electrical insulation. The battery submodule designed in this thesis should meet the requirements of air cooling and adopt an open case. The battery protection unit consists of an upper base, two side end covers, and a lower base, as shown in Figure 3.9.

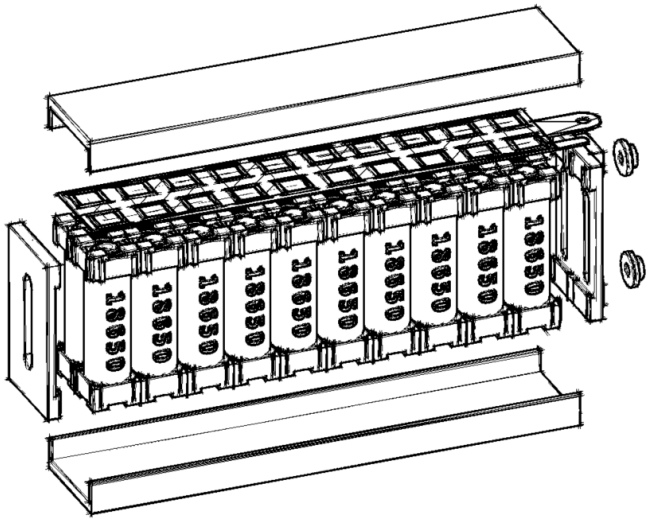


Figure 3.9: Single battery submodule with peripheral protection cases

The upper base and the lower base of the battery are respectively connected to the battery holder through trapezoidal pins, and the side end covers are designed as a trapezoidal groove, which is fixed on the holder through trapezoidal pins. In order to ensure waterproofing and dustproofing of the battery submodule, a layer of Acrylonitrile Butadiene Styrene (ABS) glue is applied before assembling the components. A lug boss was designed on the right end cover for placing conductive copper columns, and an M4 nut was inlaid under the boss. Heat will generate during charging and discharging cycles, the battery submodule requires the right and left sides open to the air. Because of good mechanical properties, and flame resistance, ABS was chosen as the material of the peripheral protection cases.

### 3.3.4 Battery submodule energy density

The energy density is an important parameter of a battery system. According to the design requirements, the energy density of the battery pack should be greater than 150 Wh/kg. Designing a battery system should meet mechanical and electrical strength requirements, more importantly reach the desired energy density. The weight of each component in the battery submodule is shown in Table 3.9.

Table 3.9: The quality and rough weight of each component in the battery submodule

| Item | Material | Unit Mass/g | Quantity | Total Mass/g |
|---|---|---|---|---|
| Upper Base | ABS | 18 | 1 | 18 |
| Bottom Base | ABS | 18 | 1 | 18 |
| Side Cover | ABS | 28 | 2 | 56 |
| Conductive pole | Brass | 4 | 2 | 8 |
| Current Collector | Brass | 12 | 2 | 24 |
| Frame holder | ABS | 17 | 2 | 34 |
| Bolts | Steel | 2 | 2 | 4 |
| INR18650-35E | - | 50 | 20 | 1000 |

The total mass of the battery submodule:

$$M = \sum_{i=1}^{n} M_i = 1.162\ kg \qquad (3.16)$$

Where $M$ is the total mass of the battery submodule and $M_i$ is the mass of each component in the battery submodule.

The battery submodule consist of 20 cells in parallel, so its total energy is

$$Q = m \bullet V \bullet C = 20 \times 3.6\ V \times 3.5\ Ah = 252\ Wh \qquad (3.17)$$

In the formula, $Q$ represents the total energy of the battery submodule, m represents the number of battery cells connected in parallel, V and C represent the voltage and capacity of the battery cells respectively.

Energy density of battery submodule:

$$E = \frac{Q}{M} = \frac{252\ Wh}{1.162\ Kg} = 216.87\ Wh/Kg \quad (3.18)$$

Where: $E$ is the energy density of the battery submodule, the energy density of the battery submodule reaches 216.87/kg, which meets the basic requirements of the design.

### 3.3.5 Fabrication of battery submodule

When a battery cell is over charged or over discharged, it will cause the degradation of the capacity, which will reduce its service life. When multiple battery cells are installed into a battery submodule, due to the difference in performance between cells the battery submodule is more likely to be over charged and over discharged, and the degradation of affected battery cell will be accelerated. At the same time, when a certain battery cell is damaged, the degradation of other cells in the same submodule will also be triggered, eventually causing the entire battery submodule to fail. Therefore it is necessary to check the consistency of the batteries before welding them together.

Battery consistency inspection often includes using the voltage matching method, capacity matching method, resistance matching method, and full dynamic characteristics matching method. The matching of the full dynamic characteristics of cells can better determine the consistency of the battery cells, but because of it is a complicated process, it is less likely to be used in engineering, whereas the internal resistance matching and voltage matching methods are easy to implement and are able to reflect the cell consistency well.

The internal resistance range of the battery cell found cell used in this research was in the range $21.4\,m\Omega$ - $22.4\,m\Omega$, the maximum difference is 4.08%. The voltage range is 3 .58 V-3.60 V, and the difference is less than 5%, confirming that the battery cells showed a high consistency.

Spot welding is used for welding the current collector and the battery terminals. Resistance spot welding uses heat to melt the weldment. When spot welding, special attention need to be paid to avoid excessive welding temperature, which damages the internal parts and burns the outer shell of the battery cell. Before the battery pack is welded, the quality of the welding apparatus must be inspected. In this thesis, a battery and a sample of nickel strips were first welded. The quality of the welding joint was confirmed by observing whether there were phenomena such as surface burns or missed welding.

The welding machine used in this thesis is shown in Figure 3.10. When holding the battery cell, it must be welded fast and accurately to prevent high temperatures from damaging the internal structure of the battery. Since the battery submodule has been assembled between the battery cell and the battery holder before welding, there is no need to redesign the clamp to fix the battery cells, which greatly simplifies the processing. Figure 3.11 shows the battery submodule after finishing spot welding.

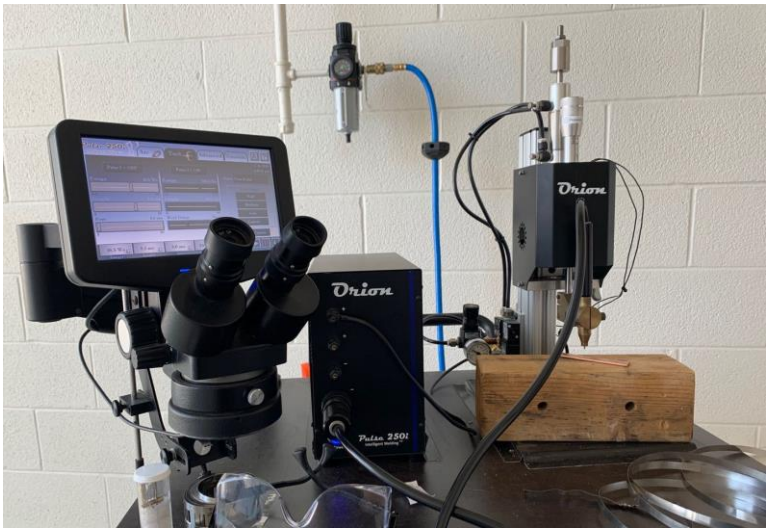


Figure3.10: The welding machine.

Figure3.11: Sample welding submodule.

**Assembly of battery submodule**

Figure 3.12 shows a view of the battery submodule. The upper base of the battery submodule is mainly used to fix the conductive copper column and provide for voltage measurement. The side end cover is mainly used to protect the positive and negative current collectors and provide electrical insulation. The lower base is used to buffer the external shocks to the battery submodule. The terminal cap holders are able to link the battery cells together and withstand limited external force of 60N. Before spot welding the battery submodule was assembled using the cap holders, temperature sensors, side end covers and the conductive copper column. The upper and the lower bases were assembled after welding.

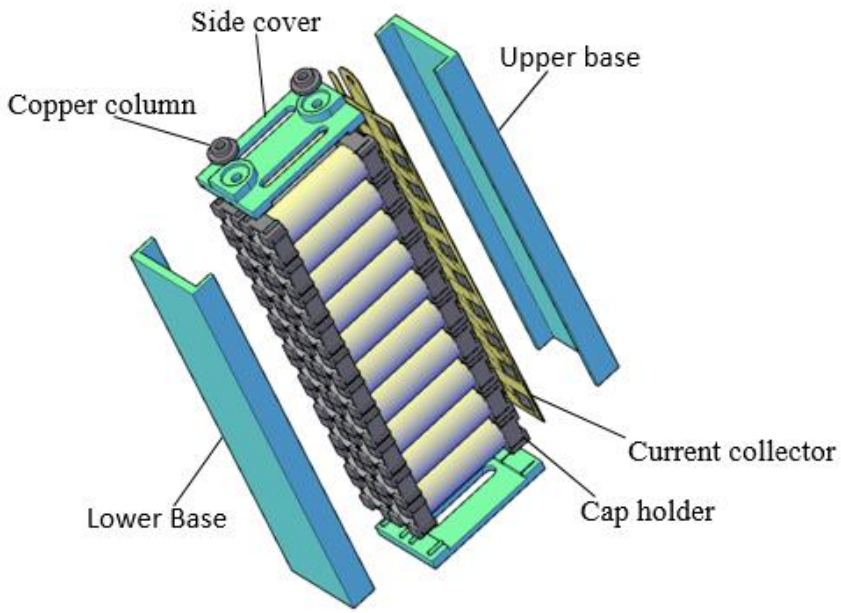


Figure3.12 Extended view of the battery submodule.

**Chapter summary**

This chapter outlined the design of a cylindrical battery pack and submodule. The overall design of the battery submodule was discussed, and different series and parallel cell configurations were compared. From the perspective of battery consistency, reliability and operating cost, the configuration of one submodule was made with 20 parallel cell connections, and the battery pack consisted of 13 submodules stacked in series. The energy density of one battery submodule reaches 216.87Wh/kg, which meets the design requirements.

# Chapter 4

# Battery Testing Setup

Different tests are conducted to determine specific parameters and properties of batteries. This chapters introduces the experimental setup used for the characterization of lithium-ion battery cells [30, 31] as outlined in Figure 4.1.

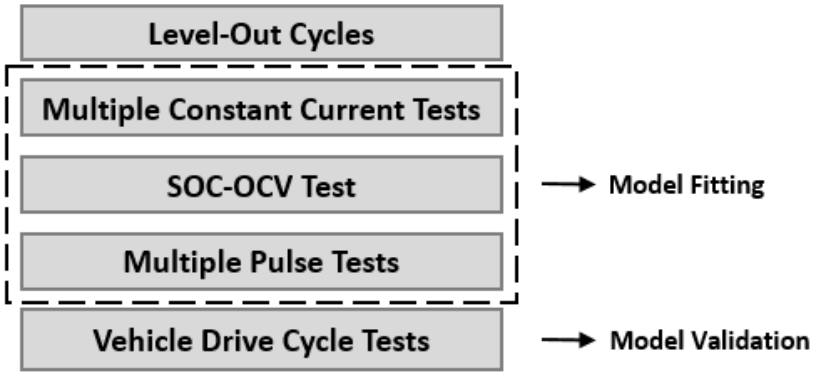


Figure 4.1: Overview of applied characterization tests.

## 4.1 Test Setup Components

This research considered characterization of a prismatic cell for its potential use in a second battery module. The prismatic cell selected is a new super-capacity prismatic cell of 280 Ah. This chapter provides an overview of tests and the equipment used for the characterization of this cell.

### 4.1.1 Battery Selection

Lithium-ion battery cathode materials are mainly divided into four types: Lithium Cobalt Oxide (LCO), Lithium Manganese Oxide (LMO), Lithium iron Phosphate (LFP), and ternary materials of Nickel Manganese Cobalt Oxide (NMC) or Nickel Cobalt Aluminium Oxide (NCA). Among them, LFP and NMC/NCA batteries are currently the mainstream in the market. The five key indicators to evaluate a lithium-ion battery are energy density, cost, safety, cycle life, and power density. At this stage NMC/NCA with higher energy density has attracted the most attention in the EV field. However, a higher energy density bring potential safety problems, including battery fire (e.g. frequent spontaneous combustion of Tesla model S series).

### 4.1.2 LFP Battery Advantages

**High safety performance**

The P-O bond in the LFP crystal is stable and difficult to decompose [32]. Even at high temperature or overcharged, it will not heat up and collapse or form strong oxidizing substances like lithium cobalt oxide. A LFP battery does not puncture to explosion and is not easily burned when overcharged, making large-capacity easier and safer to use compared with ordinary LCO and NMC/NCA batteries.

**Long cycle life**

The cycle life of a conventional lead-acid battery is from about 300 times up to 500 times, while a LFP battery has a cycle life of more than 2,000 times under 1C-rate standard charge/discharge. LFP batteries have a theoretical cycle life of 7- 8 years used under the proper conditions [33].

**Good high temperature performance**

LFP batteries have a wide operating temperature range from -20°C to +75°C and have high temperature resistance. The peak value of LFP can reach 350°C - 500°C with high-temperature characteristics, while LCO and LMO are only around 200°C [34].

**Cost performance**

Resource prices of nickel, cobalt, and manganese fluctuate greatly and the processing costs are high. The natural resources of iron and phosphorus are abundant, and the manufacturing costs are lower correspondingly. Because of this, there are increasingly more new energy vehicle OEMs developing larger-scale LFP batteries. Tesla will switch from NMC/NCA materials to LFP in all standard-range cars to increase profit margins while not raising selling prices.

**LFP batteries also have shortcomings:**

- Poor low-temperature performance.
- Low compaction density and the volume of equal capacity is larger than NMC/NCA batteries.
- The consistency issue of LFP battery also needs attention，it is not suitable as a cylindrical cell where a large number of connections are required.

Three large-capacity LFP battery cells were compared through multi-dimensional, and the one with the highest energy density and the most stable performance was selected. Table 4.1 lists the detailed parameters of these three LFP cells.

Table4.1：Parameters comparison of three large-capacity LFP cells.

| Item | | Specification | | |
|---|---|---|---|---|
| Model | | LiFePO4 120 Ah | LiFePO4 200 Ah | LiFePO4 280 Ah |
| Manufacturer | | Chuangning | Chuangning | EVE |
| Capacity | | 120 Ah | 202 Ah | 280 Ah |
| Voltage | | 3.2 V | 3.2 V | 3.2 V |
| Internal resistant | | ≤0.4 mΩ | ≤0.5 mΩ | ≤0.25 mΩ |
| Weight | | 2.7 kg ± 0.1 kg | 3.9 kg ± 0.1 kg | 5.22 kg ± 0.05 kg |
| Energy Density | | 142.22 Wh/kg | 165.74 Wh/kg | 171.65 Wh/kg |
| Discharge | Discharge Cut-off Voltage | 2.8 V | 2.5 V | 2.5 V |
| | Max discharge current at room temperature | 1C-rate constant current | 0.5C-rate constant current<br>1C for 30 s | 1C –rate constant current |
| Charge | Charge cut-off voltage | 3.7 V | 3.65 V | 3.65 V |
| | Max charge current at room temperature | 1C-rate constant current | 0.5C-rate constant current<br>1C for 30 s | 1C-rate constant current |
| Operating temperature range | Charging | 0℃ ~ 55℃ | -20℃ ~ 55℃ | 0℃ ~ 55℃ |
| | Discharging | -20℃ ~ 55℃ | -30℃ ~ 55℃ | -20℃ ~ 55℃ |

The 280 Ah LFP prismatic cell has a firm aluminum shell and is manufactured by EVE Energy Co. provided in Figure 4.2. Its terminals have a structure of double aluminum poles with internal

screw of size M6 that will be used for connecting the terminals. Each terminal can bear a torsion of 8 N-m. The effective depth of threaded holes is 6 mm, enough to mount the fixture frame.


Figure 4.2 Comparison of three high-capacity prismatic cells.

### 4.1.2 Digatron cell cycler

In this research, the Digatron MCT-ME cell cycler was used for battery characterization. This tester is reliable and easy to customize with specifications listed in Table 4.3.

Table 4.3: Specification of Digatron cell cycler [36]

| | |
|---|---|
| **Voltage** | 0 - 5V |
| **Unit Current** | 75 A per channel |
| **Total number of channels** | 8 |
| **Channels operation** | Parallel connected only |
| **Series operation** | Series connections cannot be made |
| **Accuracy / Resolution** | ± 0.1% FS / 16 bits |
| **Command & data log rate** | Up to 10 Hz |
| **Temperature Sensing** | AD592 sensor, ± 0.5°C accuracy |
| **Control Software** | Battery Manager Workstation |

The Digatron cell cycler shown in Figure 4.3 consists of 8 channels, and each channel can provide up to 5V/75A output. It should be noted that the 8 channels can be connected in parallel to increase the current to up to 600 A, but not in series, so the maximum output voltage of the cycler is 5 V. The cycler has different functional modules including a power module, a temperature sensing module, and a voltage sensing module as shown in Figure 4.4.

Figure 4.3: Digatron battery cell cycler.

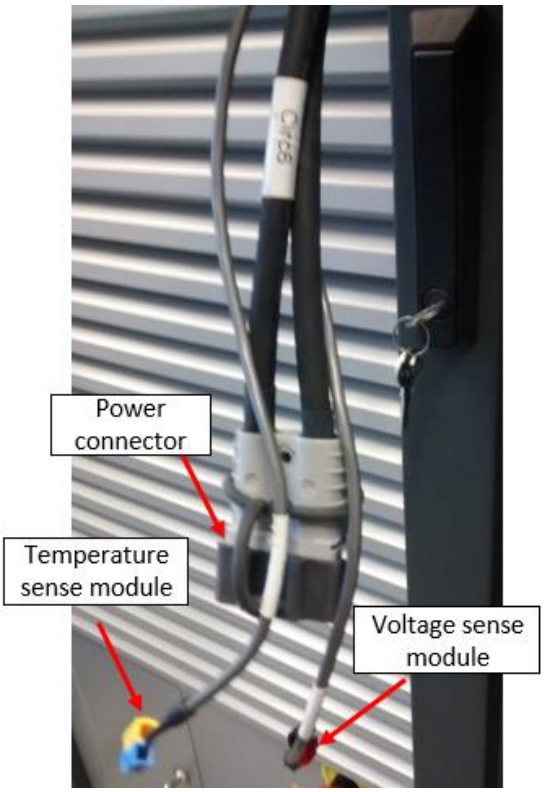


Figure 4.4: Functional modules of the cycler.

### 4.1.3 Experimental Chamber

Characterization tests for batteries need to be performed within a certain temperature range, so a chamber with controlled ambient temperature is required. Figure 4.5 shows a chamber from Thermotron with temperature control. This chamber has a Product Temperature Control Unit

(PTCU) and a thermocouple system to adjust the temperature rise rate of the product, also with a user-defined temperature offset. The environmental chamber temperature was set to 20C.

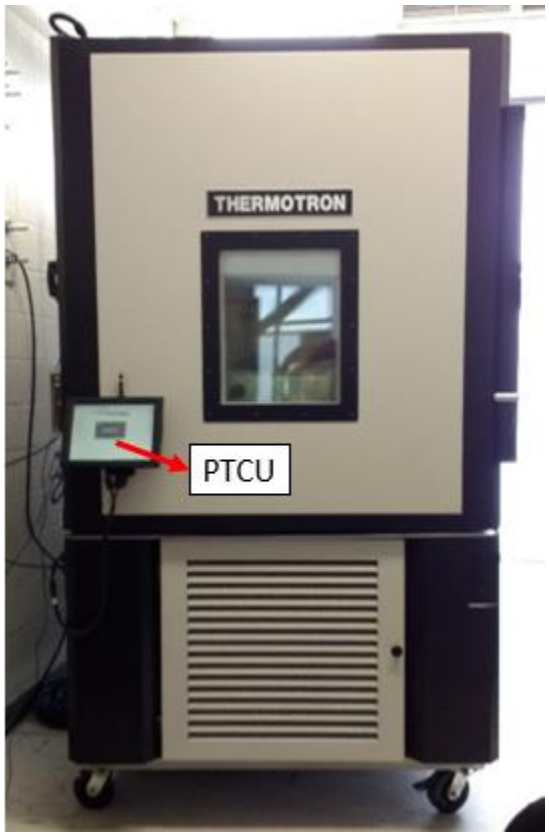


Figure 4.5: Thermotron temperature control chamber.

### 4.1.4 Connection Set

During battery characterization tests care was taken to avoid exceeding the rated voltage limit, bad connections between the electrical parts causing a short circuit or an open circuit, or an excessive load current causing local overheating. In addition to the safety protection mechanisms provided by the experimental chamber, other measures related to the physical connection between the tester and the battery cell, as shown in Figure 4.6, taken included:

- Use of proper cable sets to connect the 280 Ah battery with 4 paralleling channels of Digatron cycler, which can bear up to 300 A current load ensuring the battery can work up to 1C-rate.
- Connection of a temperature sensor to the testing battery cell. Upon receiving signals from the sensor, the control unit can regulate the temperature by varying the charging current: if the temperature is getting too high, the cycler will reduce the current requested by the actual program step or skip the charging/discharging step according to the temperature threshold.
- Further charging/ discharging after the cut-off voltage setting has a great impact on the battery health, hence the voltage sensor needs to be connected in real time and prevent the battery from over charging/discharging. For the 280 Ah prismatic cell the cut-off charging voltage is 3.6 V and the cut-off discharging voltage is 2.55 V.
- A fuse box was added in between the battery terminals and Digatron cycler to protect the battery from overheating under an excessive load current.

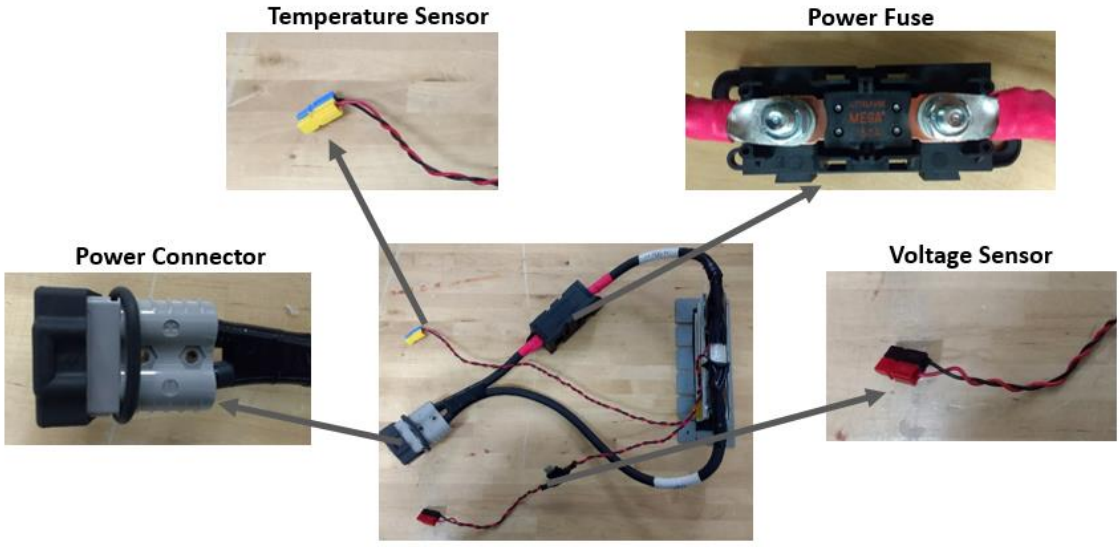


Figure 4.6: Battery safety connection set.

### 4.1.5 Rack and Fixture

During the charging and discharging process of lithium-ion batteries there is a certain pressure from gas generated inside the cell (empirical data 0.3 - 0.6 MPa). Under constant pressure, the deformation of the battery shell wall gets significant with a large force-bearing area. The swelling problem of prismatic batteries is quite common, especially for those of large capacity, which might cause increasing internal resistance, as well as partial electrolyte exhaustion and even shell rupture, seriously affecting the cycle life of a battery. Building a suitable battery fixture can help reduce the occurrence of swelling problems. Normally a prismatic cell requires external clamping between two strips of metal with a specific clamping force to keep it from expanding as shown in Figure 4.7. Also the cell needs to be fixed on a rack to prevent vibrations. Both racks and fixtures must be insulated and nonflammable in case that the connection becomes loose causing a short circuit.

Figure 4.7: The common external clamping fixture for prismatic cell.

Racks and fixtures need to be individually customized for the testing cells. This thesis used a thermal camera to capture the heat distribution of the battery surfaces. Thermal pictures indicate the temperature is relatively uniform on the surface. Given the requirement of measuring the

temperature of each cell surface, one side of the battery was placed on an insulating supporting rack and zip ties were used to fix it in place; this helped maximize the heat dissipation capacity of each surface without any active cooling method.

Considering that the shell thickness and material of this 280Ah prismatic cell have been confirmatively strengthened, the shell expansion is almost negligible, hence it is acceptable to place this prismatic cell on the insulated platform with any clamping plates presented in Figure 4.8, simplifying the layout structure for better heat dissipation.

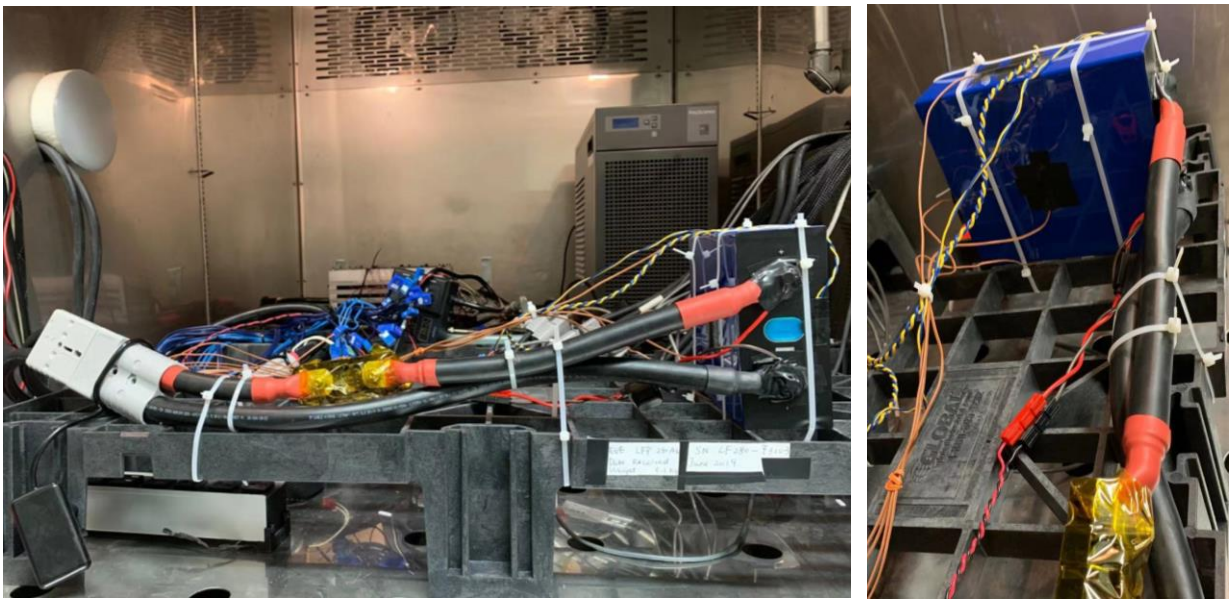

Figure 4.8: Fixture layout a) Front view b) Side view.

In accordance with the laboratory regulations, the important parameter information of the testing battery needs to be identified in advance during the test, including but not limited to the following attributes:

- The nominal capacity.
- The rated current and voltage.

- Manufacturer, product serial number, and battery chemistry.

### 4.1.6 Thermocouples

Thermocouples (TC) are a commonly used for temperature measurement. They directly measure the temperature and converts the thermal signal into an electromotive force signal. There are several types of thermocouples classified on the basis of durability, temperature ranges, resistance, and unmatched characteristics. Table 4.4 presents a comparison of major thermocouple types in detail. There are some important rules which must be taken into consideration. Red is always the negative terminal of a thermocouple regardless of the type.

Table 4.4: Comparison of thermocouple types [38].

| Standard Calibration | | Material | Temp Range | Accuracy | Premium Grade | Accuracy |
|---|---|---|---|---|---|---|
| "J" | + | Iron | 32 F to 1400 F | +/- 4 F or 0.75% | "JJ" | +/- 2 F or 0.4% |
| | - | Constantan | | | | |
| "K" | + | Chromel | 32 F to 2300 F | +/- 4 F or 0.75% | "KK" | +/- 2 F or 0.4% |
| | - | Alumel | | | | |
| "T" | + | Copper | -320 F to 700 F | +/- 2 F or 0.75% | "TT" | +/- 1 F or 0.4% |
| | - | Constantan | | | | |
| "E" | + | Chromel | 32 F to 1600 F | +/- 3 F or 0.75% | "EE" | +/- 1.8 F or 0.4% |
| | - | Constantan | | | | |
| "N" | + | Nicrosil | 32 F to 2300 F | +/- 4 F or 0.75% | "NN" | +/- 4 F or 0.4% |
| | - | Nisil | | | | |

"T" type thermocouples were selected because of the following characteristics.

- High temperature sensitivity.
- Wide temperature ranges to sub-zero.

- Lower costs.
- Durable and long lasting.

### 4.1.7 Thermocouple Placement

A thermal camera was used to capture the temperature distribution on each surface of the prismatic cell during the 1C-rate discharge test from top view, right view, and back view respectively. In Figure 4.9 the maximum temperature of each surface appears at the geometric center, and the heat dissipation capacity of different surfaces is almost the same.

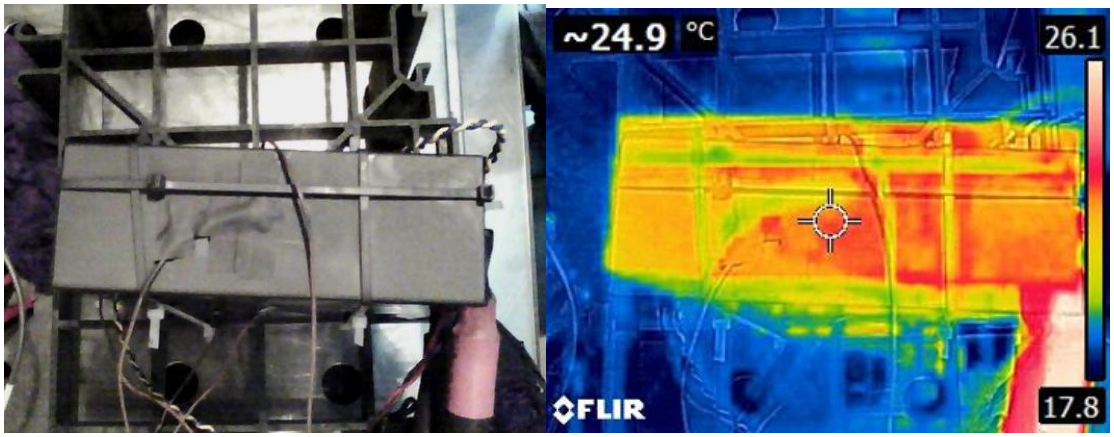


a) Top view.

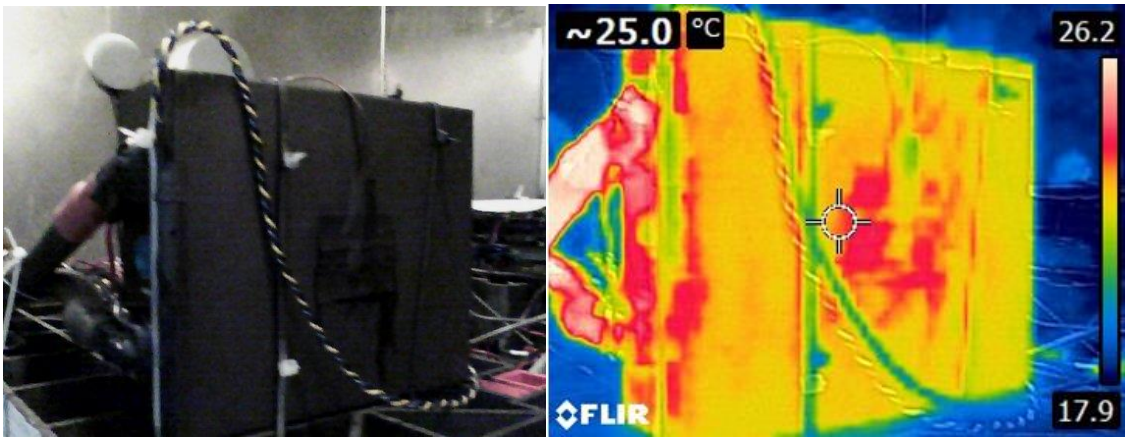


b) Right view.

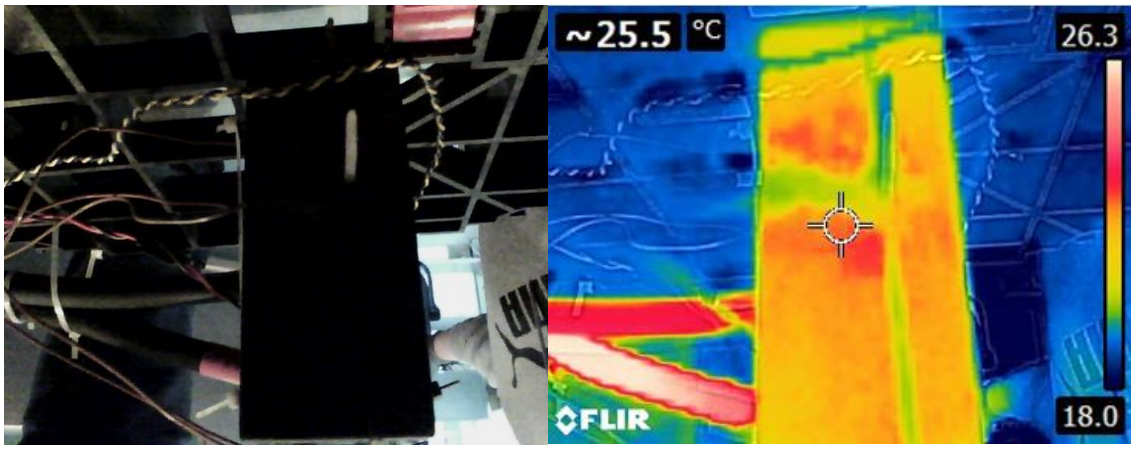


c) Back view.

Figure 4.9: Temperature Distribution of a 280 Ah Prismatic cell.

Since the shell case of the 280 Ah prismatic cell has been reinforced, no fixture is needed because the volume expansion of the cell during testing would be negligible, therefore five "T" type thermocouples were directly glued on battery surfaces with insulation foam and insulating tape as shown in Figure 4.10. Four TCs were placed at the surface geometric center, and one TC was placed right beside the venting hole because some tests have shown that heat accumulates more in between the two terminals of a prismatic cell [39], the temperature data from the thermocouples was monitored in real-time.

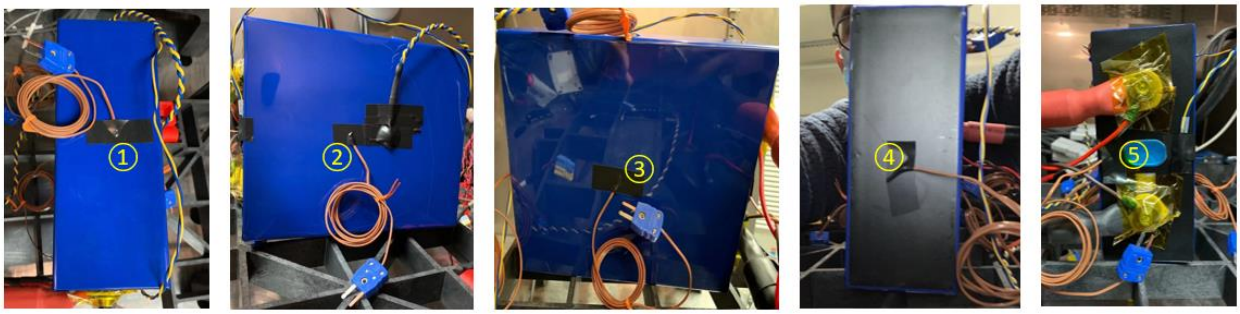


1) Top view. 2) Right view. 3) Left view. 4) Bottom View. 5 ) Front view.

Figure 4.10: Thermocouple placement.

## 4.2 Test Software

After setting up the experimental hardware, remote desktop control was used to monitor and manage the experiment in real time. [40] The test system set up is shown in Figure 4.11.

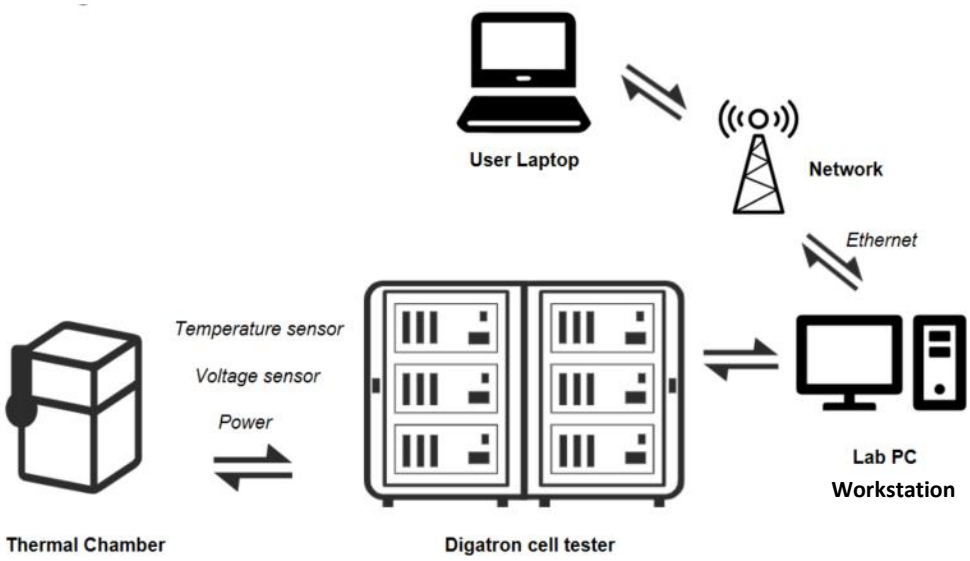


Figure 4.11: An overview of the component connections.

### 4.2.1 Battery Manager Workstation Software

Battery Manager Workstation is an application software connected to the hardware setup to control the Digatron on user's end. The workstation has a user-friendly interface and clearly reflects the real-time status of experiments in a timely manner, and also supports remote control allowing easy operation of the tests. The monitoring parameters could also be easily customized according to specific requirements.

### 4.2.2 Program

Battery Manager Workstation has its own script editing language, and an example program of 0.5C-rate constant current charging test is shown in Figure 4.13:

- The operator is the specific operation to be performed.
- Nominal value is the parameter values needed to be set.
- Limit is the cut-off boundary of parameters such as the upper and lower temperatures.

| Step | Label | Operator | Nominal Value | Limit | Action | Registration |
|---|---|---|---|---|---|---|
| | ! | Add = 1 IsSet Conditional for every circuit that is syned with this one | | | | |
| 1 | | PAU | | 1 sec | | 1 sec |
| 2 | | SET | TSW = 25 | | | |
| 3 | | PAU | | > 20 C & < 30 C | | 1 sec |
| 4 | | PAU | | 15 min | | 1 sec |
| 5 | | SET | Qty1 = 0 | | | |
| 6 | | CHA | Vchg V 0.5 ACN1 | < CV_Icut A | | 1 sec |
| 7 | | ADD | Cnt 1 | | | |
| 8 | | PAU | | 60 sec | | 1 sec |

Figure 4.13: Basic program: 0.5C-rate constant current charge test.

Generally the program above can be named Master Charge and classified as a basic program, which can be cited in a customized characterization test program. Figure 4.14 shows a 1C-rate charging test program for a 280 Ah prismatic cell, the upper and lower boundary of the voltage and temperature were set according to the battery's specification sheet and directly refer to the basic program Master Charge to simplify the script. Incorrect program steps can cause the test to be interrupted prematurely. Experimental programs written on the workstation must be carefully checked before operation.

Battery Manager Workstation also provides ways to view the experimental results and parameters. Figure 4.15 shows the terminal voltage changes in real time. Furthermore, experimental results can be exported to Excel and to Matlab for later analysis.

| | Step | Label | Operator | Nominal Value | Limit | Action | Registration |
|---|---|---|---|---|---|---|---|
| | | ! | Set cycle count value at begining test, used to track battery cycles throughout testing | | | | |
| | 1 | | SET | Cnt = 1 | | | |
| | 2 | | SET | RLevel = 3 | | | |
| | | ! | Set battery protection values, A is discharge current, A_not_Abs is charge current | | | | |
| | 3 | | SET | | < 2.5 V<br>> 3.65 V<br>> 55 C<br>< -20 C<br>< -285 A<br>> 285 A_notAbs | ERR 2<br>ERR 2<br>ERR 3<br>ERR 3<br>ERR 4<br>ERR 4 | CharCyc |
| | 4 | | PARALLEL | 2<br>3<br>4<br>6 | | | |
| | | ! | Set Test Temperature, will charge at 10degC and perform all tests at TempSet value | | | | |
| | 5 | | SET | TempSet = 20<br>TempLow = 10<br>TempHigh = 30 | | | |
| | | ! | Set minimum voltage for drive cycle and other tests, will regulate voltage to this value when reached or end test st | | | | |
| | 6 | | SET | Vmin = 2.55 | | | |
| | | ! | Set maximum voltage for drive cycle tests and charging, will regulate voltage to this value when reached | | | | |
| | 7 | | SET | Vchg = 3.6 | | | |
| | 8 | | SET | Vmax = 3.6 | | | |
| | | ! | Set current cut off for charging | | | | |
| | 9 | | SET | CV_Icut = 2.8 | | | |
| | | ! | 1C charge test 1 | | | | |
| | 10 | | SET | Ah = 0<br>Wh = 0 | | | |
| | 11 | | FILE | Ch1Charg | | | |
| | 12 | | Master_Charge | | | | |
| | 13 | | STO | | | | |

Figure 4.14: Basic program - 0.5C-rate constant current charge.

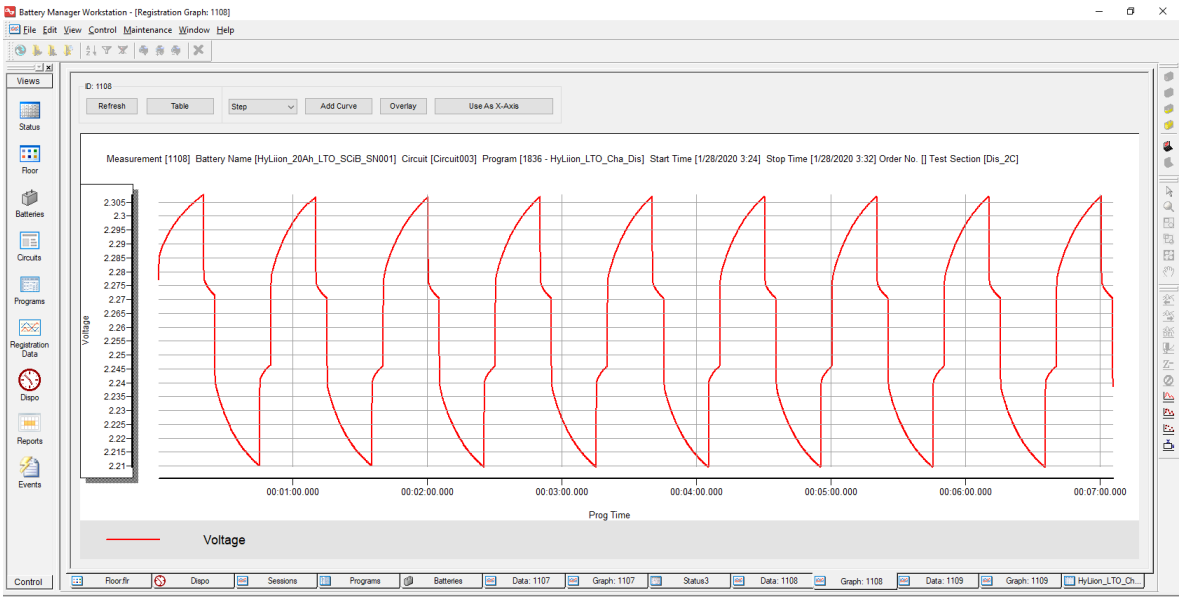


Figure 4.15: Measured voltage output in graph.

## 4.2.3 Temperature Reading

Five “T” type thermocouples were arranged and placed on the surfaces of the tested prismatic cell to obtain the temperature data. Labview Thermocouple Reader was used to collect data in real time, as shown in Figure 4.16. The data was saved and exported directly to Excel for later analysis.

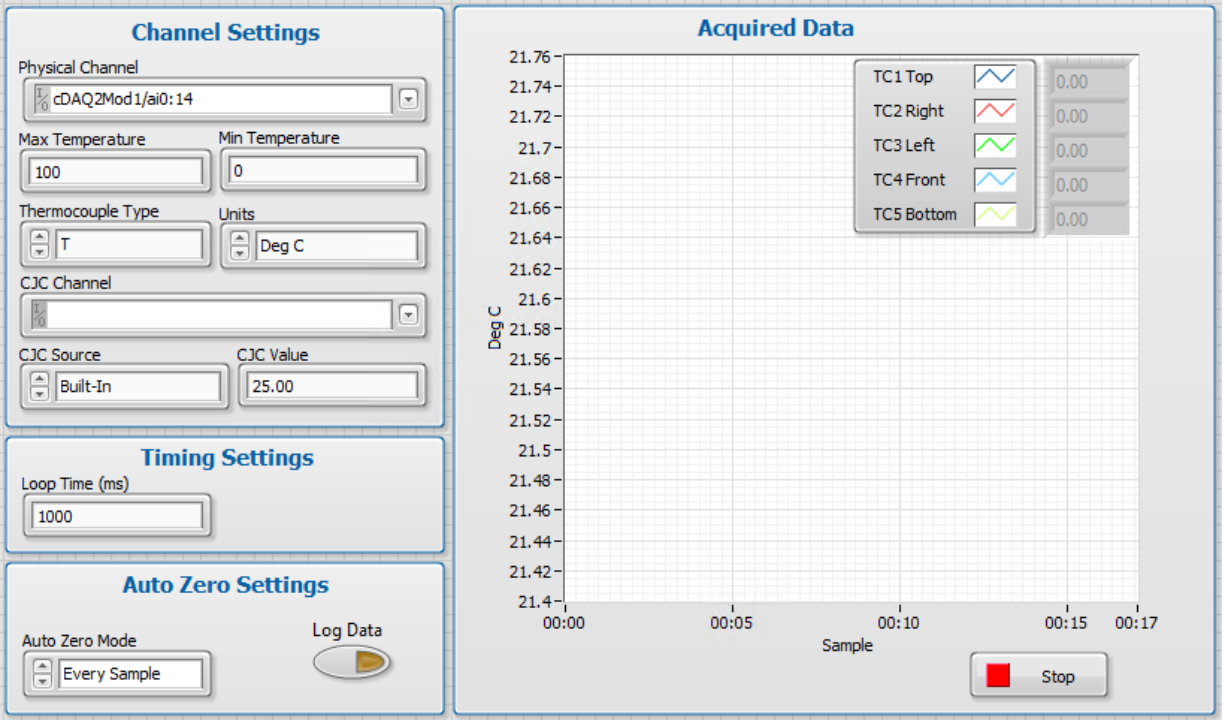


Figure 4.16：Main interface of Labview Thermocouple Reader.

# Chapter 5

# Characterization Tests and Improved Pulse Tests

Specific characterization tests are often conducted on lithium-ion batteries. In this chapter, Level-out test, SOC-OCV test, and the Pause Charge test will be explained and performed. The results are used to build a battery simulation model [41]. A LFP battery cell (3.2 V 280 Ah) was selected with a reinforced aluminum shell manufactured by EVE Energy Co., Table 5.1 presents its specification sheet.

Table 5.1: Parameter limits of 280 Ah Prismatic Cell. [42]

| Specification | | Upper Limit Value | Lower Limit Value |
|---|---|---|---|
| Voltage [V] | | 3.65 | 2.5 |
| Current [A] | | 280 [Charging] | -280 [Discharging] |
| Operating Temperature[°C] | Charging | 0 | 55 |
| | Discharging | -20 | 55 |

Safety limits need to be set to prevent over charging/over discharging during the test. Test current and voltage must not exceed the upper and lower limit values for preventing:

- Dramatic battery capacity loss results in early aging.
- Mechanical damage like electrolyte leakage, overheating and other safety hazards.

In addition, batteries must be tested and operated within the proper temperature ranges. The tests were conducted at 20°C, at which the battery has a better performance and the experimental results can be generalized [43]. It is also necessary to ensure that the battery is relaxed regularly between charging/discharging phases to achieve a good performance.

## 5.1 Level-out Test

Due to the self-discharge characteristics of lithium-ion batteries, at least 10 cycles of level-out tests should be run under test temperature of 20°C to activate the battery cells before characterization tests, which better ensured the accuracy and reliability of the experimental results. However, considering that the tested battery had a large capacity of 280 Ah, 5 cycles level-out tests were conducted. The specific steps are shown below in Figure 5.1:

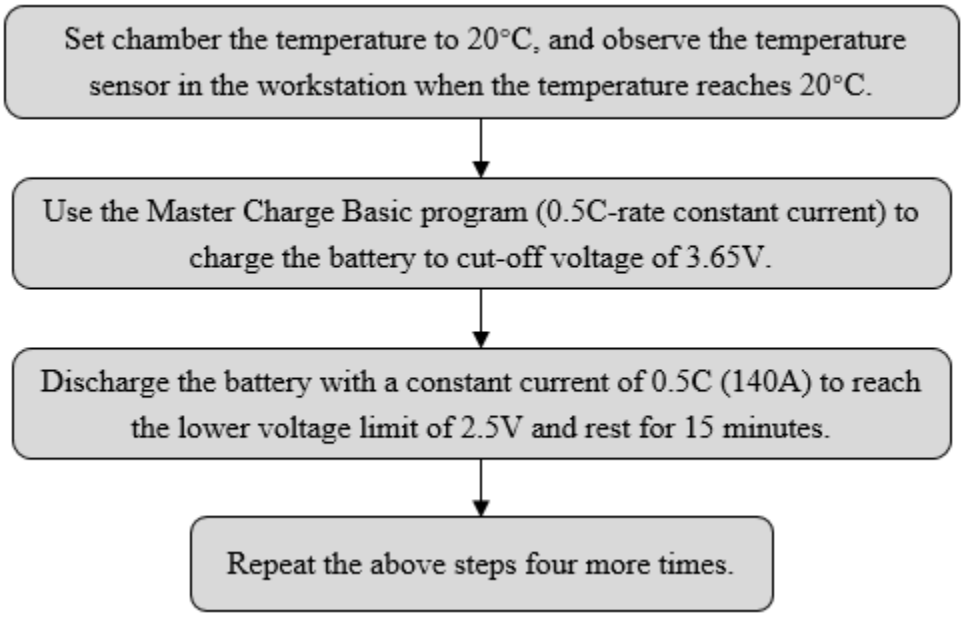


Figure 5.1: Flow Chart of Level-out Experimental Steps.

Figures 5.2 and 5.3 respectively provide a visual schematic of the single level-out cycle and entire 5 level-out cycles, showing the current input and the measured voltage results during the experiments.

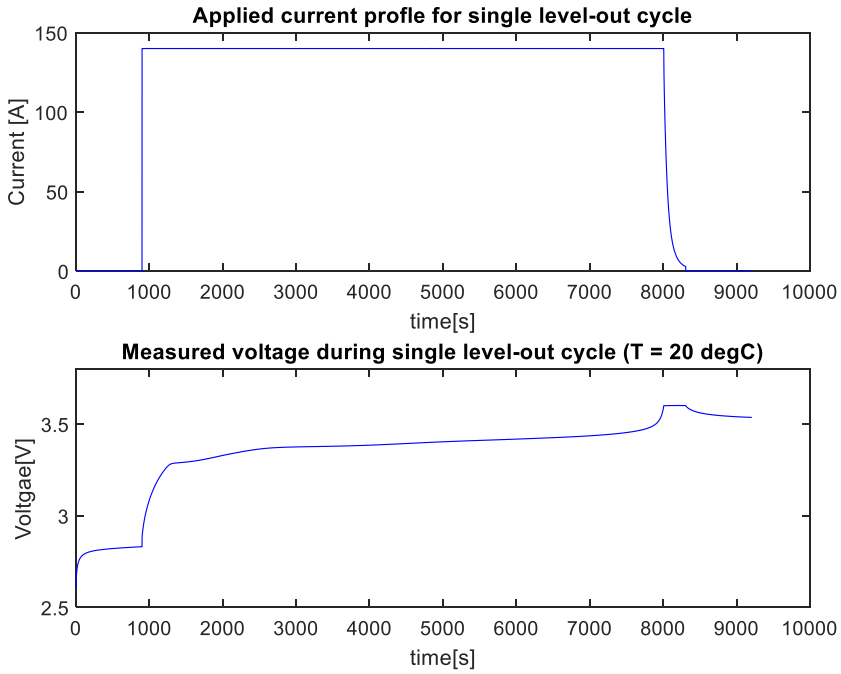


Figure 5.2: Current Input and Measured Terminal Voltage of Single Level-out Test.

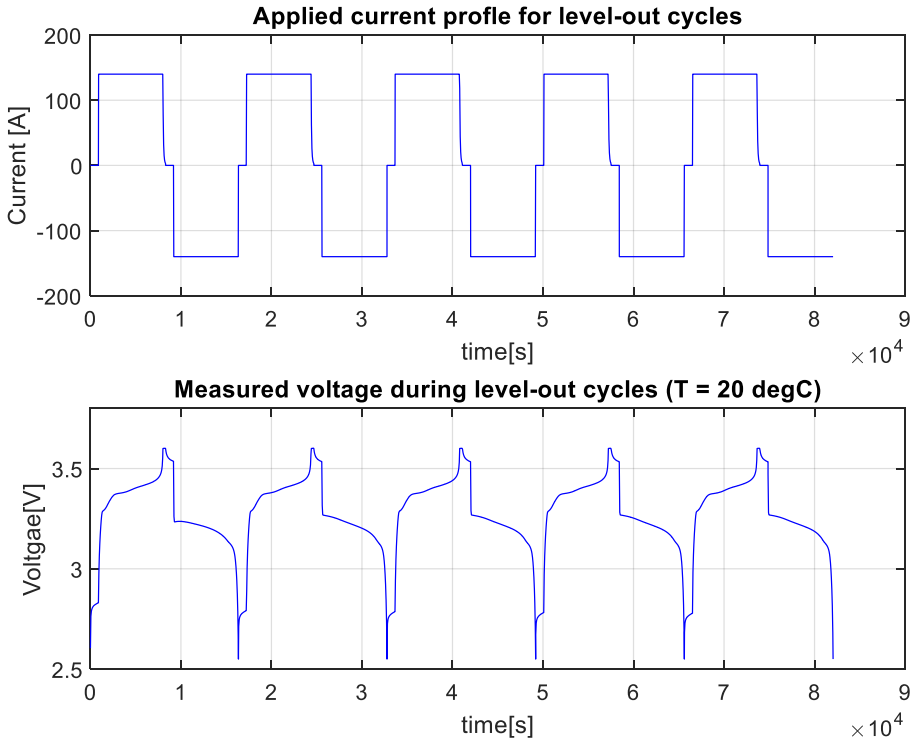


Figure 5.3: Current Input and Measured Terminal Voltage of Entire 5 Level-out Tests.

The battery capacity comparison of 5 level-out cycles is shown in Figure 5.4. It can be seen the capacity measured in the first charging cycle is much lower than rated 280 Ah, mostly due to the self-discharge of the battery during storage after leaving the product line. From the electrochemical point of view, the input power is often not completely converted to the active material for electric charges to use, but partly consumed (such as in irreversible side reactions), therefore the discharge capacity should be always less than the charge capacity. This is the concept of the battery's Coulombic efficiency, which is defined as the ratio between the discharge capacity and the charge capacity, which is often less than 100%. For current lithium-ion batteries, the Coulombic efficiency can basically reach 99.9% and above. Figure 5.5 presents the Coulombic efficiency during level-out tests.

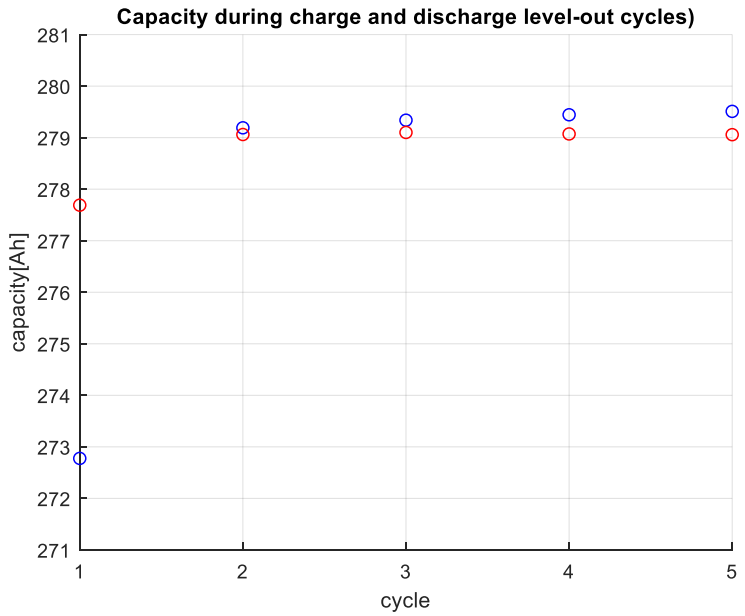


Figure 5.4: Capacity Comparison of Charging and Discharging Cycles.

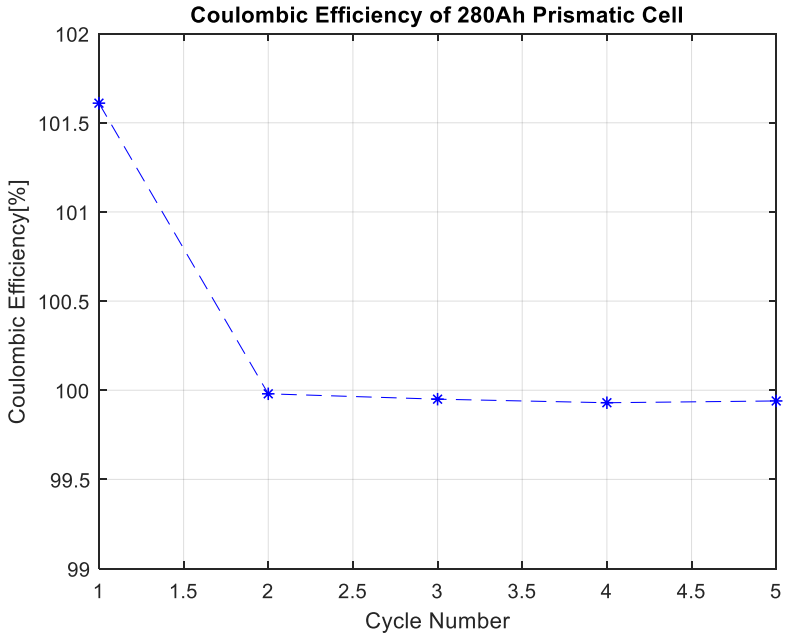


Figure 5.5: Coulomb Efficiency during Level-out Tests.

## 5.2 SOC-OCV Test

The correlation between Open Circuit Voltage (OCV) and State of Charge (SOC) is a very important characteristic for a lithium-ion battery in the SOC calibration process, so the OCV-SOC curve was mostly used for characterization [44]. Under ideal circumstances, every OCV value has only one SOC corresponding to it.

In State of Charge (SOC) estimation, the initial SOC is critically important, which is usually obtained through this OCV-SOC curve correlation. Generally, after the electric vehicle has been running for a period of time, or before the vehicle rests and starts again, the Battery Management System (BMS) will generate this curve to correct the initial SOC value, and then obtain an updated SOC value through a certain algorithm. Therefore, the correlation between SOC and OCV is related to the accuracy of the SOC estimation.

The relationship curve between SOC and OCV is generally obtained by depolarizing the battery using a small current, usually discharging the battery at a fixed rate of 0.05C to the lower cut-off voltage, and then charging the battery at a fixed rate of 0.05C to the upper cut-off voltage, recording the terminal voltage of the battery accordingly. When the extremely small current goes through internal resistance inside the battery, according to Ohm's Law the voltage generated should be negligible, hence the measured terminal voltage can be approximated as OCV. The SOC is calibrated to 100% when the battery is fully charged and 0% when it is fully discharged. As the cycle progresses, this OCV-SOC curve will have a slight shift, but generally the change is not significant. The specific steps are shown below in Figure 5.6.

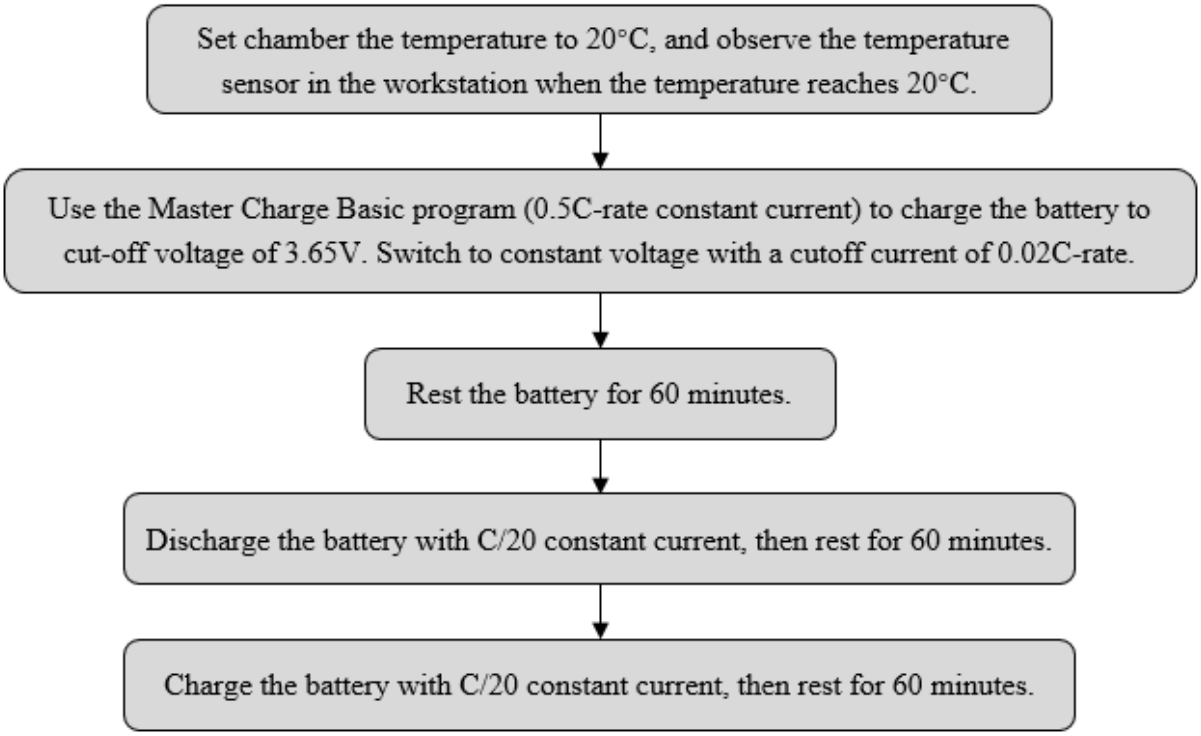


Figure 5.6: Flow Chart of OCV-SOC Experimental Steps.

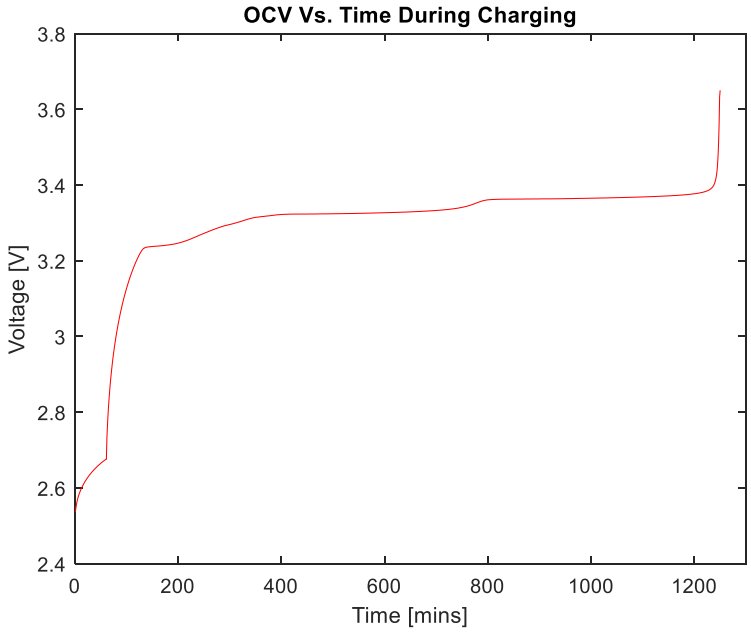


a) Measured Voltage during C/20 Charging.

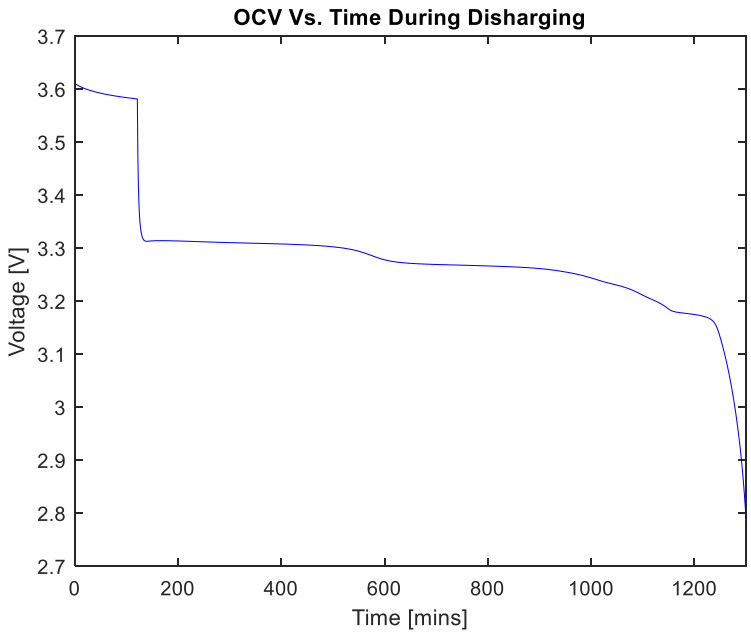


b) Measured Voltage during C/20 Discharging.

Figure 5.7: Voltage Changes with Applied C/20 Constant Current.

Figure 5.7 (a) and (b) show the voltage changes during C/20 constant current charging and discharging phases. Figure 5.8 shows the resampled OCV-SOC relationship during charging and discharging phases.

Experience shows that the battery needs to rest for a while after being charged and discharged to obtain a relatively stable and accurate voltage value. Therefore 60 minutes of relaxation time was added in the middle of each charge and discharge process, which was very necessary.

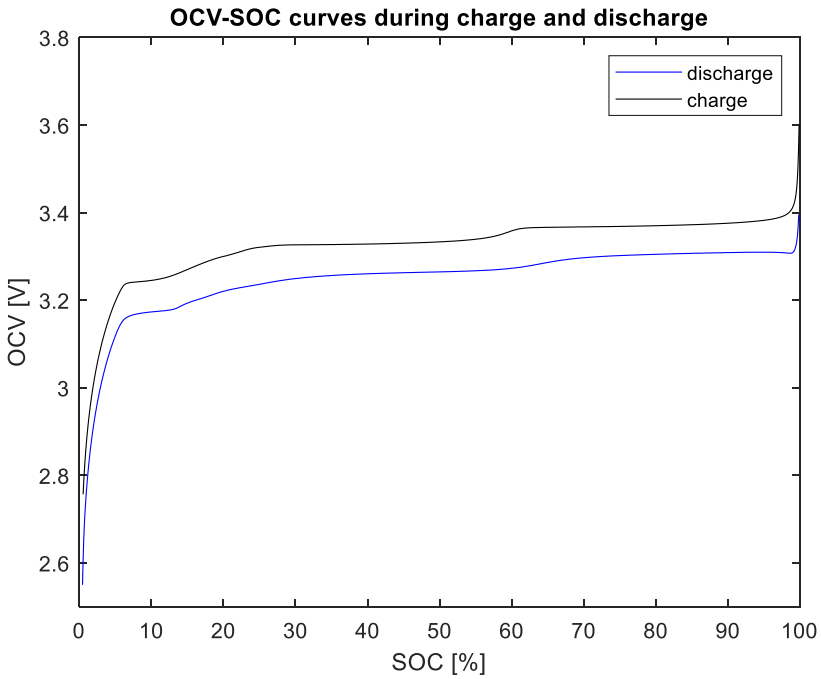


Figure 5.8: OCV-SOC Curves during Charging and Discharging After Resampling.

It can be observed the OCV-SOC curves of charging and discharging have deviations due to polarization and ohmic effects happening inside the battery, in order to neutralize these differences a common method is to average the charging curve and the discharging curve to obtain an actual OCV-SOC curve. The green line in Figure 5.9 is our battery's OCV-SOC relationship curve at room temperature. The OCV-SOC characteristics of a battery varies at different test temperatures.

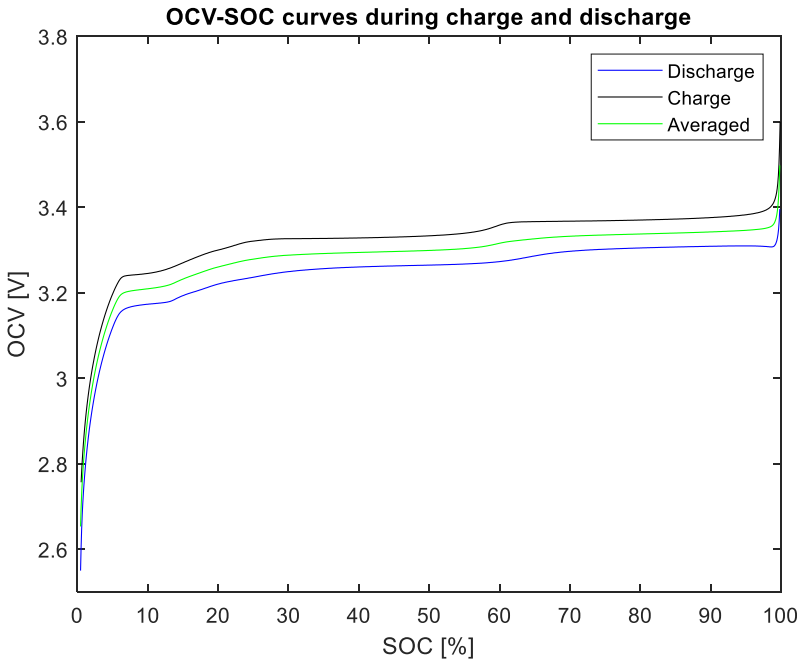


Figure 5.9: Averaged OCV-SOC Curve at Room Temperature (20°C)

The curve of this 280 Ah prismatic cell has a large slope at the beginning and end of the OCV-SOC test, where OCV changes significantly. While there is a flat stage from 10% SOC to 98% SOC, where OCV changes slowly and slightly. In order to quantify the relationship between SOC and OCV, a polynomial fitting function in Matlab was applied (polyfit) using the least squares method to fit the experimental data with the 9th degree fitting order to obtain the relationship[43], shown in equation (5.1). Figure 5.10 shows the comparison of the polynomial fitting curve and the experimental OCV-SOC curve. The Root Mean Square Error (RMSE) of 9th degree polynomial is shown in Figure 5.11, and the mean RMSE is 8.1 mV which is acceptable.

$$U_{OCV} = 2.2761\times10^{-15}\times SOC^{9} - 1.0875\times10^{-12}\times SOC^{8} + 2.2024\times10^{-10}\times SOC^{7} - 2.4602\times10^{-8}\times SOC^{6} + 1.6524\times10^{-6}\times SOC^{5} - 6.8246\times10^{-5}\times SOC^{4} + 0.0017\times SOC^{3} - 0.0244\times SOC^{2} + 0.1828\times SOC + 2.6719 \quad (5.1)$$

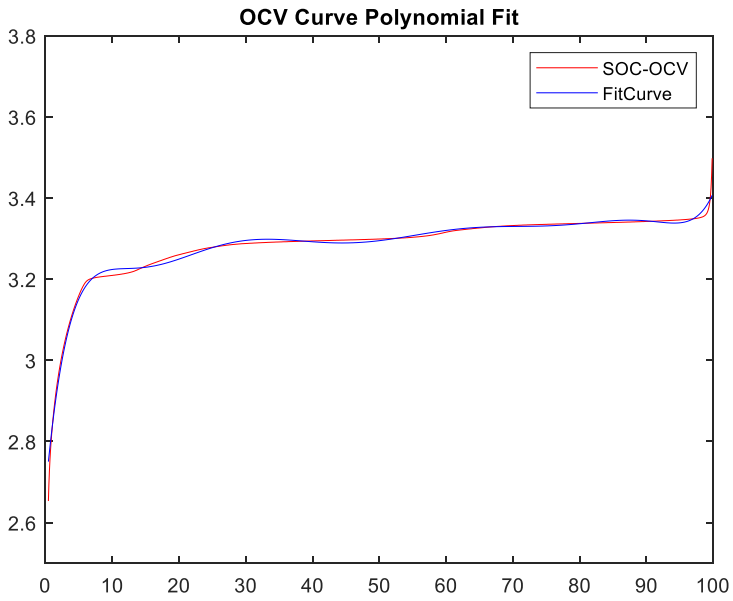


Figure 5.10: Polynomial Fitting OCV-SOC Curve.

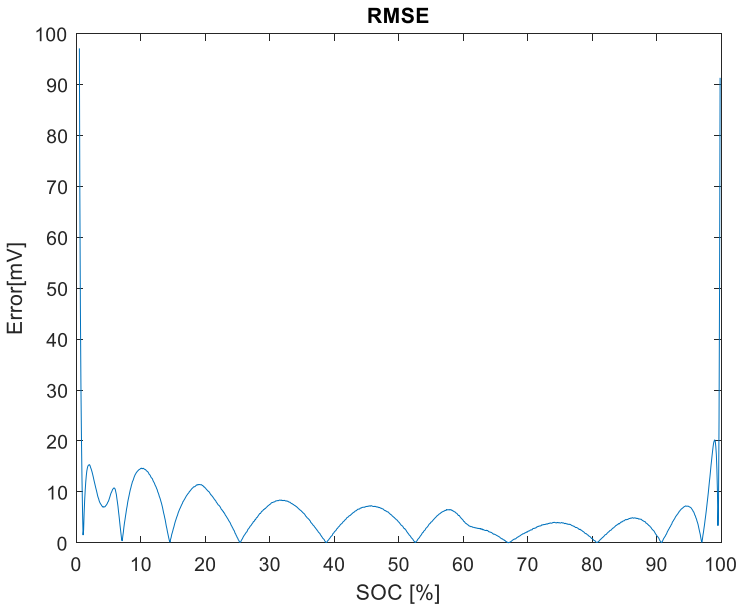


Figure 5.11: RMSE of 9th Degree Polynomial OCV-SOC Fit.

## 5.3 Different C-rates Test

From the above experiments it is observed that the measured voltage of the 280 Ah LFP battery cell drops rapidly at the beginning and the end of a discharge process, and the voltage stays almost flat in the middle. The discharging trends vary with different types of lithium-ion batteries, mainly in the slope of the OCV-SOC characteristic curve.

Constant current of 0.1C, 0.2C, 0.5C, and 1C were used to discharge the LFP 280 Ah prismatic cell, and then observe the OCV changes with the decreasing capacity. Because of the constant current discharging, Time axis can easily be converted to inverse of capacity. The specific steps are shown below in Figure 5.12:

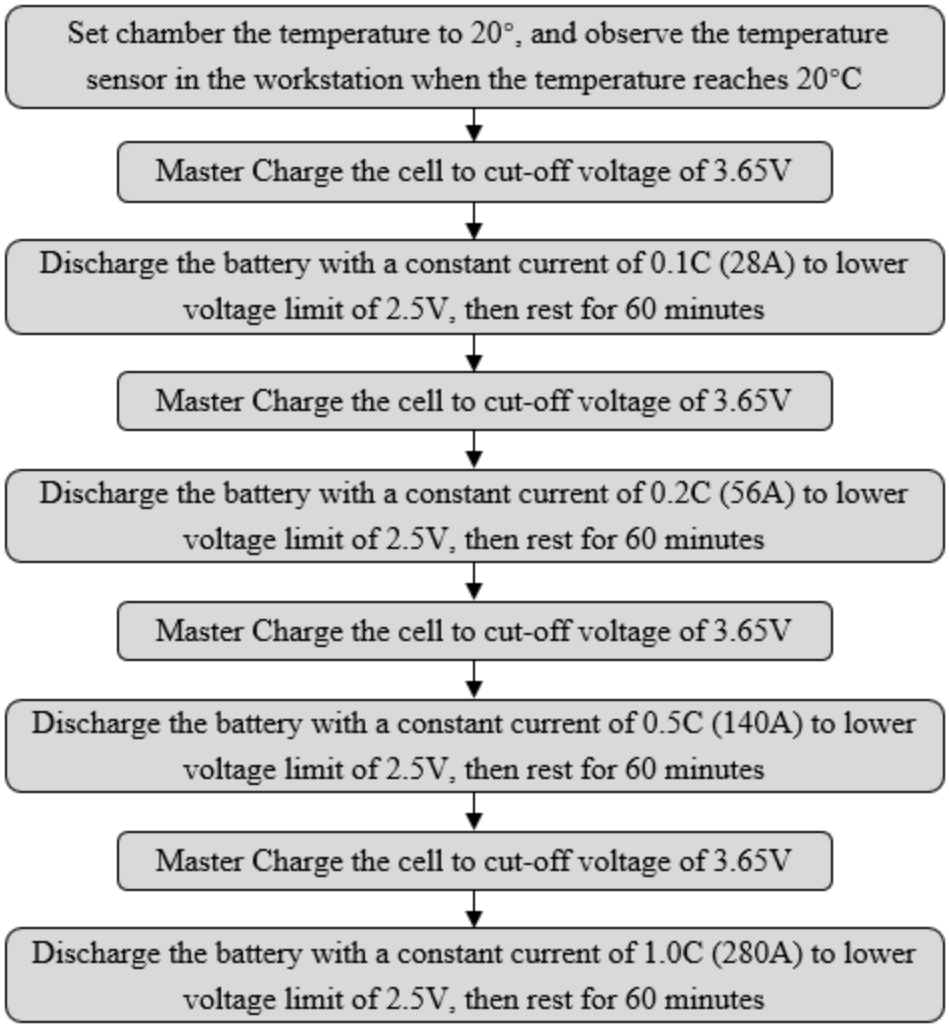


Figure 5.12: Flow Chart of Different C-rates Experimental Steps.

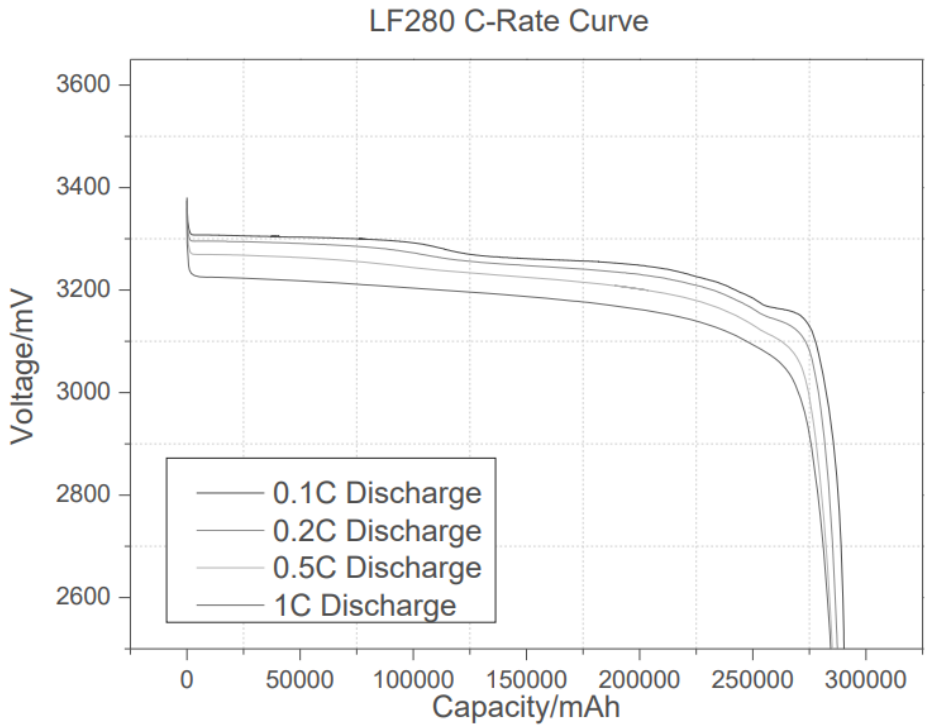


Figure 5.13: Discharge curves of LFP 280 Ah battery at different discharging ratio.

Figure 5.13 shows the discharge curves of LFP 280 Ah prismatic cell at different discharge rates of 0.1 C, 0.2 C, 0.5 C, and 1C at an ambient temperature of 20 ℃. It can be seen that there is always a stable discharge flat stage for different rates. In addition, the voltage platform decreases with discharge rates increasing. This is because larger current results in the voltage drop increasing due to the existence of the internal resistance inside the battery. On the other hand, a larger discharging current will also increase the polarization of the battery, which will also lower the voltage platform.

The discharged capacity of the LFP 280 Ah prismatic cell at different C-rates is shown in Figure 5.14. The battery capacity will decrease with increasing discharging rates. The discharged capacity is very close to the nominal 280 Ah at small 0.1 C-rate, while the discharged capacity at 1C-rate is only about 98% of its nominal capacity. This indicates that there is a certain negative correlation between the discharging rate and the battery capacity.

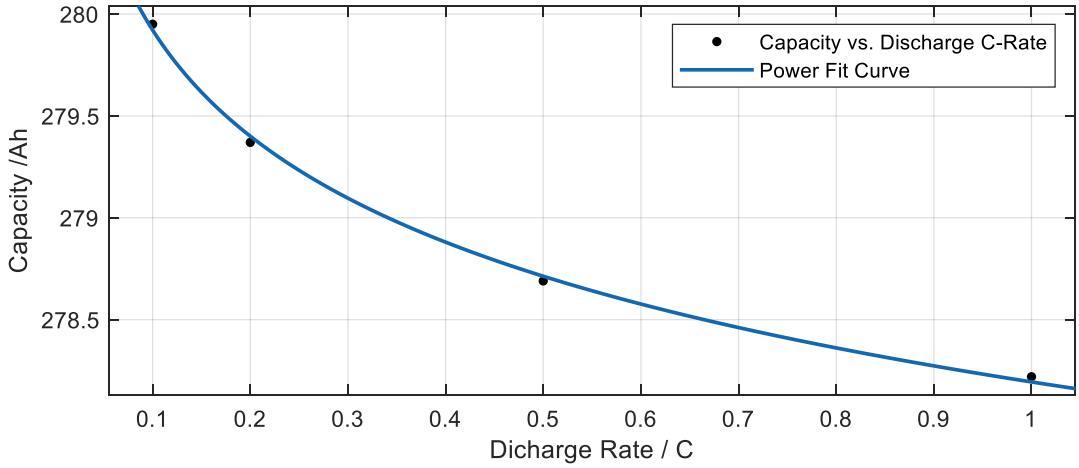


Figure 5.14: Curve Fit of Discharge Capacity at Discharging Rate.

Peukert [45] found an empirical formula for constant discharging current versus continuous discharging time/capacity in a constant current discharging test of lead-acid batteries, as follows:

$$I^P \times t = constant \qquad (5.2)$$

In equation (5.2), *I* is the discharge current, *p* is the Peukert coefficient, and *t* is the maximum discharging time. This equation gives the relationship between the discharging current and the maximum discharging time, but it is difficult to define the maximum discharging time in an actual application. Researchers have revised and linked the maximum discharge time to the discharged capacity of the battery, and introduced a power function relationship between the discharged capacity and the discharging current. They concluded that a power function relationship was satisfied between the discharge capacity and the discharging C-rates. [45]

Curve-fitting the power function relationship of discharged capacity and discharging C-rates in Figure 5.14 results in the following equation.

$$\mathrm{Q} = 279.89 \times K^{-0.002105}, X^2 = 0.9915 \qquad (5.3)$$

In equation (5.3), Q is the discharged capacity, K is the discharging C-rates, and $X^2$ is the correlation coefficient of the curve-fitting, which indicates the degree of fit to the original data, and its value is between 0 and 1. The larger $X^2$ is, the better the fit is. In Figure 5.14, the correlation coefficient between capacity and discharging rate is 0.9915 after fitting with a power function, which indicates that the capacity and discharging rate are correlated to the power function rule.

## 5.4 Improved Pulse Test and Parameter Identification

The equivalent circuit method was used to model and simulate the response of the LFP 280 Ah prismatic cell. The equivalent circuit model consists of several circuit elements, and the parameters of each element needs to be determined through pulse tests and parameter optimization. By observing its dynamic characteristics in a current pulse, analyzing and processing the curves and data of current and voltage, the ohmic resistance and polarization parameters with SOC can be obtained. The aging characteristics of the lithium-ion battery can also be evaluated by continuous pulse tests.

Hybrid Pulse Power Characterization (HPPC) is the most widely used pulse test, which is the process of applying a pulse discharge, followed by rest time, and then repeating these steps until the battery discharge cut off. An example HPPC test current is shown in Figure 5.15, starting with an initial SOC at 90%.

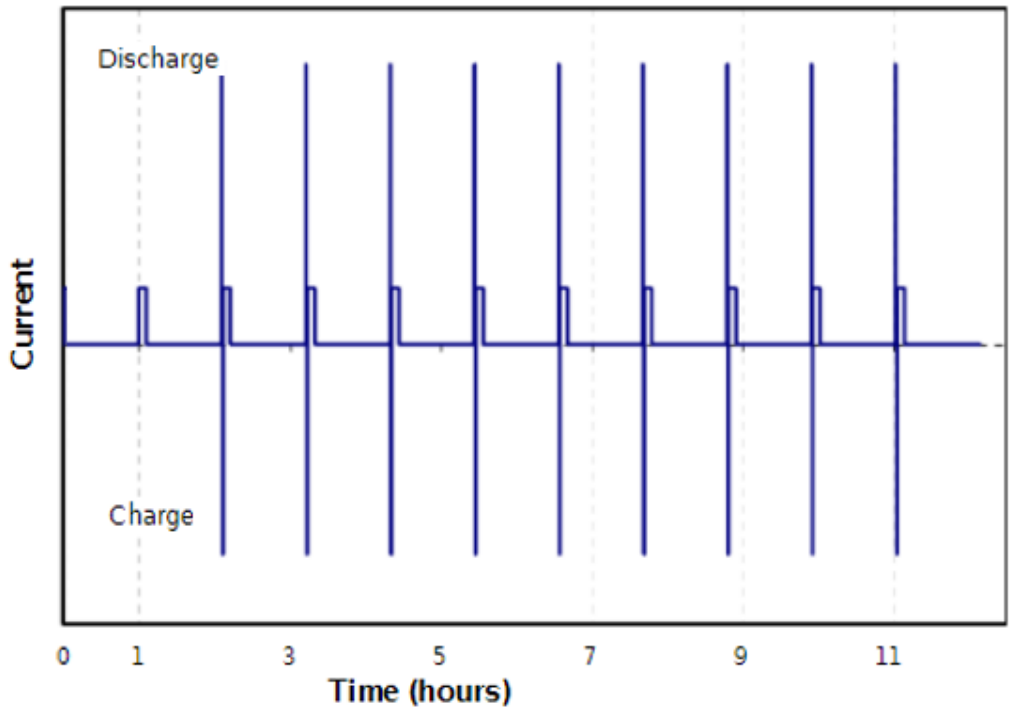


Figure 5.15 Current Profile of One Typical HPPC Test.

The typical HPPC test applies several pulses, and accordingly obtains a set of model parameters at every 10% SOC drop. The model parameters change with SOC and are updated through this process.

In addition, in the process of using conventional HPPC test data for model parameter identification, one set of data is used to represent the charging and another for the discharging condition. It is necessary to differentiate model parameters for charging from discharging. In this thesis a pulse test with a modified number of pulses is proposed in Figure 5.18 and 5.19. The pulse width for the 280 Ah LFP high-capacity battery cell was accordingly changed, and the "charge pulse test" data was used to identify the characteristic parameters in the charging direction, while in the discharging direction another "discharge pulse test" data was used. In this way, the actual dynamic variation of the battery can be described more accurately [46]. Figures 5.16 and 5.17 show the experimental steps of the improved pulse discharge test and charge test respectively.

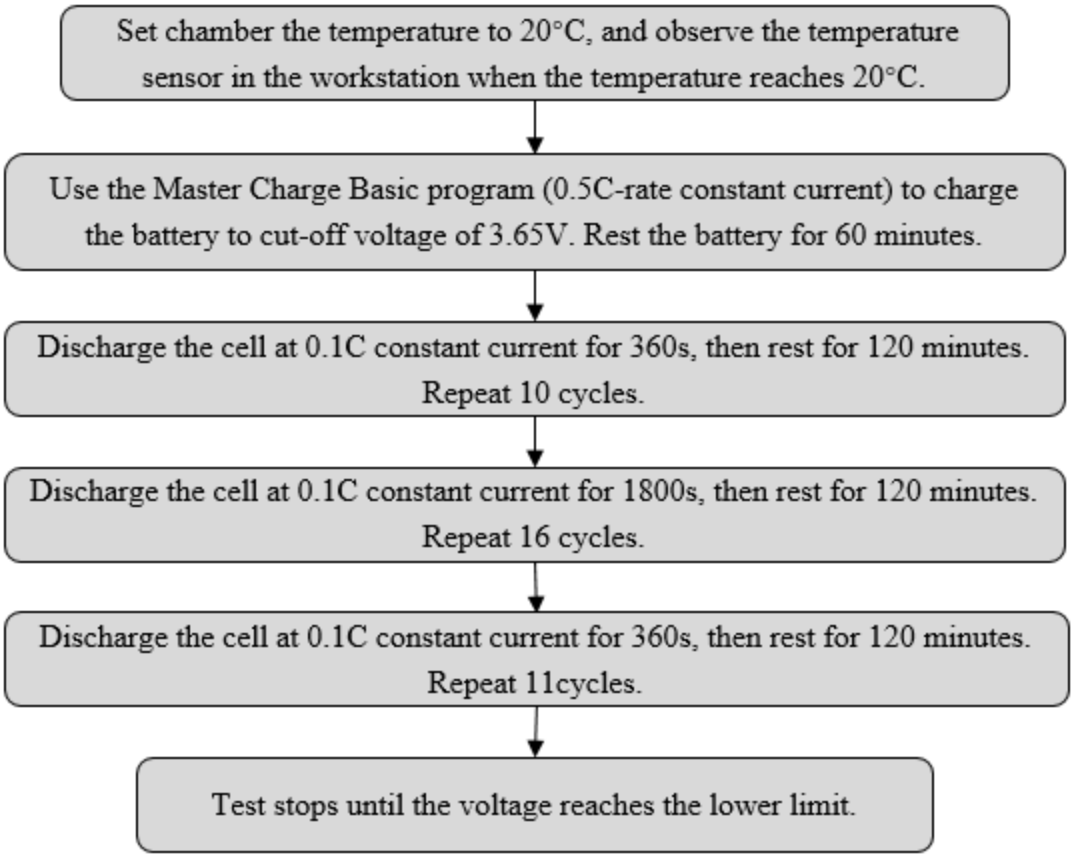


Figure 5.16: Flow Chart of Improved Pulse Discharge Test.

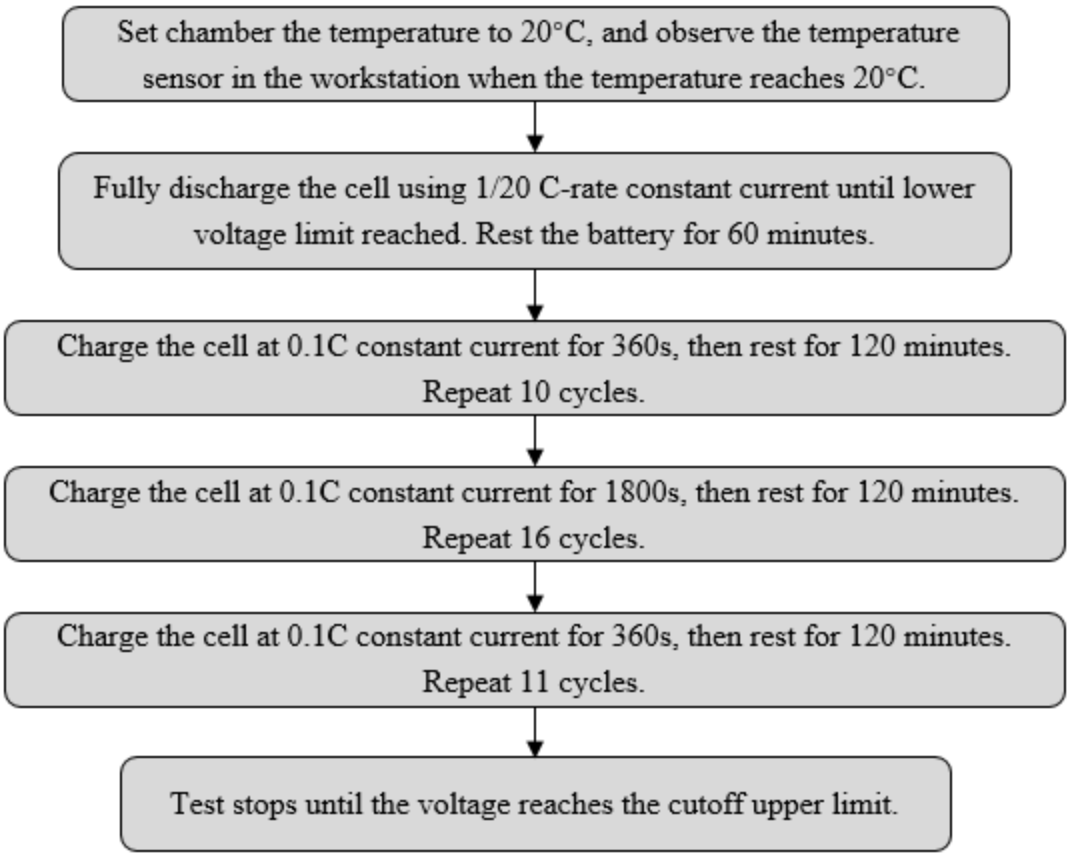


Figure 5.17: Flow Chart of Improved Pulse Charge Test.

The model parameters and the actual characteristics of the LFP 280Ah battery change significantly in between the 0%-10% and 90%-100% SOC intervals. The proposed improved pulse test applied more pulses in these two intervals, where the pulse width lasted 1% SOC, while in the remaining 10%-90% SOC the pulse width was 5% SOC.

The improved pulse test divides SOC into 36 segments by percentage, taking the pulse charge test as an example: from 0% to 10% SOC, a 10-segment test was conducted with a fixed charging rate of 0.1C pulse current (28 A), each segment completed 1% SOC charging. From 10% to 90% SOC, a 16-segment test was conducted with a fixed charging rate of 0.1C pulse current (28 A), each segment completed 5% SOC charging. From 90% to 100%, another 10-segment test was

conducted with a fixed charging rate of 0.1C pulse current (28 A), each segment completed 1% SOC charging. The measured voltage during each segment was recorded at each SOC point, combining with the battery equivalent circuit model to identify the model parameters [47].

The improved pulse test split the entire experimental process into 36 smaller phases, making it easier to obtain the parameters for the model. Experimental data profiles of improved pulse charging tests and discharging tests are presented in Figures 5.18 and 5.19 respectively. This method proved to be more suitable for LFP batteries to collect the parameters of the equivalent circuit model. In chapter 6 the data from the improved pulse tests will be analyzed and a simulation model is developed for the LFP 280 Ah prismatic battery cell.

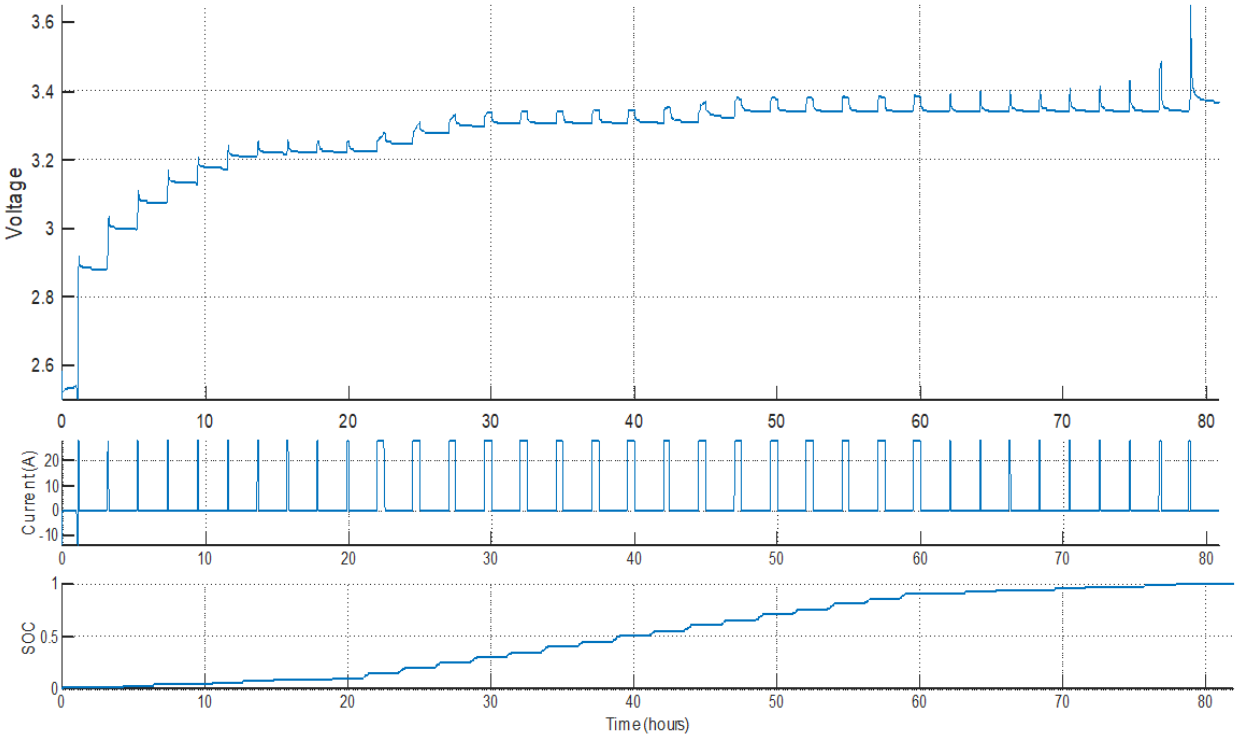


Figure 5.18: Experimental Data Profiles of Improved Pulse Charging Test.

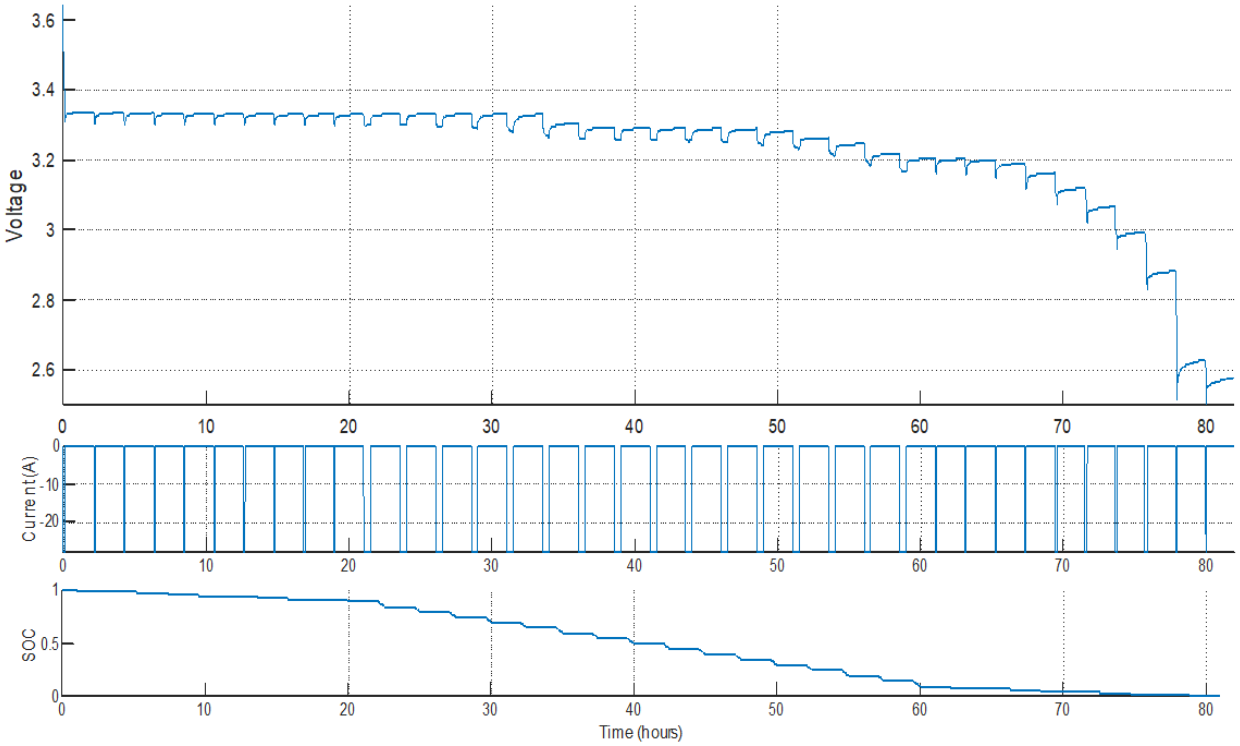


Figure 5.19: Experimental Data Profiles of Improved Pulse Charging Test.

# Chapter 6

# Battery Model and Parameter Identification

## 6.1 Battery management system

The main function of a Battery Management System (BMS) is to monitor the operation and the health condition of the battery, and control the operation of the battery to meet the performance and safety requirements [48]. The BMS needs to estimate SOC of the battery, maintain cell balancing, manage battery operation to prevent overheating, and ensure operational safety. The BMS functions are shown in Figure 6.1. The BMS is regarded as a core technology for the electric vehicle industry, in which the accuracy of SOC estimation determines the merits of a BMS.

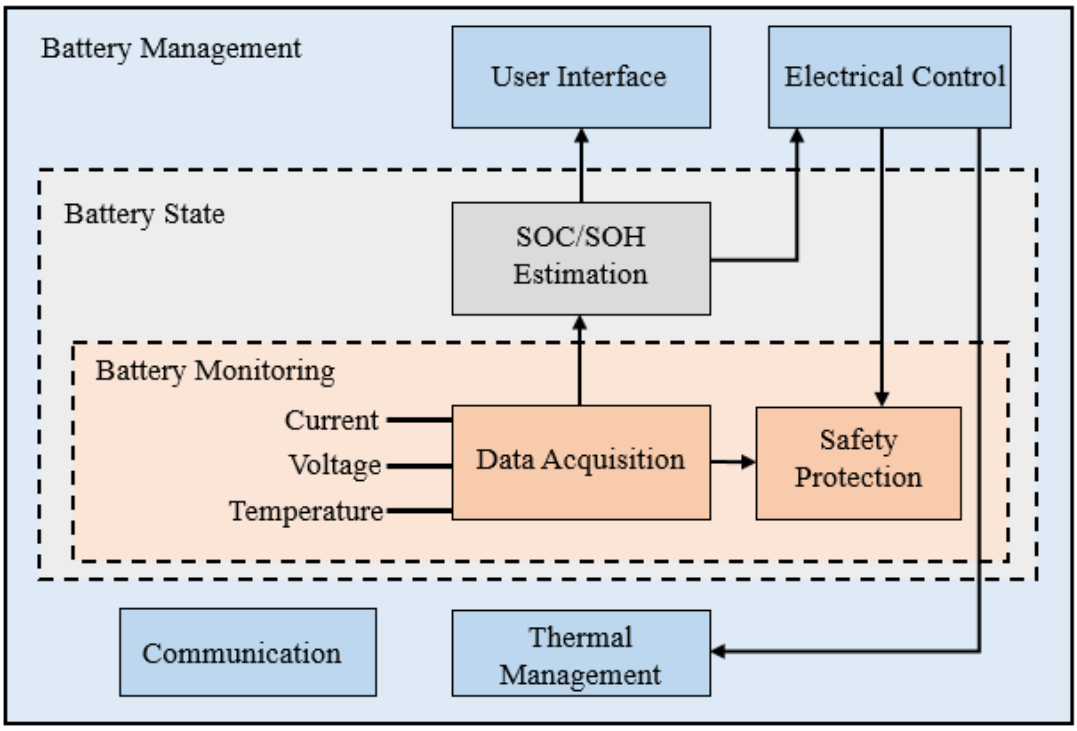


Figure 6.1: A Generic Structure of Battery Management System.

## 6.2 Lithium-ion battery studying model

Battery model models are instrumental to SOC estimation key to the efficient operation of BMS. Current battery models can be divided into equivalent circuit models, empirical, and electrochemical models [48].

Electrochemical models are based on the chemical reactions inside a battery, and describe the internal reactions in a mathematical form during the charging and discharging process [49]. Due to the complexity of the chemical reaction, the electrochemical model is correspondingly complex and needs to be simplified before it can be used. Electrochemical models have also been proposed to describe the thermal characteristics and aging process of the battery and updating the battery parameters accordingly [49] [50].

When describing the characteristics of the battery, the actual accuracy of models are not usually high. Therefore, the electrochemical models are more commonly used to guide the development and production of the battery, and less used in the BMS.

The equivalent circuit model uses a circuit network to describe the characteristics of the battery. It is composed of voltage sources, resistors, capacitors, and other circuit elements [51]. The equivalent circuit model does not explicitly capture the internal chemical reactions of a battery, and has a relatively simple structure, making it easy to compute. Because of its simplicity, it is widely used for SOC estimation in battery management systems.

In this thesis, a first-order Thevenin model is used to establish the equivalent battery model of a 280 Ah prismatic cell. [52] The proposed improved pulse charge and discharge tests are conducted on the battery to obtain the model parameter. The model is then verified experimentally by using Urban Dynamometer Driving Schedule (UDDS) simulation.

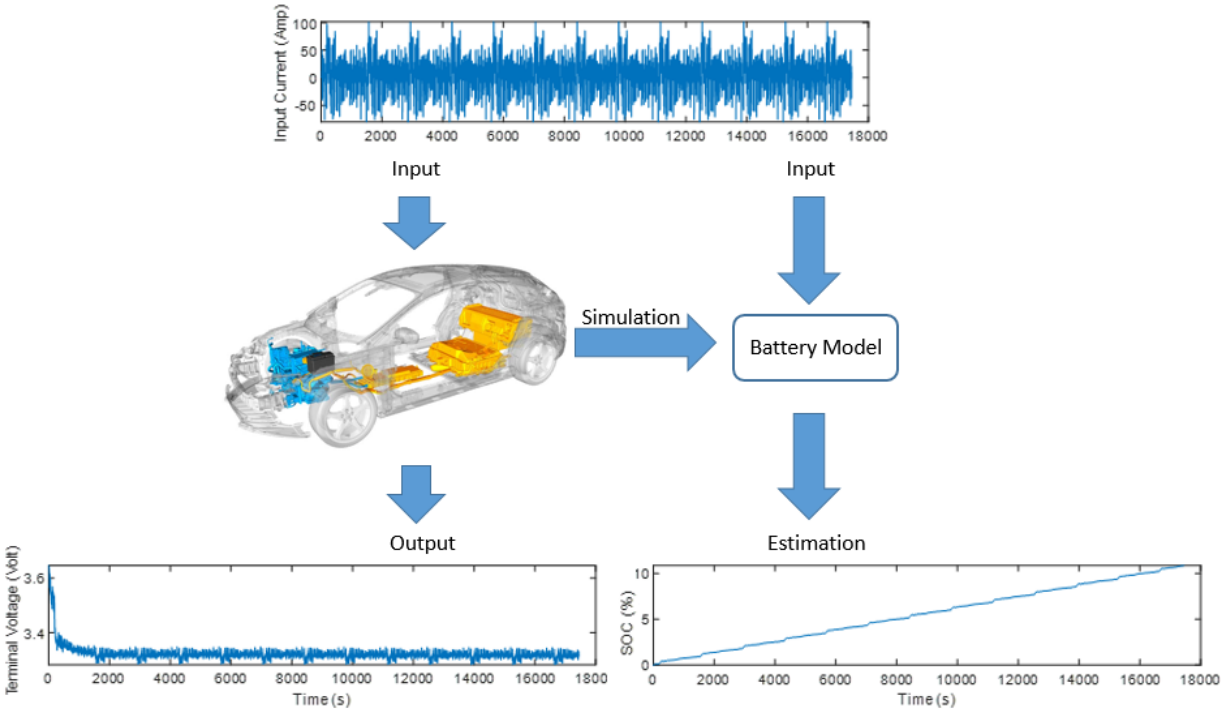


Figure 6.2: Schematic of Battery Model Simulation.

## 6.3 Equivalent Circuit Model for Lithium-ion Batteries

A battery model is a mathematical representation of battery characteristics. Battery models are categorized as electrochemical, empirical, or equivalent circuit models. The equivalent circuit model has a simple structure and good accuracy, which is more suitable for BMS implementations.

The equivalent circuit model needs to consider the following aspects:

1. The model parameters should have a clear meaning, and to a certain extent should be consistent with the reaction mechanism of the battery.
2. The model should have good accuracy and adaptability, and describe the battery characteristics under a variety of conditions.
3. The model structure should be reduced to its level of dynamic significance.

At present, the most commonly used equivalent circuit models are mainly Rint model, Thevenin model, and General Non-Linear (GNL) comprehensive model.

### 6.3.1 Rint Model

The Rint model is the simplest battery model, also known as the internal resistance equivalent circuit model, first introduced by the Idaho National Laboratory. It can be viewed as a series connection of a resistor with an ideal voltage source [49], as shown in Figure 6.3.

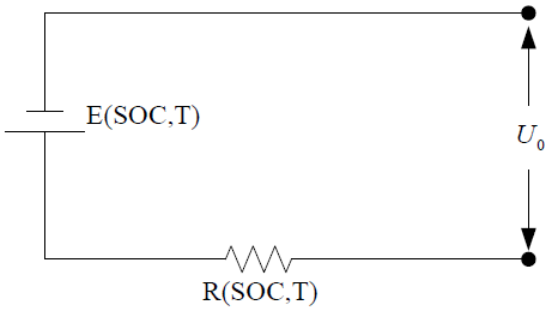


Figure6.3: Equivalent model of internal resistance.

Where E is from the ideal voltage source and is equal to the open circuit voltage; R is the internal resistance of the battery; and $U_0$ is the terminal voltage, which is measured in real time. The ideal voltage source and the internal resistance are treated as a constant in the model, which leads to insufficient accuracy, because the electrochemical reaction will change the concentration of the internal electrolyte solution, and the internal resistance of the battery is actually a time-varying state. This is not reflected in the simple equivalent circuit model. The model therefore is only suitable for use in constant current charging and discharging.

### 6.3.2 Thevenin Equivalent Circuit Model

The Thevenin equivalent circuit model, also known as the RC Model, takes into account that the chemical reactions inside the battery are nonlinear and adds RC parallel pairs to the internal resistance equivalent model[53][54]. The model is shown in Figure 6.4.

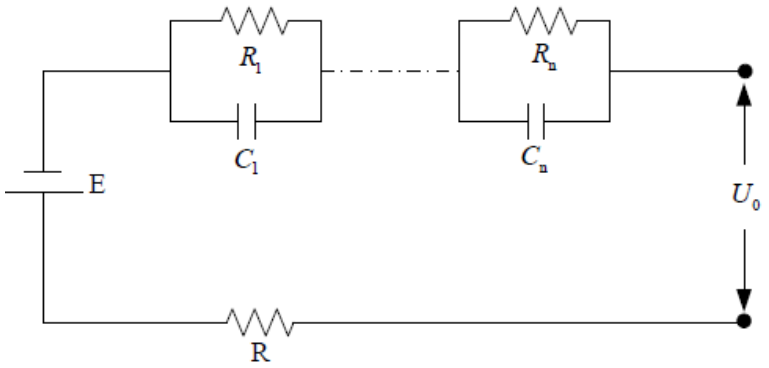


Figure6.4: Thevenin equivalent circuit model.

The Thevenin battery model consists of an ideal voltage source E, several RC pairs, and an internal resistance R, as shown in Figure 6.4. R is the ohmic internal resistance of the battery, which is used to describe the purely resistive characteristics of the battery. The variables $R_1$ and $C_1$ in the RC link are the polarization resistance and the polarization capacitance respectively, which are used to describe the polarization characteristics caused by the electrode deviating from the equilibrium electrode potential during charging and discharging. The number of RC pairs indicates the order of the Thevenin model. A higher order provides a higher accuracy battery model, but the calculation will be more complex accordingly. Obviously, it is necessary to select the appropriate numbers of RC pairs in accordance with the actual situation.

Compared with the Rint model, the Thevenin battery model has extra RC pairs, which make up for the shortcomings of the Rint model in terms of dynamic characteristics. The Thevenin battery model parameters are easy to obtain, and the structure is simple and clear. It is currently a widely used circuit model. However, since E is an ideal voltage source, the Thevenin battery model cannot express the process of the open circuit voltage variation with SOC, so this model is only suitable for describing battery characteristics under a specific SOC value, and the dynamic characterization has some errors across the whole charge/discharge cycles.

### 6.3.3 General Non-Linear (GNL) Comprehensive Model

The GNL comprehensive model adds parallel resistor and series capacitors on the basis of the Thevenin equivalent model [55]. The equivalent circuit is shown in Figure 6.5.

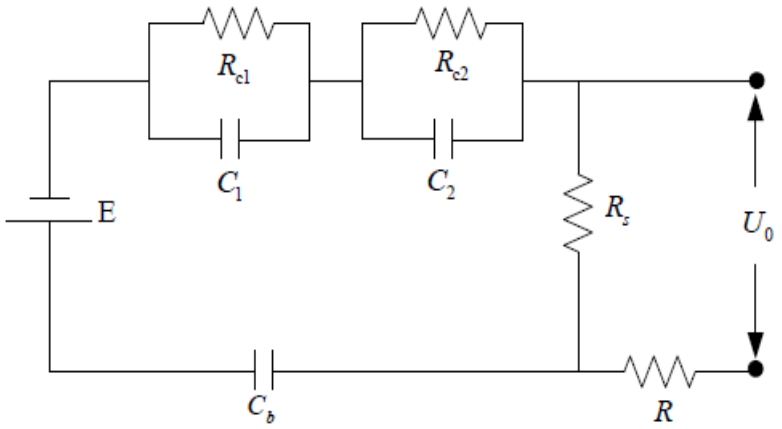


Figure 6.5: GNL Comprehensive Model.

The Thevenin equivalent circuit model considers polarization effect but does not consider the self-discharge of the battery. The GNL Comprehensive Model introduces the self-discharge internal resistance $R_s$ representing the self-discharge effect, because the open-circuit voltage is related to the charge level of the battery, and so the introduction of capacitor $C_b$ represents the open circuit voltage affected by SOC [56]. The accuracy of this model is high, but it is difficult to identify the parameters and build the simulation model.

In summary, the Rint model is suitable for a simple constant current charging and discharging cycle whose real-time errors cannot be neglected. The Thevenin model uses RC parallel pairs that can reduce polarization and concentration errors, while the number of the RC pairs depends on the complexity, age and condition of the battery. The GNL model adds a battery self-discharge pair but its parameters are hard to identify and need to be obtained through careful measurements and experimentation. In order to more accurately characterize the variation of the open-circuit voltage with SOC, the ideal voltage source in the Thevenin model could be regarded as a controlled voltage source related to SOC, and their relationship can be extracted as an OCV-SOC relationship, so that the Thevenin model has a high accuracy over the whole SOC cycle of the battery. The first-order Thevenin model is used in this thesis after considering its computational complexity and accuracy.

## 6.4 Parameter Identification

The first-order Thevenin model is the equivalent circuit model with only one RC pair, shown in Figure 6.6.

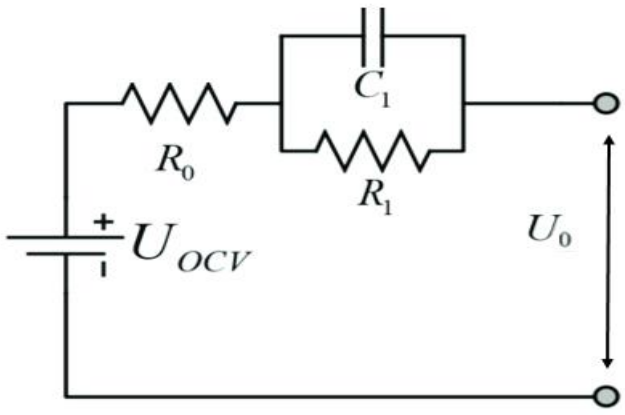


Fig.6.6 First-order RC equivalent circuit model.

Where $U_0$ refers to the terminal voltage of the battery, $U_{OCV}$ refers to the open-circuit voltage of the battery, $R_0$ represents the ohmic internal resistance, $R_1$ represents the polarization resistance, and $C_1$ represents the polarization capacitance. Considering that the ohmic resistance values are different during charging and discharging cycles, an improved first-order RC equivalent model is applied.

### 6.4.1 Improved First-Order RC Model

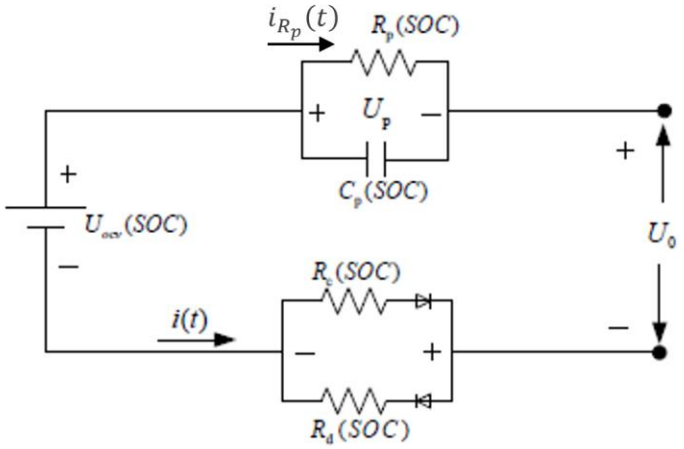


Fig.6.7: Improved first-order RC equivalent circuit.

As shown in Figure 6.7, $R_c$ represents the ohmic internal resistance of the charging cycle while $R_d$ represents this for the discharging cycle. The charging circuit and the discharging circuit are separated by two diodes. The equivalent circuit equations of the battery are contained in equations (6.1) to (6.4). The SOC (t) in the following equations reflects its time dependence. [57].

Equivalent circuit discharging equation is:

$$U_0 = Uocv(SOC(t)) - R_p * i_{R_p}(t) - R_d(t) * i(t) \qquad (6.1)$$

Equivalent circuit charging equation is:

$$U_0 = Uocv(SOC(t)) - R_p * i_{R_p}(t) - R_c(t) * i(t) \qquad (6.2)$$

Polarization branch current relationship equation is:

$$i_{R_p}(t+1) = exp(-\frac{1}{R_p C_p}\Delta t) * i_{R_p}(t) + (1 - exp(-\frac{1}{R_p C_p}\Delta t)) * i(t) \qquad (6.3)$$

SOC (t) is time variant as follows:

$$SOC(t+1) = SOC(t) - \frac{\Delta t}{Q}\eta * i(t) \qquad (6.4)$$

Where SOC[t] is the value of the SOC at time t, Q is the nominal capacity of the battery, and $\eta$ is the discharge efficiency.

In order to better identify the parametric values of RC pairs and estimate SOC effectively at each stage of charging and discharging, the proposed improved pulse charge and pulse discharge test was conducted on the 280 Ah LFP prismatic cell.

### 6.4.2 Modified Pulse Width and Pulse Numbers

Due to the huge amount of experimental data, in order to better analyze and estimate the parameters in the model the entire experimental process was split into smaller pulses, making it easier to observe. In order to ensure that the performance of the tested battery at different SOC phases can be well presented during each pulse, uneven pulse width was applied, and the overall test was broken down into 36 pulse breakpoints [56][57]. The voltage and current curves of the 36-pulse tests are shown in Figure 6.8. The beginning 10% and ending 10% period both adopted an interval width of 1% SOC, while in the middle 80% period an interval width of 5% SOC was selected. As such, more data was measured in the ranges where the battery's state changed significantly, which is better for characterizing the performance of the battery cell.

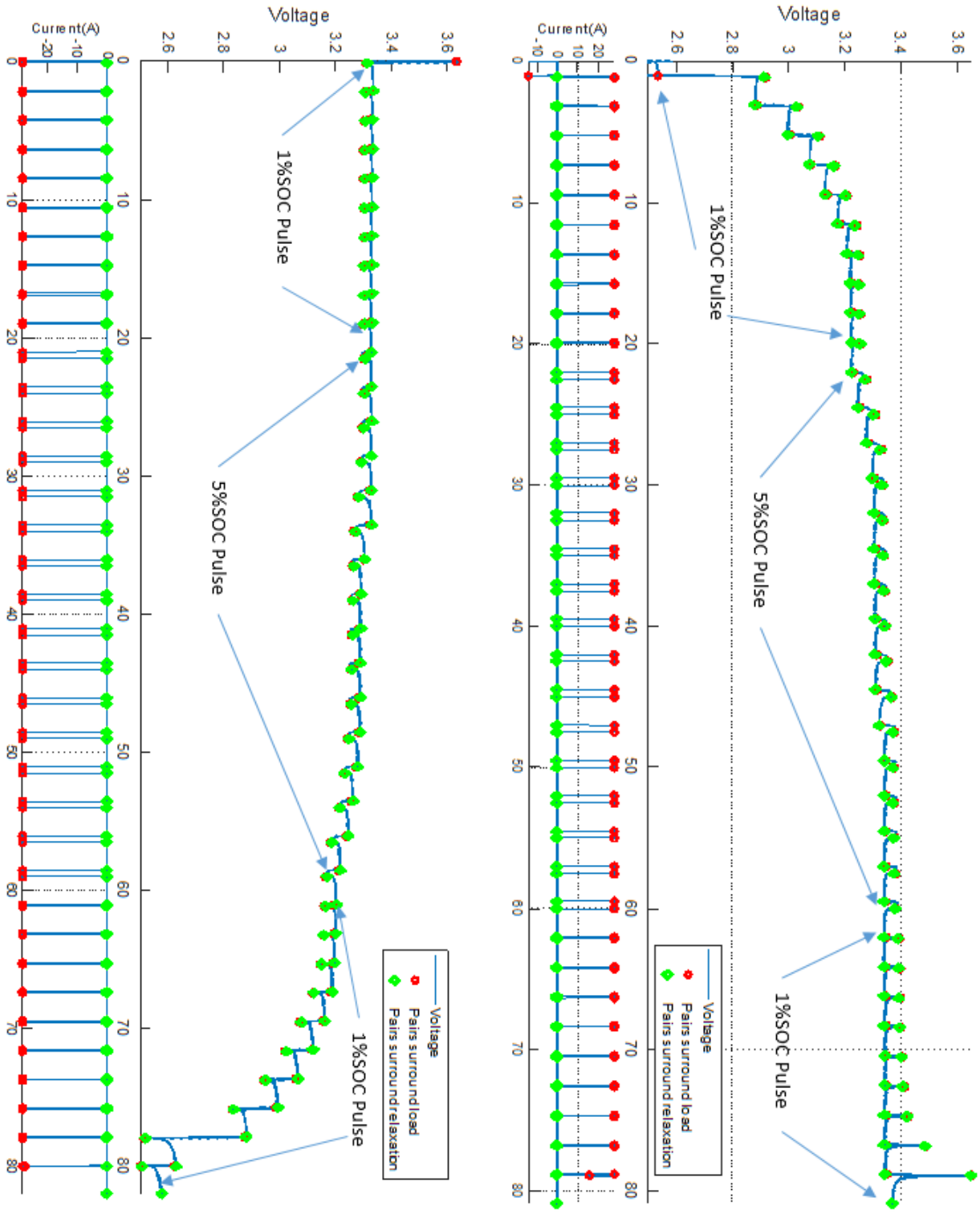


Fig 6.8 (a) 1% - 5% - 1% SOC Pulse Discharge. (b) 1% - 5% - 1% SOC Pulse Charge.

### 6.4.3 Parameter Estimation

To better understand the layered pulse, the single pulse in the 60% SOC phase during a discharge cycle is used as example. As can be seen from Figure 6.9, a single pulse can be divided into three segments according to the variation of the measured battery voltage:

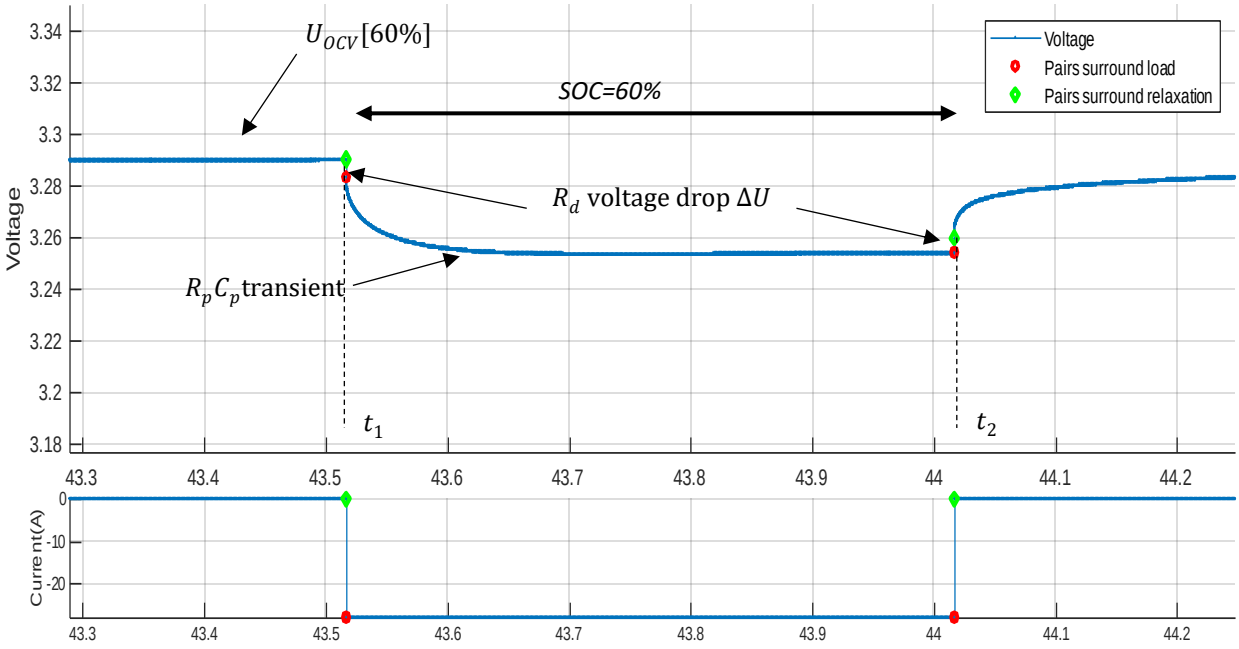


Fig 6.9: Pulse Discharge single wave at 60% SOC.

This includes:

1- Static equilibrium period $t_1$ and $t_2$: take $t_1$ as example, the battery pulse discharge current rises instantaneously from 0 A to 28 A, at which time the battery terminal voltage drops to near 3.29 V. For a moment the battery is neither discharged nor charged, and the capacitor voltage does not change abruptly, but the terminal voltage of ohmic internal resistance changes instantaneously at $t_1$, producing a small voltage drop $\Delta U$, according to Ohm's law:

$$\Delta U = I * R_d \qquad (6.6)$$

2- Discharge pulse period $t_1$- $t_2$:at this stage the battery is discharged with a constant current of 28 A. The voltage drop is composed of two parts: the ohmic voltage and the polarization voltage. Due to the sudden increase of the discharge current, the ohmic voltage drops quickly and the slope of the curve is large, then the $R_pC_p$ parallel pair takes charge, the polarization voltage decreases exponentially and so the slope of the curve decreases gradually later at this stage.

3- Relaxation period: after $t_2$, the pulse current drops to 0A again. No current goes through the ohmic resistance $R_d$ so the ohmic voltage can be ignored. The battery open circuit voltage $U_{OCV}$ should be equal to the measured terminal voltage plus the terminal voltage of the $R_pC_p$ pair. In the meanwhile the capacitor tends to discharge within $R_pC_p$ parallel circuit, causing the terminal voltage of the $R_pC_p$ pair to be exponentially decreasing, while the measured terminal voltage will increase conversely in the relaxation stage until it reaches $U_{OCV}$ under this SOC.

### 6.4.4 Initial Values of Model Parameters

The improved equivalent circuit model accounts for the changing value of the ohmic resistance with respect to charging and discharging operation. In order to estimate the initial value of the ohmic resistance, pulse tests were conducted under 36 small segments with a pulse width of 1% - 5% - 1% SOC. 36 values of the ohmic resistance were calculated and are shown in Figure 6.10. They were averaged to obtain an initial value for the improved model setup in Equations 6.7 and 6.8. The following assumptions were made:

- Any prior relaxation had settled.
- Starting SOC value was 100% for the discharge cycle and 0% SOC for charge cycle.

- Starting voltage of the first pulse equals the OCV at 100% SOC for the discharge cycle, and the starting voltage equals the OCV at 0% SOC for charge cycle.

$$\overline{R_c} = \sum R_c(i) = 0.2302\ \text{m}\Omega \qquad (6.7)$$

$$\overline{R_d} = \sum R_d(i) = 0.2296\ \text{m}\Omega \qquad (6.8)$$

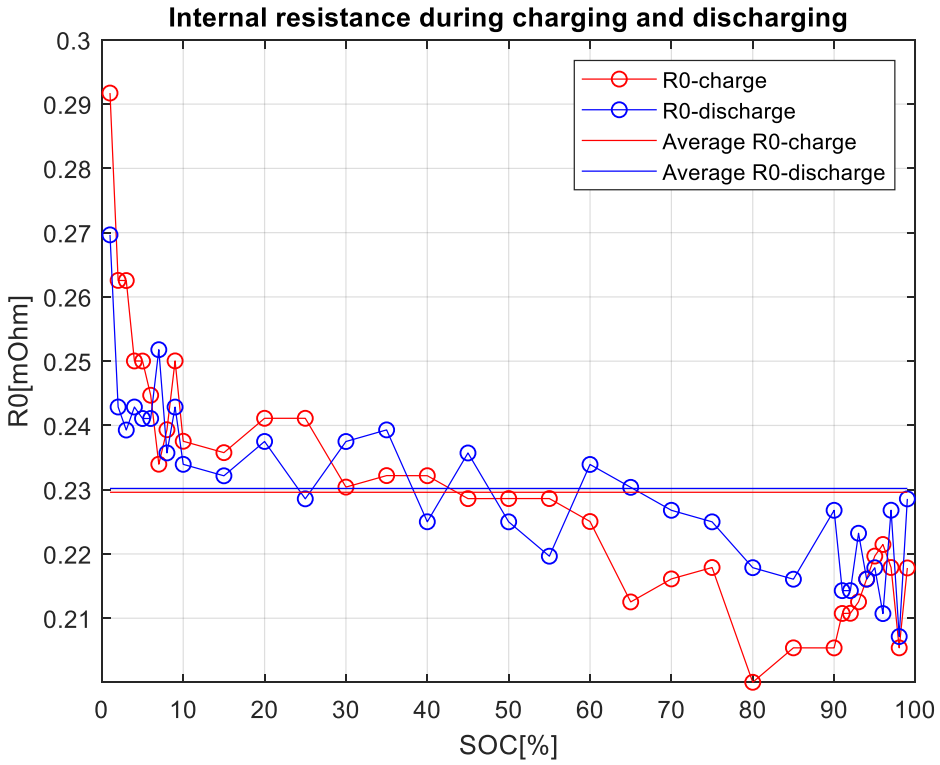


Figure 6.10: Ohmic Internal Resistance during Charging and Discharging Pulse Tests.

The initial values of the polarization parameters $R_p$ and $C_p$ cannot be obtained directly, while the polarization parameter $R_p$ can be assumed to be within an order of magnitude of the ohmic internal resistance $R_0$ and taken to have a similar value. The initial $R_p$ was taken directly as 0.23 mΩ, while for the initial value of polarization capacitance $C_p$ the empirical value of 2000 KF was chosen. The Genetic Algorithm (GA) optimization method was then used to perform parameter optimization

on these two parameters to make the equivalent circuit model fit the actual performance of the battery cell.

## 6.5 The Optimization Process using Genetic Algorithms

The Genetic Algorithm (GA) is an optimization method that imitates the mechanism of natural selection and the Darwinian evolution theory. It is a method to search for optimal solutions by simulating the natural evolutionary process as shown in Figure 6.11.

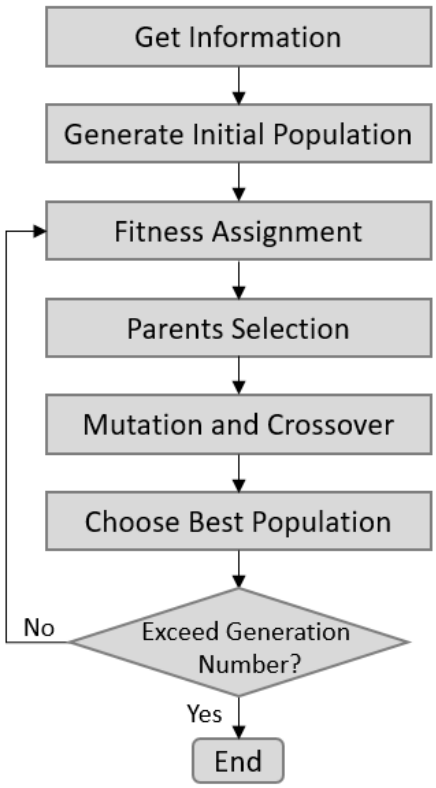


Figure 6.11: Flow Diagram of Regular Genetic Algorithm.

Based on the empirical assessment of the initial population, the approximate solution with increasingly better fitness is generated by generation-by-generation evolution according to the

principle of fitness and diversity. In each generation, individuals are selected to become parents according to their fitness, and the population representing the new set of solutions is generated by combining the parents using a crossover operation while injecting diversity by using random mutation. As the number of generations' increases, the individuals in the population get closer to the optimal value. [61]

In this research, a first-order equivalent circuit battery model is parametrised using by using experimental data and the Genetic Algorithm shown in Figure 6.12.

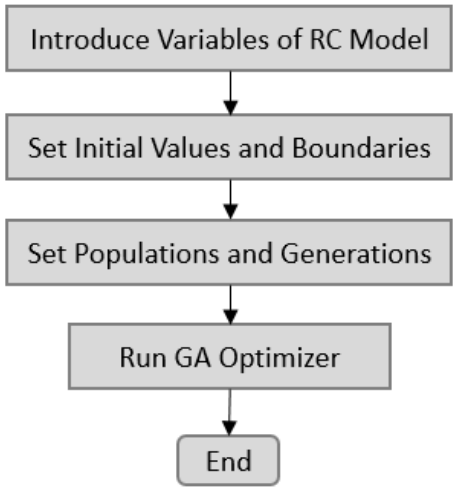


Figure 6.12: Flow Diagram of Genetic Algorithm Parameters Optimization.

**Building the battery simulation model**

The first-order RC model was chosen as the object of study in this thesis because it has fewer parameters to identify and better for its use in a BMS. The Simulink simulation platform was used to build the first-order RC equivalent circuit battery model as shown in Figure 6.11. By applying the corresponding identified parameters to the model, the simulation output results were compared

with the actual experimental results of the battery cell to verify if the model would correctly reflect the actual working process of the tested 280 Ah prismatic battery cell. [58] [60]

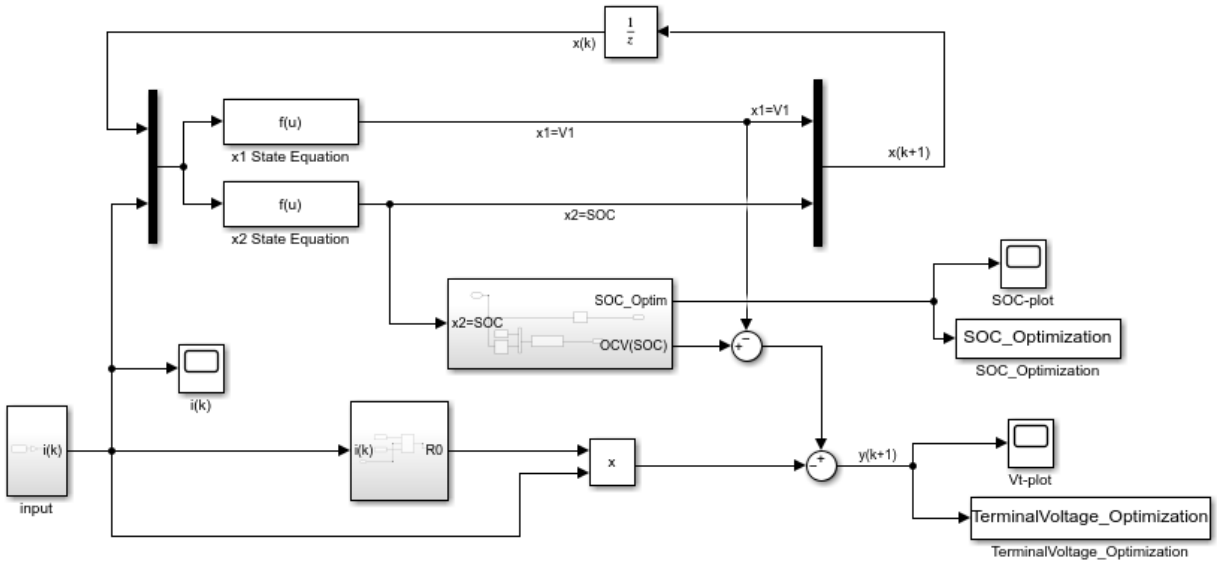


Figure 6.13 Improved First-Order RC Equivalent Circuit Battery Model.

## 6.6 Validation using Driving Schedule

Considering that the operating conditions used for parameter identification differ significantly from the actual driving conditions of the vehicle, the battery equivalent model has practical significance only if it can reflect the actual driving conditions of the electric vehicle, keeping relative error within an acceptable range. United States Environmental Protection Agency (EPA) developed several driving schedules for assessing vehicle emissions and fuel economy. Among these, the Urban Dynamometer Driving Schedule (UDDS) is the most commonly used. [59] [62] Figure 6.14 shows the Speed-Time characteristics of the UDDS drive cycle.

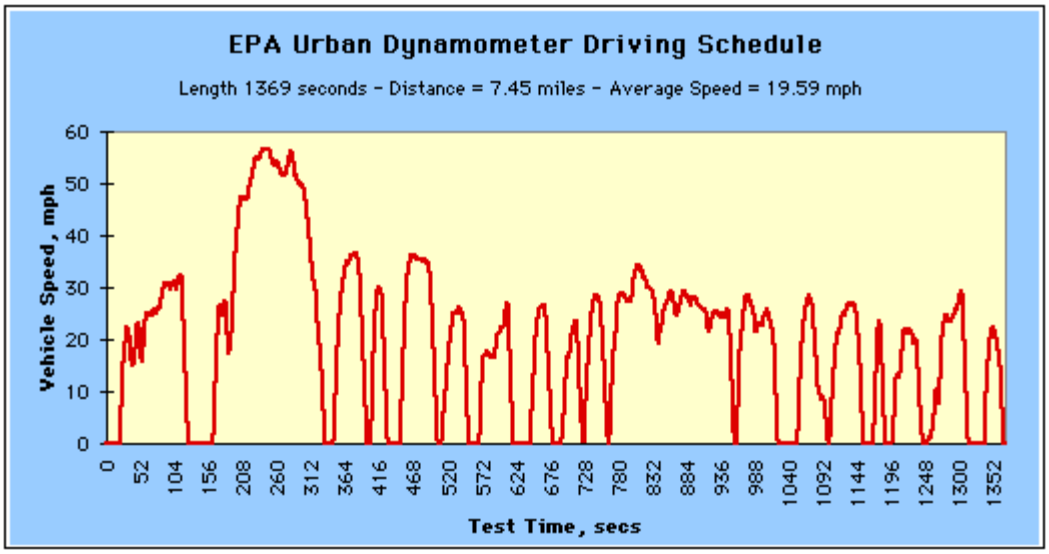


Figure 6.14: Speed-Time Characteristic of UDDS Drive Cycle.

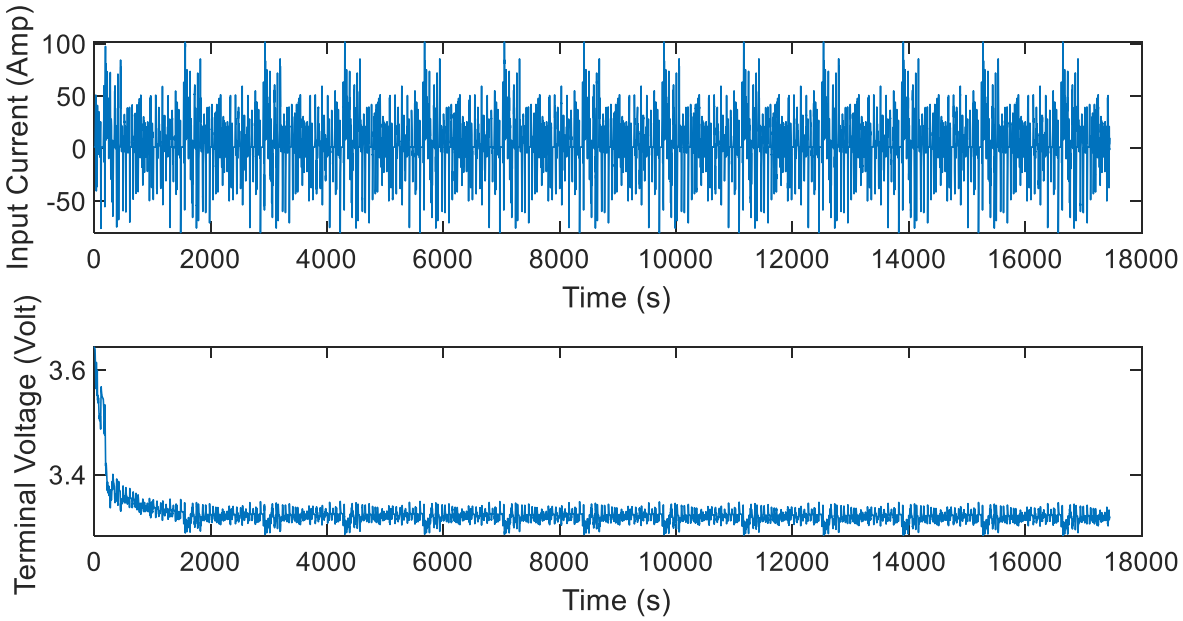


Figure 6.15: Empirical Data Profiles of Applied UDDS Driving Cycle.

Figure 6.15 shows the empirical measured data using the experimental setup described in Chapter 4. The current profile of several repeated drive cycles and the corresponding measured terminal voltage are present in Figure 6.15.

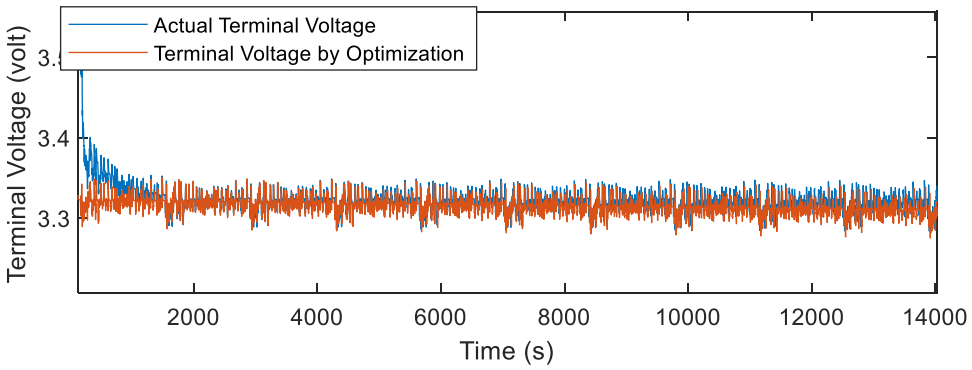


Figure 6.16 Fitting curves of measured terminal voltage and simulated terminal voltage.

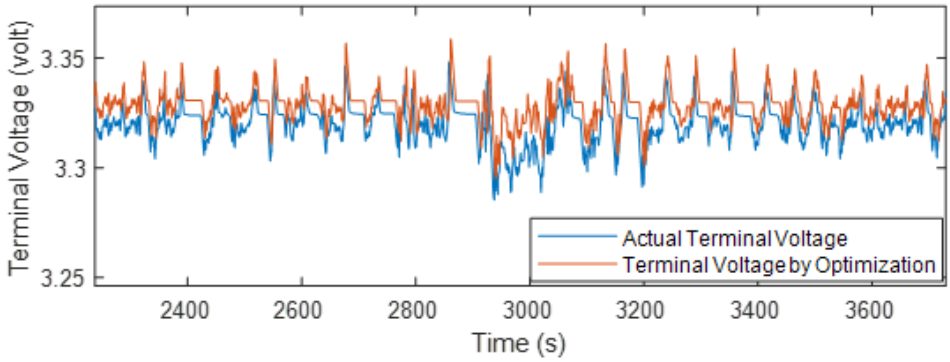


Figure 6.17: Fitting Curves of the terminal voltage in one zoomed UDDS cycle.

By the improved the pulse test and model parameter identification method the results of several entire cycles of UDDS tests were analyzed. There is a comparison between measured data and simulated data shown in Figure 6.16, after applying UDDS drive cycles there was an obvious fitting error at the beginning, mainly because of the intensity of the electrochemical reaction at the beginning of an empty battery, causing the characteristic parameters of the high capacity battery changed extremely drastically, therefore that modeling errors is difficult to control under the rapid dynamics change in battery model. The voltage drop of the battery was large, resulting in an obvious error which made curve fitting of the characteristic parameters not accurate. However, as the driving test proceeded, the modeling accuracy improved, resulting in a reduction in simulation error.

Figure 6.17 provides zoomed simulation results between the simulation data and empirical data from one single UDDS cycle. The relative error of the simulated output from the first-order RC equivalent model compared to the experimental measured data is also shown in Figure 6.18. The beginning error is unavoidable to a certain extent as it is difficult to capture rapid parametric change in the battery model in this region by simply using an equivalent circuit model of a low order. This phenomenon needs to be considered when estimating this high-capacity 280Ah battery states based on the battery model.

When ignoring the pulse data error under the unstable battery condition at the beginning stage, the average error of the simulated voltage is 0.0266 V, which is about 0.7% of the 3.5 V nominal voltage. This average residual has the same magnitude as the noise present in the measurements, indicating that the model accuracy is acceptable.

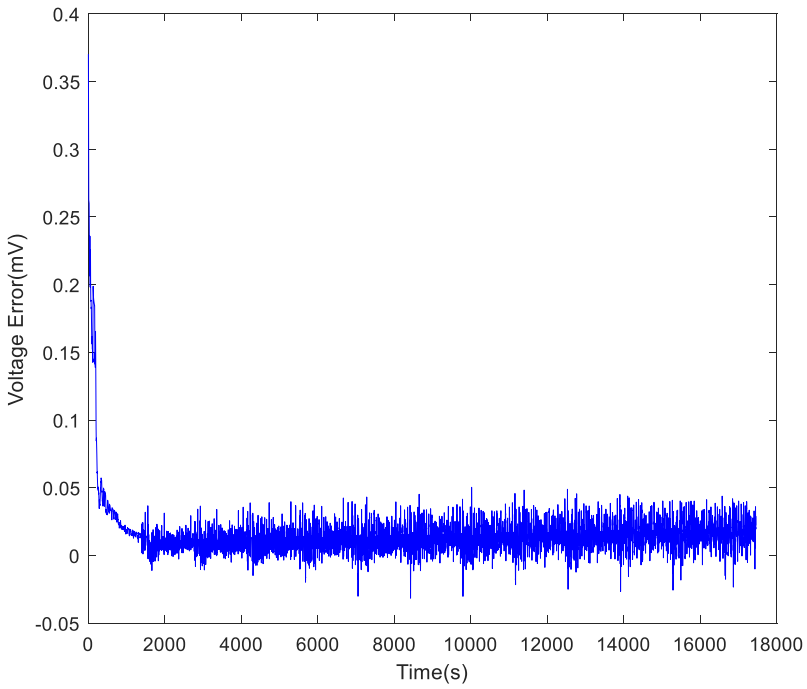


Figure 6.18: Simulated voltage error curve in real time.

In this chapter, an equivalent circuit model with one RC pair was established and presented shown in Figure 6.13, the simulated model has been validated by applying UDDS driving cycles with comparing empirical data and measured data. This first-order equivalent circuit model will be used in the later design of the second cylindrical battery pack for Ford Focus EV.

# Chapter 7

# Conclusion and Future Work

## 7.1 Conclusion

This thesis considers two topics. The first pertains to the design of a battery pack for a Ford Focus electric vehicle model and a consideration of its performance and prototyping. In this relation, the following work was completed:

(1) The basic parameters and design of a 48V battery pack using cylindrical battery cells was completed to meet the electrical and mechanical design requirements. The battery pack consists of 13 stacking submodules of 20 cells connected in parallel to achieve designing configuration.

(2) One battery submodule was partly assembled. The conductivity of current connectors in the battery submodule and the welding joints between different cell units were checked. The layout and fixed structure of the battery submodule were designed to accommodate passive air cooling for weight reduction.

The second topic involved testing, characterization and modeling of a 280 Ah prismatic battery cell of high capacity. A simulation model of the battery cell was derived for use in later studies involving the design of a future battery module. The main associated contributions were as follows:

(1) An improved pulse test method was proposed and applied for the characterization of the prismatic cell. An equivalent circuit model of the battery cell was derived and the charcaterization test data was used for model parametrization in conjunction with the GA optimization method.

(2) A simulation model using the prismatic cell's equivalent circuit model was developed and validated by using the Urban Dynamometer Driving Schedule (UDDS) cycle. The simulated results were compare to empirical data to confirm the validity of the first-order RC model.

## 7.2 Future Work

According to the design requirements, the battery module should have a higher energy density and capacity, and therefore the proposed design can benefit from further optimization of the layout and structure, to reduce its volume and mass. Passive air-cooling method is adopted which has low heat dissipation efficiency that may lead to a large local temperature difference., The resulting inconsistency in temperature distribution will accelerate battery aging, so the cooling structure needs to be further optimized.

Although the equivalent circuit model proposed in this thesis based on the improved pulse tests has attained acceptable results, the maximum value of the modelling error appears in the beginning is comparatively high. A more complex model with a higher order should be considered to improve the overall accuracy. The pulse tests are also suggested to be conducted under 0.1 C-rate, 0.2 C-rate, 0.3 C-rate and 0.5C-rate respectively, which would better help parameterize the equivalent circuit model and improve the accuracy of simulation.

# References

[1] Al-Maamary H. M. S., Kazem H. A., Chaichan M. T., Renewable energy and GCC States energy challenges in the 21st century: A review [J]. International Journal of Computation and Applied Sciences. 2017, 2(1):11-18.

[2] US EPA, About the U.S. Electricity System and its Impact on the Environment, https://www.epa.gov/energy/about-us-electricity-system-and-its-impact-environment, 2017.

[3] Wei X., Yimin M., Feng Z., Lithium-ion Battery Modeling and State of Charge Estimation. Integrated Ferroelectrics 200(1): 59-72-2019.

[4] Farmann A., Waag W., Marongiu A., Sauer D. U., Critical review of on-board capacity estimation techniques for lithium-ion batteries in electric and hybrid electric vehicles [J]. Journal of Power Sources, 2015, 281: 114-130.

[5] Inside EV's, Zero Chevrolet Volt Batteries Replaced So Far Due to "General Capacity Degradation", https://insideevs.com/news/330098/zero-chevrolet-volt-batteries-replaced-so-far-due-to-general-capacity-degradation/.

[6] Drive.com, Toyota, Nissan and Honda join forces, https://www.drive.com.au/news/toyota-nissan-and-honda-join-forces/, 2018.

[7] Shashank Arora, Weixiang Shen, Ajay Kapoor, Review of mechanical design and strategic placement technique of a robust battery pack for electric vehicles, Renewable and Sustainable Energy Reviews, Volume 60, 2016, Pages 1319-1331, ISSN 1364-0321,

[8] Ali, M. U., Zafar, A., Nengroo, S. H., Hussain, S., Alvi, M. J., & Kim, H.-J. (2019). Towards a Smarter Battery Management System for Electric Vehicle Applications: A Critical Review of Lithium-Ion Battery State of Charge Estimation. Energies, 12(3), 446. D oi: 10.3390/en12030446

[9] Chen X., Shen W., VO T. T., et al. An overview of lithium-ion batteries for electric vehicles [C]//2012 10th International Power & Energy Conference (IPEC). IEEE, 2012: 230-235.

[10] Batteryuniversity.com, BU-205: Types of Lithium-ion,

https://batteryuniversity.com/article/bu-205-types-of-lithium-ion, 22-Oct-2021.

[11] Edited by Folkson, R. Alternative Fuels and Advanced Vehicle Technologies for Improved Environmental Performance, 2014. Woodhead Publishing Series in Energy (57).

[12] Li J., Cheng Y., Jia M., et al. An electrochemical–thermal model based on dynamic responses for lithium iron phosphate battery [J]. Journal of Power Sources, 2014, 255: 130-143.

[13] Geisbauer C., Wöhrl K., Koch D., et al. Comparative Study on the Calendar Aging Behavior of Six Different Lithium-Ion Cell Chemistries in Terms of Parameter Variation [J]. Energies, 2021, 14(11): 3358.

[14] Sony, High-power output cylindrical lithium ion battery fit for high-power supply also announced - https://www.sony.com/en/SonyInfo/News/Press_Archive/200412/04-060E-2004.

[15] Sahraei E, Meier J, Wierzbicki T. Characterizing and modeling mechanical properties and onset of short circuit for three types of lithium-ion pouch cells [J]. Journal of Power Sources, 2014, 247: 503-516.

[16] Choi J., Aurbach D. Promise and reality of post-lithium-ion batteries with high energy densities. Nature Reviews Materials 1, 16013 (2016). https://doi.org/10.1038/natrevmats.2016.13.

[17] The Electropedia, Woodbank Communications Ltd., Battery Performance Characteristics, https://www.mpoweruk.com/performance.htm, 2005.

[18] US Department of Energy, Energy Efficiency & Renewable Energy, https://www.energy.gov/eere/vehicles/vehicle-technologies-office, 2021.

[19] Peng Zhang et al 2017 IOP Conference Series: Materials Science and Engineering. 199 012134.

[20] V. Pop, H. J. Bergveld, P. H. L. Notten and P. P. L. Regtien, "State-of-charge indication in portable applications," Proceedings of the IEEE International Symposium on Industrial Electronics, 2005. ISIE 2005, pp. 1007-1012 vol. 3, doi: 10.1109/ISIE.2005.1529061.

[21] Comparison of Kalman Filter-based state of charge estimation strategies for Li-Ion batteries W Wang, D Wang, X Wang, T Li, R Ahmed, S Habibi, A Emadi, 2016 IEEE transportation electrification conference and expo (ITEC), 1-6

[22] Ho V., Li-ion Battery and Gauge Introduction [J]. Taiwan: Richtek Technology Corporation, 2014.

[23] US Solar Institute, Depth of discharge (DOD), https://www.myussi.com/glossary/depth-of-discharge/2020.

[24] Libattery.ofweek.com, Research on SOC estimation of lithium iron phosphate battery, https://libattery.ofweek.com/2016-02/ART-36001-11001-29063789.html, 2016.

[25] Xiangzhe L., Fang S., Daoyong, L. Electric vehicle power supply system [M]. Beijing: Chemical Industry Press, 2011.11. [18].

[26] 2013 Ford Focus Electric Advanced Vehicle Testing – Baseline Testing Results, INL/MIS-15-34211 • January 2015.

[27] Yu Zhisheng Automobile theory [M] Beijing: China Machine Press, 03, 2009.

[28] Wang Zhenpo, Sun Fengchun, Lin Cheng. Analysis of Inconsistency on the Service Life of Power Battery Packs [J]. Journal of Beijing Institute of Technology, 2006, 26(7): 577-580.'

[29] US Department of Energy, Battery Test Manual for Plug-In Hybrid Electric Vehicles [R]. Idaho Falls. U.S.Department of Energy Vehicle Technologies Program, 2008.03.

[30] Yanhui M., Research on heat dissipation structure of NiMH battery pack for hybrid electric vehicle [D]: [Master's Thesis] Shanghai: Shanghai Jiaotong University, 2009.

[31] Haifeng D., Nan W., Review of research on inconsistency of lithium ion battery for vehicle power [J]. Automotive Engineering, 2014, 36 (2): 181-187.

[32] Nizam M., Maghfiroh H., Rosadi R. A., et al. Design of battery management system (BMS) for lithium iron phosphate (LFP) Battery [C], 2019, 6th International Conference on Electric Vehicular Technology (ICEVT). IEEE, 2019: 170-174.

[33] Oswal M., Paul J., Zhao R. A comparative study of lithium-ion batteries [J]. University of Southern California, 2010: 2419-2430.

[34]Ko Y., Choi W. A new SoCSOC estimation for lfp batteries: Application in a 10 ah cell (hw 38120 l/s) as a hysteresis case study [J]. Electronics, 2021, 10(6): 705.

[35]Digatron Power Electronics, Test cycles from Digatron Power Electronics, https://www.digatron.com/en-us/Products/Laboratory/Cycler/Cell-Tester

[36] DIGATRON MCT-ME cycler, https://www.digatron.com/enus/Products/Laboratory/Cycler/Cell-Tester/MCT-ME.

[37] Thermotron temperature control chamber, https://thermotron.com/equipment/temperature-chamber/?gclid=Cj0KCQiAu62QBhC7ARIsALXijXS6sgVQDwzUdxfFQbbBrsuvVqkpefJK4wD2PEw4PTt9DxoFKPXy8vQaAuTPEALw_wcB.

[38] Smart Sensors Inc., Replacing Thermocouples: Room for Improvement? http://www.smartsensors.com/goldy1.htm.

[39] Ye Y., Saw L. H., Shi Y., et al., Effect of Thermal Contact Resistances on Fast Charging of Large Format Lithium Ion Batteries, Electrochim. Acta, vol. 134, pp. 327–337, 2014.

[40] Reliable state of charge and state of health estimation using the smooth variable structure filter HH Afshari, M Attari, R Ahmed, A Delbari, S Habibi, T Shoa.

[41] Roscher M. A., Bohlen O. S. , and Sauer D.U., Reliable state estimation of multi-cell lithium-ion battery systems, IEEE Transactions on Energy Conversion, vol. 26, no. 3, Sep. 2011.

[41] Evlithium, EVE LF280 Lifepo4 3.2V 280 Ah Power Lithium ion Battery for RV solar system storage, https://www.evlithium.com/hot-lithium-battery/946.html.

[42] Batteryuniversity.com, Bu-205: Types of lithium-ion, https://batteryuniversity.com/learn/

Article/types of lithium ion.

[43] Thanagasundram S., Arunachala R., Makinejad K., et al, A cell level model for battery simulation, in European Electric Vehicle Congress, Brussels, Belgium, 11, 2012.

[44] Reduced-coupling coestimation of SOC and SOH for lithium-ion batteries based on convex optimization D Xiao, G Fang, S Liu, S Yuan, R Ahmed, S Habibi, A Emadi, IEEE Transactions on Power Electronics 35 (11), 12332-12346 Control Engineering Practice 77, 1-14.

[45] Cugnet M. G, Dubarry M., Liaw B. Y., Peukert's law of a lead-acid battery simulated by a mathematical model [J]. ECS Transactions, 2010, 25(35): 223.

[46] Jackey R., Saginaw M., Sanghvi P., et al. Battery model parameter estimation using a layered technique: an example using a lithium iron phosphate cell [J]. SAE Technical Paper, 2013.

[47] Huria, T., Rechargeable lithium battery energy storage systems for vehicular applications, http://etd.adm.unipi.it/t/etd-04262012-182954/, Ph.D. thesis, Department of Energy and Systems Engineering, University of Pisa, 2012.

[48] Cheng K. W. E., Divakar B. P., Wu H., et al. Battery-management system (BMS) and SOC development for electrical vehicles [J]. IEEE Transactions on Vehicular Technology, 2010, 60(1): 76-88.2010, 10-11.

[49] He H. W., Xiong R., Guo H., et al. Comparison study on the battery models used for the energy management of batteries in electric vehicles [J]. Energy Conversion and Management, 2012, 64: 113-121.

[50] Li J., , Wang L., Chao L., et al. State of Charge estimation based on a simplified electrochemical model for a single LiCoO2 battery and battery pack [J]. Energy, 2017, 133: 572-583.

[51] Hein S., Danner T., Latz A. An electrochemical model of lithium plating and stripping in lithium ion batteries [J]. ACS Applied Energy Materials, 2020, 3(9): 8519-8531.

[52] Piao C., Yang X., Teng C, et al. An improved model based on Thevenin model for nickel metal hydride power battery [C]. 2010. International Conference on Optics, Photonics and Energy Engineering (OPEE), IEEE.

[53] Farmann A., Waag W., Sauer D. U. Adaptive approach for on-board impedance parameters and voltage estimation of lithium-ion batteries in electric vehicles [J]. Journal of Power Sources, 2015, 299: 176-188.

[54] Allafi W., Uddin K., Zhang C., et al. On-line scheme for parameter estimation of nonlinear lithium ion battery equivalent circuit models using the simplified refined instrumental variable method for a modified Wiener continuous-time model [J]. Applied Energy, 2017, 204: 497-508.

[55] Ding X., Zhang D., Cheng J., et al. An improved Thevenin model of lithium-ion battery with high accuracy for electric vehicles [J]. Applied Energy, 2019, 254: 113615.

[56] Jackey, R., Plett, G., and Klein, M., Parameterization of a Battery Simulation Model Using Numerical Optimization Methods, SAE Technical Paper 2009-01-1381, 2009, doi: 10.4271/2009-01-1381.

[57] Continuous piecewise-linear, reduced-order electrochemical model for lithium-ion batteries in real-time applications M Farag, M Fleckenstein, S Habibi, Journal of Power Sources 342, 351-362.

[58] Deland, S., Optimization of Hydroelectric Flow with MATLAB, Dec. 2012.

[59] Jackey R., da Cunha A. and Gazzarri J., Webinar: Automating Battery Model Parameter Estimation using Experimental Data,

http://www.mathworks.com/videos/automating-battery-model-parameter-estimation-using-experimental-data-81987.html.

[60]Miller S., Hybrid-Electric Vehicle Model in Simulink, http://www. mathworks.com/matlabcentral/fileexchange/28441-hybrid-electric-vehicle-model-in-simulink 17 Apr, 2014.

[61] Zhang L., Wang L., Hinds G., et al. Multi-objective optimization of lithium-ion battery model using genetic algorithm approach [J]. Journal of Power Sources, 2014, 270: 367-378.

[62] A comparative study of Li-ion battery models and nonlinear dual estimation strategies MS Farag, R Ahmed, SA Gadsden, SR Habibi, J Tjong, 2012 IEEE Transportation electrification conference and expo (ITEC), 1-8